Phase Dynamics of Irregular Oscillations

Dissertation

zur Erlangung des Doktorgrades
'doctor rerum naturalium' (Dr. rer. nat.)
der Mathematisch-Naturwissenschaftlichen Fakultät

der

Universität Potsdam

vorgelegt von
Justus Tilmann Caspar Schwabedal
aus Sankt Augustin

Potsdam, September 2010

Published online at the
Institutional Repository of the University of Potsdam:
URL http://opus.kobv.de/ubp/volltexte/2011/5011/
URN urn:nbn:de:kobv:517-opus-50115
http://nbn-resolving.org/urn:nbn:de:kobv:517-opus-50115

“Intelligenz ist wie das Facettenauge einer Fliege.”

– P. E. S.

Allgemeinverständliche Zusammenfassung

Viele Systeme in der Natur zeigen ungleichmäßige Rhythmen, ohne dass eine äußere Kraft sie dabei beeinflusst. Zum Beispiel variiert die Rhythmik der Atmung ständig in ihrer Tiefe und Dauer. Zum Zwecke des besseren Verständnisses werden solche Rhythmen in vereinfachter Weise durch ihre Phasen beschrieben. Diese Beschreibung wird in zwei Arbeitsschritten vorgenommen, erstens der Unterteilung des Rhythmus in seine Phasen und zweitens der Zuordnung verschiedener Systemzustände zu einer Phase. Beide Arbeitsschritte liegen jedoch im Ermessen des Beobachters und sind deshalb nicht allgemeingültig: Zum einen wird der ungleichmäßige Rhythmus willkürlich in kürzere oder längere Phasen unterteilt. Zum anderen werden Systemzustände unterschiedlicher Amplitude, also z.B. der Atemtiefe, unbegründet derselben Phase zugeordnet. Im Rahmen der vorliegenden Doktorarbeit wird eine verfeinerte Phasenbeschreibung vorgenommen, die zu einem gewissen Grade allgemeingültig ist. Beide genannten Arbeitsschritte werden dabei separat verfeinert.

Die Unterteilung des Rhythmus in seine Phasen als ersten Arbeitsschritt ist charakterisiert durch die Schnelligkeit, mit der die jeweiligen Phasen durchlaufen werden. Daher soll in der Arbeit die Phasengeschwindigkeit dazu verwendet werden, die Phase in eine allgemeingültige Form zu bringen. Für vom Zufall bestimmte Systeme ist die Phasengeschwindigkeit jedoch nicht eindeutig feststellbar. In der Arbeit sollen daher auch mehrere Varianten einer mittleren Phasengeschwindigkeit vorgestellt werden, die eine allgemeingültigere Phasenbeschreibung erlauben. Dabei ist je nach Anwendungsbereich eine andere Variante nützlich. Vorteil einer allgemeingültigen Phasenbeschreibung ist dabei, dass auch die von ihr abgeleiteten Größen erweiterte Gültigkeit erlangen: So kann im Ergebnis die Kopplung zwischen miteinander in Verbindung stehenden Systemen allgemeingültig beschrieben werden. Dies wird in der Arbeit anhand von Beispielen näher dargelegt.

Auch der zweitgenannte Arbeitsschritt der Zuordnung verschiedener Systemzustände zu einer Phase soll in allgemeingültiger Weise ermöglicht werden. Diese Zuordnung soll nach dem Kriterium der zukünftigen Unterscheidbarkeit vorgenommen werden: Demnach sind all diejenigen Systemzustände einer Phase zuzuordnen, die in Zukunft nicht unterschieden werden können. Betrachtet man zwei Zustände einer Phase, so lässt sich das Kriterium dadurch überprüfen, dass man für beide Zustände getrennt die Zeit misst, die vergeht, bis sie jeweils nach einer Periode wieder in derselben Phase sind. Die gemessenen Zeiten müssen dann für die derselben Phase zugeordneten Zustände identisch sein. Für vom Zufall bestimmte Systeme ist es wiederum nötig, die mittlere Zeit für eine Rückkehr in dieselbe Phase zu berechnen. Für Rhythmen sogenannter chaotischer Systeme hingegen erweist sich, dass das Kriterium nur annäherungsweise erfüllt werden kann. Für solche Systeme ist eine Phasenbeschreibung daher nur begrenzt möglich.

Gemeinsam erlauben beide verfeinerten Arbeitsschritte eine allgemeingültige Phasenbeschreibung ungleichmäßiger Rhythmen, wodurch auch komplizierte rhythmische Vorgänge in der Natur präziser beschrieben werden können.

Abstract

Many natural systems embedded in a complex surrounding show irregular oscillatory dynamics. The oscillations can be parameterized by a phase variable in order to obtain a simplified theoretical description of the dynamics. Importantly, a phase description can be easily extended to describe the interactions of the system with its surrounding. It is desirable to define an invariant phase that is independent of the observable or the arbitrary parameterization, in order to make, for example, the phase characteristics obtained from different experiments comparable.

In this thesis, we present an invariant phase description of irregular oscillations and their interactions with the surrounding. The description is applicable to stochastic and chaotic irregular oscillations of autonomous dissipative systems. For this it is necessary to interrelate different phase values in order to allow for a parameterization-independent phase definition. On the other hand, a criterion is needed, that invariantly identifies the system states that are in the same phase.

To allow for a parameterization-independent definition of phase, we interrelate different phase values by the phase velocity. However, the treatment of stochastic oscillations is complicated by the fact that different definitions of average velocity are possible. For a better understanding of their differences, we analyse effective deterministic phase models of the oscillations based upon the different velocity definitions. Dependent on the application, a certain effective velocity is suitable for a parameterization-independent phase description. In this way, continuous as well pulse-like interactions of stochastic oscillations can be described, as it is demonstrated with simple examples.

On the other hand, an invariant criterion of identification is proposed that generalizes the concept of standard (Winfree) isophases. System states of the same phase are identified to belong to the same generalized isophase using the following invariant criterion: All states of an isophase shall become indistinguishable in the course of time. The criterion is interpreted in an average sense for stochastic oscillations. It allows for a unified treatment of different types of stochastic oscillations. Using a numerical estimation algorithm of isophases, the applicability of the theory is demonstrated by a signal of regular human respiration. For chaotic oscillations, generalized isophases can only be obtained up to a certain approximation. The intimate relationship between these approximate isophase, chaotic phase diffusion, and unstable periodic orbits is explained with the example of the chaotic Rössler oscillator.

Together, the concept of generalized isophases and the effective phase theory allow for a unified, and invariant phase description of stochastic and chaotic irregular oscillations.

Contents

Chapter 1

Introduction

Our curiosity is excited by physical objects that show dynamical patterns. If the same pattern is repeated cyclically without any forceful influence of an external rhythm, a purpose of its own is ascribed to the dynamical process and it is desirable to understand the structure of its dynamics and its interactions with its surrounding. It seems natural to divide the pattern into certain phases that define a consecutive time course in a circular fashion. The associated phase variable describes in which part of the cycle the system currently resides. In its applications, may they be as complicated as the rhythms of the human brain or as simple as the dynamics of a pendulum clock, the phase provides the foundation for a global understanding of dynamical properties [89].

In a physical context, a 2π-periodic phase variable provides a simplified description of autonomous oscillations shown by natural, synthetic or mathematical systems [1, 42, 63]. Simple examples of autonomous dissipative systems fueled by an energy source can show regular limit-cycle oscillations for which a phase description – a monotonic parameterization of the limit-cycle – is straightforward. But their dynamics can also be more complicated: Irregularities in frequency and amplitude may be present in the oscillations. Then, amplitude variables have to be taken into account in order to quantify deviations from the stereotypical oscillation [40]. In some cases, the irregularity can be described best as the effect of a random forcing, i. e. noise. Noise is either a perturbation to regular oscillations, or it is substantial in the sense that it induces oscillations in the system which would equilibrate otherwise [64, 46, 6]. In other cases, the irregularity is of a non-random nature interpreted as the presence of deterministic chaos [49, 72, 73]. Both types of irregular oscillations can only be parameterized by a single phase variable if certain *states are identified to be in the same phase*. The standard procedure of phase reduction extends the definition of phase starting from a limit-cycle: Those states are identified that become indistinguishable in the course of time in which they contract to the same state of the limit-cycle [89]. Therefore, the procedure is not applicable for those systems that show irregular oscillations unless they are weakly noise-perturbed.

An oscillating system embedded in a complex surrounding can be described more realistically by taking into account their interactions. These are usu-

ally constrained to be weak in some sense[1]. The state of weakly interacting limit-cycle oscillators remains close to the limit-cycle, allowing for a perturbative approach to be valid. The phase dynamics of such oscillators has been extensively studied in different setups such as, two, three and many of the oscillators interacting globally or in networks via continuous or pulse-like coupling [20, 37, 38, 42, 52, 63, 79, 87, 89]. Usually, the coupled oscillators interact pairwise. A continuous pairwise interaction is characterized by two coupling functions, each one quantifying the phase-dependent force exerted on the other phase variable. The coupling function can be inferred from oscillatory data, allowing for an easily interpretable method of signal processing [8, 40, 41, 58, 84, 85]. In pulse-like interactions, a short pulse kicks the phase of the oscillator to a new value. The difference between the old and the new value can be characterized by the phase resetting curve [10, 55, 59]. The curve has been used to characterize different types of neuronal oscillators [10]. For an invariant definition of interaction functions, such as the coupling function or the phase resetting curve, the phase variable has to be obtained in a non-arbitrary parameterization that is normally provided by the limit-cycle of the oscillating system. Therefore, the theory of phase dynamics has only a restricted applicability that, for example, does not allow a description of interacting noise-induced oscillations [30, 60, 69].

The goal of this thesis is an invariant phase description of irregular oscillations. For this, those states of the oscillations that belong to the same phase must be identified in an invariant way. Furthermore, the phase of stochastic oscillations has to be defined independent of the initially arbitrary parameterization to be able to formulate an invariant phase description of interactions.

For an invariant phase description of stochastic oscillations, they are modeled by effective deterministic phase oscillators. The theory is easily extended to describe continuous and pulse-like interactions by the definition of an effective coupling function and a stochastic phase resetting curve, respectively. Furthermore, the problem of phase reduction of irregular oscillations is addressed. Following the paradigm of Ref. [89], we identify states *to be in the same phase if they become indistinguishable in the course of time*. The approach leads to a phase variable that is to a certain extent invariant under transformations of the state space.

In Chap. 2, the current model and the first passage model of effective phase dynamics are presented in detail. The current model can be extended to describe continuous interactions of oscillations as demonstrated by the simple example of periodically forced stochastic oscillations. The first passage model, on the other hand, describes the stochastic phase resetting curve of stochastic oscillations that are subject to a brief pulse. In Chap. 3, the concept of standard isophases is generalized for a treatment of stochastic and chaotic oscillations. A numerical scheme is presented that allows for an estimation of the generalized isophases from data. It is shown by examples, that the theory is applicable to noise-induced, noise-perturbed as well as non-Markovian

[1]For strong interactions, the notion of system might not apply.

stochastic oscillations in a unified way. Furthermore, the applicability of the scheme to observed oscillations is illustrated by a biophysical example. For chaotic oscillations, it is shown that generalized isophases can only be approximated. The relations of chaotic phase diffusion, unstable periodic orbits and approximate isophases is discussed.

We continue the introduction with a biophysical example of interacting irregular oscillations with which we explain certain difficulties of a phase description (Sec. 1.1). Then, different theoretical models of irregular oscillations are discussed: In the simplest case, a limit-cycle oscillator allows for a perturbative phase description of weakly perturbed and interacting oscillations (Sec. 1.2). Some oscillations are better described by generically stochastic oscillators that show, for example, noise-induced oscillations. For these, the notion of oscillation can be ill-posed what drives the concept of phase description to its limits (Sec. 1.3). After all, the irregularity of oscillations may not be the result of randomness, but deterministic chaos. Then, chaotic oscillators are the natural model of choice, for which oscillations can be characterized by their unstable periodic orbits (Sec. 1.4).

1.1 Irregular Oscillations

Autonomous irregular oscillations are immanent in biophysical systems [20]. Well-known examples are the oscillations shown by the human heart, as well as the human respiration. However, the observable patterns are not perfectly recurrent, but show variability in frequency and amplitude. Therefore, it may not be straightforward to identify an oscillation, or even harder, the phases of the oscillatory cycle in an observable-invariant fashion. On the other hand, a phase description of interacting oscillations yields the profit of an easily interpretable quantification of their interaction. Let us explain the problems of a phase description of irregular oscillations with the examples of the **electrocardiogram (ECG)** and breast belt measurements of the regular human respiration.

Regular human respiration measured by the tension of a breast belt $\rho(t)$ gives an approximately sinusoidal signal for which their is not much ambiguity in the definition of oscillation (cf. top left plot of Fig. 1.1). However, the dynamical pattern $E(t)$ of single beat of the human heart in the ECG shows multiple features of variable amplitude[2] (top plot of Fig. 1.2). For example, the highest peaks, the R-peaks, can serve as markers in between which the heart is said to perform one "oscillation" – its phase grows by 2π. This notion of oscillation has been motivated biologically by matching characteristic heart movements to features of the ECG pattern.

The construction of a phase variable $\varphi(t)$ must start somewhere on the cycle of the heart beat[3]. To be specific, we can identify all states $E(t_j)$ for which the

[2]Usually, there are three peaks named P, R and T, and two valleys named Q and S, but there can be a fourth peak (see Ref. [74] or any textbook on human physiology).

[3]Being a cycle, there is no generic beginning.

ECG shows a local maximum of the R-peak to be in the same phase $\varphi(t_j) = 0$. Knowing only one phase of the cycle, we can already calculate a coarse-grained instantaneous heart period – the so called **beat-to-beat interval (BBI)**: $T_j = t_{j+1} - t_j$. Let us note that such an approach is applied in theoretical models of stochastic oscillations as well [30, 66]. Problematically, the marker-based procedure for a calculation of BBIs is not invariant because it depends on the marker and the observable: Let us consider the signal $E(t)$ and its time derivative $\dot{E}(t)$ as a two-dimensional state space of the dynamics. The states of zero phase correspond to a curve in the state space (bottom left plot of Fig. 1.2). The BBIs are nothing but the return times to that curve (bottom right plot). However, if the electrodes[4] were placed at slightly different positions, the state space would be transformed, nonlinearly. Most likely, the states defined by the new maxima of R-peaks would not be the same as before resulting in quantitatively different BBIs[5]. We find: A marker-based definition of phase is neither optimal nor invariant.

For a definition of BBIs we needed only one phase of the ECG signal, and we have chosen the R-peak. Principally, one is interested in defining a phase variable for all states of the ECG, but this is not easy because variations of most features corresponding to other values of the phase are usually too large for a reliable detection. This is different for the almost sinusoidal dynamics of regular human respiration (cf. top left plot of Fig. 1.1). Using the Hilbert transformation $H_x(t)$, a two-dimensional state space $(H_\rho,\ \rho)$ is obtained that allows for the definition of polar coordinates whose phase variable $\varphi(t)$ characterizes respiratory oscillations to a certain extent [63]. As for the ECG marker, the curves of constant phase defined by the radial beams (red lines) are neither optimal nor invariant[6].

If two oscillating systems interact, an imprint of the interaction is left in their phase dynamics, that is observable in the phase dependence of their instantaneous frequencies. The interaction of the human respiration and heart beat can be observed by the well-known respiratory sinus arrhythmia – the dependence of the heart beat on the respiratory phase [27]. The effect can be readily seen by displaying the BBIs T_j obtained from the ECG as a function of respiratory phase $\varphi(t_j)$ (cf. bottom plot of Fig. 1.1): On average, the inspiratory phase $\varphi(t_j) \approx 0$ is accelerant whereas the expiratory phase $\varphi(t_j) \approx \pi$ is decelerant. The data shows a large amount of noise that has several potential sources. For example, it is well-known that the arrhythmia depends on the amplitude of respiration, as well, which is averaged over in the phase description. However, as it is strongly suggested from the discussion above, we claim that a certain amount of noise, seen in the bottom plot of Fig. 1.1, is due to the inaccurateness in the definitions of respiratory phase and BBIs.

[4]The ECG is measured with surface electrodes that are placed on the skin of the upper part of the body at certain positions.

[5]The implied randomness of the chosen observable is a form of measurement noise. Its amplitude depends on the scattering width of states and on the speed of transition of the curve relative to the mean frequency.

[6]This can be seen easily by a slight shift of the origin in Fig. 1.1.

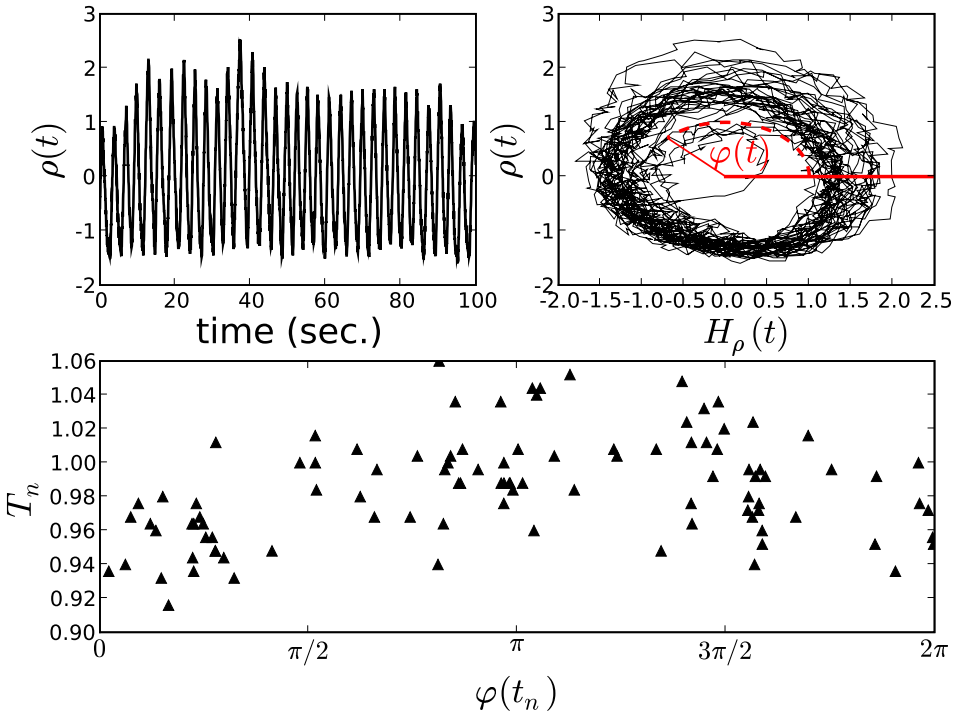

Figure 1.1: A time segment of regular human respiration $\rho(t)$ (top left plot) is embedded via the Hilbert transform H_ρ (black line in top right plot). In this state space, polar coordinates define an arbitrary phase variable of the respiration $\varphi(t)$ (red lines). The BBIs $T_n = t_{n+1} - t_n$ of a simultaneously measured ECG signal (cf. Fig. 1.2) as a function of the phase $\varphi(t_n)$ at the time of the R-peak t_n revealed the well-known respiratory sinus arrhythmia – the dependence of heart period on the respiratory phase (black triangles in bottom plot). The shown data was obtained from subject `fly05` of the "fantasia database" [21] (sampling rate: 256 Hz).

1.2 Description of Irregular Oscillations as Regular Oscillations

There are certain conditions under which irregular oscillations may be described by regular oscillations shown by limit-cycle oscillators [32, 43, 81]. One has to be sure that only weak extrinsic forces perturb the regular dynamics. Then, a phase description based on limit-cycle oscillators can yield a good approximation, too. The approach was employed to describe systems under the influence of short pulses [9, 26, 50], of other oscillators [42, 63], and of white or colored noise [22, 45, 82, 90]. Notably, stochastic synchronization of neuronal oscillators could be modeled quantitatively [54].

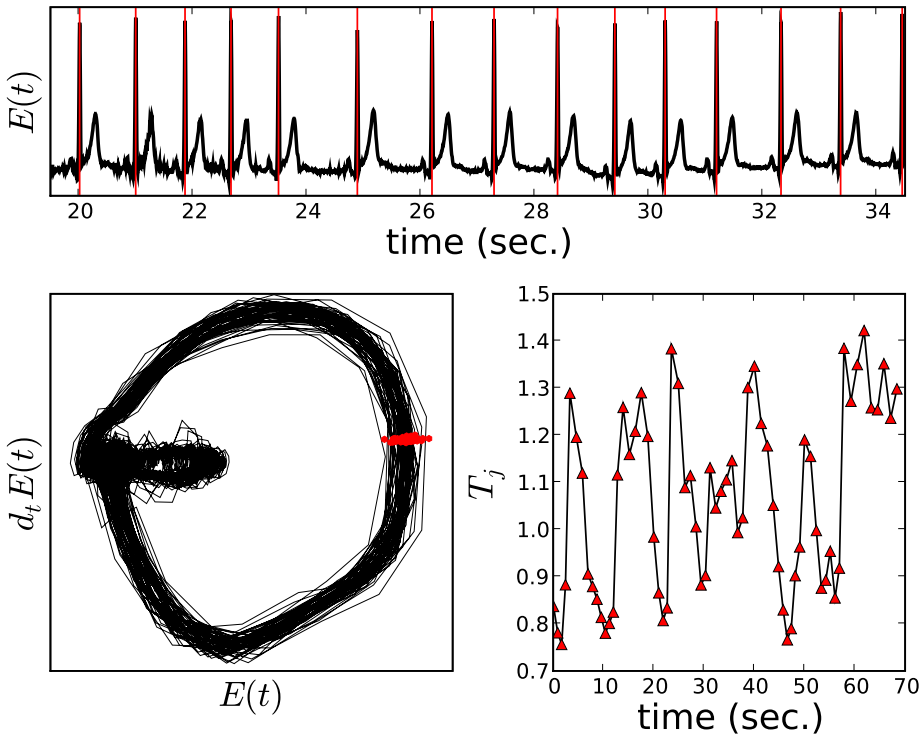

Figure 1.2: The ECG signal $E(t)$ shows a slightly aperiodic return of a stereotypical dynamical pattern (black line in top plot). The marker-based approach to identify the tip of the R-peak (red vertical lines) can be mapped to the choice of a certain curve in the state space $(E(t),\ \dot{E}(t))$ (red points in bottom left plot). Therefore, the resulting BBIs T_j at times t_j (red triangles in bottom right plot) depend on the marker as well as on the observable. The data was measured from a 25-year old male subject using a standard Holter monitor (sampling rate: 256 Hz).

1.2.1 Standard Phase Reduction

Autonomous regular oscillations are shown by a limit-cycle oscillator [89, 78]

$$\dot{\mathbf{x}} = F(\mathbf{x}) \ . \tag{1.1}$$

Asymptotically, each state that lies in the basin of attraction reaches a stable period T limit-cycle $\mathbf{x}_0(t+T) = \mathbf{x}_0(t)$ which serves as the backbone of the standard phase reduction procedure: Each state $\mathbf{x}_0$ on the cycle can be identified with a phase $\theta(\mathbf{x}_0) \in [0, 2\pi)$ in a one-to-one fashion. The identification should be performed such that the phase as a function of time is strictly monotonous if it is considered as an *unwound*[7] variable that is not taken modulo 2π. In this way a phase variable is introduced on the cycle. There are two degrees of freedom which are not fixed by the definition of phase. First, the phase $\theta = 0$ has to be matched to a certain state $\mathbf{x}_0$ on the cycle. Choosing another state $\mathbf{x}_0'$ leads to a constant phase shift. Second, the monotonous parameterization

[7]The unwound phase is also sometimes called unwrapped.

of the cycle is arbitrary. Therefore, its dynamics $\dot{\theta} = h(\theta)$ is described by an arbitrary positive function $h(\theta)$. One can chose $\dot{\theta} = \frac{2\pi}{T}$. In this parameterization θ is a time-like variable. Starting from an arbitrary parameterizing phase α that obeys the phase dynamics $\dot{\alpha} = h(\alpha)$, a uniformly rotating phase variable θ can always be obtained by the transformation

$$\theta = S(\alpha) = \frac{2\pi}{T} \int_0^\alpha \frac{d\alpha'}{h(\alpha')} \ . \tag{1.2}$$

Let us note that a stochastic phase variable can only rotate uniformly on average. However, the notion of average uniformity is ambiguous because the notion of average speed is. Therefore in Chap. 2, we will distinguish between the arbitrarily parameterized *protophase* and the *phase* that has a special parameterization, for clarity.

The irregularity of oscillations is modeled as an external perturbation to the dynamics of oscillator (1.1). Even though it might be weak or short leading only to small deviations of the state from the limit-cycle, the definition of $\theta(\mathbf{x})$ has to be extended to states in its vicinity. One possibility is to use an arbitrary extension $\varphi(\mathbf{x})$ from the limit-cycle to its neighborhood, which then is foliated by a family of Poincaré sections $J(\varphi)$ of constant arbitrary phase φ that equals θ on the limit-cycle. The family defines cylindrical coordinates that consist of the arbitrary phase φ and amplitudes $\mathbf{a}$ parameterizing $J(\varphi)$. For example, the star-shaped set of curves of constant phase φ that define the polar coordinates, shown in the top right plot of Fig. 1.1, form a family $J(\varphi)$. The dynamics of φ may still depends on $\mathbf{a}$, whereas the goal is to define a phase that rotates independent of the amplitudes: Then, in accordance with the paradigm, differences in phase will remain whereas differences in amplitude will decay in the course of time.

For a limit-cycle oscillator (1.1), the proper family of Poincaré sections $I(\theta)$ can be defined as follows: A state $\mathbf{x}$ close to the limit-cycle will be attracted to it after some time, and asymptotically it shares the same future with some state $\mathbf{x}_0$ on the limit-cycle: (cf. Fig. 1.3):

$$\lim_{t\to\infty} ||\mathbf{x}(t) - \mathbf{x}_0(t)|| = 0 \ . \tag{1.3}$$

Then, $\mathbf{x}$ is assigned the same phase as $\mathbf{x}_0$: $\theta(\mathbf{x}) = \theta(\mathbf{x}_0)$. In this way, $\theta(\mathbf{x})$ is defined for all states that approach the limit-cycle. The set of all points with the same phase gives a Poincaré section $I(\theta)$, called *standard isophase*, for which phase dynamics decouples from amplitudes [89]. We want to stress that standard isophases are defined in the basin of attraction of a stable limit-cycle.

As an example, the Landau-Stuart oscillator is a two-dimensional system that shows a limit-cycle beyond a supercritical Hopf bifurcation. In a complex coordinate Ψ, it is governed by the dynamics [80]

$$\dot{\Psi} = (1 + i\alpha)\Psi - (1 + i\kappa)|\Psi|^2\Psi \ . \tag{1.4}$$

In polar coordinates $\Psi = re^{i\varphi}$ the dynamics is given by

$$\dot{r} = r(1 - r^2) \ , \quad \dot{\varphi} = \alpha - \kappa r^2 \ . \tag{1.5}$$

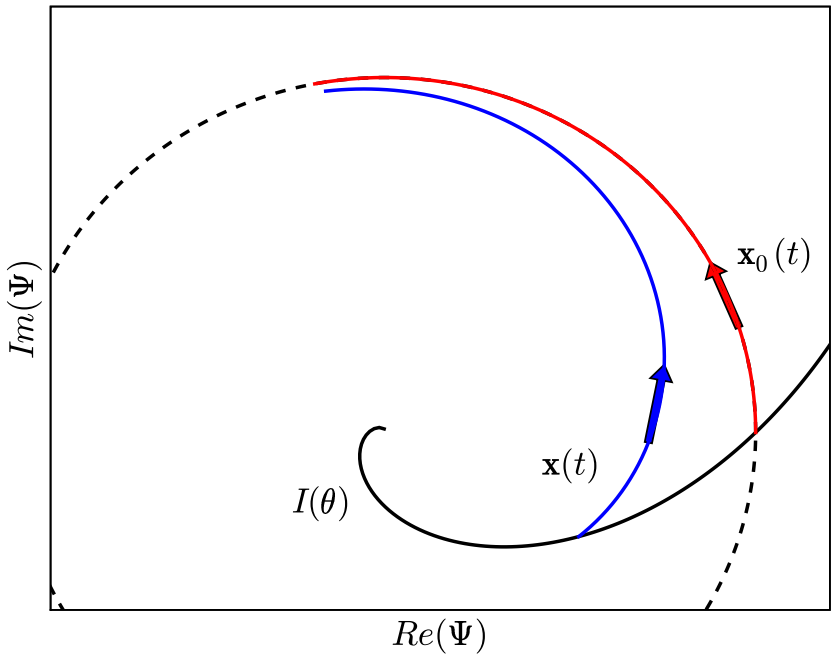

Figure 1.3: According to Eq. (1.3), a state $\mathbf{x}(t)$ (blue line with arrow) of a limit-cycle oscillator starting on a standard isophase $I(\theta)$ (black line) approaches the state $\mathbf{x}_0(t)$ (red line with arrow) starting on the intersection of the isophase and the limit-cycle (dashed line), here shown for oscillator (1.4) at parameters $\alpha = 2$ and $\kappa = 1$. For each $\mathbf{x}$, the time $T(\mathbf{x})$ to return to $I(\theta)$ is equal to the oscillation period of the limit-cycle: $T(\mathbf{x}) = T = \frac{2\pi}{\alpha-\kappa}$.

The equations have the limit-cycle solution $r(t) = 1$ and $\varphi(t) = (\alpha-\kappa)t+\varphi(0)$ with a frequency $\omega = \alpha - \kappa$. The general solution can be found, too:

$$\begin{aligned} r(t) &= \left[1 + \frac{1-r^2(0)}{r^2(0)}\mathrm{e}^{-2t}\right]^{-1/2} \quad , \\ \varphi(t) &= \omega t + \kappa \ln r(t) + \varphi(0) - \kappa \ln r(0) \ . \end{aligned} \tag{1.6}$$

From the general solution, we can find the uniformly rotating phase θ by inquiring $\dot{\theta} = \omega$. The resulting transformation

$$\theta(\varphi, r) = \varphi - \kappa \ln r \tag{1.7}$$

is an implicit definition of standard isophases: For a fixed phase θ, the solutions of Eq. (1.7) form the associated standard isophase (cf. Fig. 1.3). From the equation we see that κ governs the non-isochronicity, i. e. the amplitude dependence of the local frequency.

In Ref. [33], a generalization of phase was proposed mainly relying on the average constancy of its growth rate (cf. Eq. (1.2)), but that approach still

does not lead to an invariant phase description. In Chap. 3, we present a geometrical approach by generalizing the concept of standard isophases with which an invariant phase description can be formulated. For the generalization the following property of standard isophases is used. Let us consider a standard isophase $I(\theta)$ as a Poincaré section of the dynamics: It takes a return time $T(\mathbf{x})$ for a state $\mathbf{x}$ on $I(\theta)$ to perform one oscillation and return to $I(\theta)$. Because of the decoupling of the phase equation $\dot{\theta} = \omega$ from the amplitudes, all average return times of $I(\theta)$ are constantly equal to the oscillation period T. Not relying on the existence of a limit-cycle, the property is suitable for a generalization of standard isophases. However, in an application to chaotic dynamics it is seen that even generalized isophases may not exist. In this case, useful approximations are still possible.

1.2.2 Phase Description of Interaction

The interaction of oscillations is reflected in their phase dynamics as seen in the bottom plot of Fig. 1.1. If interactions are weak, the standard phase reduction of limit-cycle oscillators can be employed in a perturbative manner in order to derive the coupled phase equation.

In order to model interaction, we perturb the oscillator with an additional term $\Gamma(t, \mathbf{x})$ as

$$\dot{\mathbf{x}} = F(\mathbf{x}) + \Gamma(t, \mathbf{x}) \ , \tag{1.8}$$

with which random forcing given by Gaussian white noise, brief pulses given by a δ-function, or a continuous periodic forcing is modeled. We use the phase $\theta(\mathbf{x})$ of the unperturbed system, that obeys condition (1.3), in order to obtain a phase description of the perturbed oscillator [Eq. (1.8)]. We get[8]

$$\dot{\theta} = \omega + \nabla\theta(\mathbf{x})\Gamma(t, \mathbf{x}) \ . \tag{1.9}$$

The equation is not closed because, generally, the perturbed state $\mathbf{x}$ is not on the limit-cycle. However, $\mathbf{x}$ belongs to a standard isophase that intersects the limit-cycle at $\mathbf{x}_0$ (cf. Fig. 1.3). Therefore, we can close Eq. (1.9) by replacing $\mathbf{x}$ with the corresponding state $\mathbf{x}_0$ on the cycle: Then, $\theta(\mathbf{x}_0)$ is a one-to-one mapping what closes the phase equation. This *standard* procedure of *phase reduction* is only good if the state is close to the limit-cycle.

Influence of Random Forcing. A random forcing of a limit-cycle oscillator is modeled by multiplicative Gaussian white noise interpreted in the Stratonovich sense [70]:

$$\Gamma(t, \mathbf{x}) = G(\mathbf{x})\xi(t) \ .$$

In this work, $\xi(t)$ always has the property: $\langle \xi(t)\xi(t') \rangle = 2\delta(t - t')$. Performing the phase reduction, one has to be careful with the projection of states on the limit-cycle because an additional term $Y(\theta)$ arrises from correlations of noise with the amplitudes $\mathbf{a}(\mathbf{x})$ (see Ref. [90]). One gets

$$\dot{\theta} = \omega + Y(\theta) + Z(\theta)\xi(t) \ , \tag{1.10}$$

with the phase sensitivity[8] $Z(\theta) = (\nabla\theta, \mathbf{G}(\mathbf{x}_0(\theta)))$, and the amplitude term[8] $Y(\theta) = (\nabla_{\mathbf{a}}(\nabla\theta, \mathbf{G}), (\nabla\mathbf{a})\mathbf{G})$. The approximation holds only if noise is weak compared to the stability of the deterministic limit-cycle. Eq. (1.10) is an example of a *stochastic phase oscillator* (see Sec. 2.1).

Pulse-like Interaction. If the perturbation is a series of short pulses applied at times t_j with strength and direction $\mathbf{k}(\mathbf{x})$, the interaction can be modeled by

$$\Gamma(t, \mathbf{x}) = \mathbf{k}(\mathbf{x}) \sum_j \delta(t - t_j) \ .$$

The resulting phase equation is given by

$$\dot{\theta} = \omega + Z(\theta) \sum_j \delta(t - t_j) \ , \tag{1.11}$$

with the phase sensitivity[8] $Z(\theta) = (\nabla\theta, \mathbf{k}(\mathbf{y}(\theta)))$. Eq. (1.11) is good under the assumption that the state $\mathbf{x}$ stays close to the limit-cycle. Even for strong pulses, a closed phase equation can be found if its state relaxes fast enough to the cycle.

The effect of a single kick $\Gamma(t, \mathbf{x}) = \mathbf{k}(\mathbf{x})\delta(t - t')$ that is applied at a phase $\theta(t') = \alpha$ is described by the *phase resetting curve* $\mathrm{PRC}(\alpha, \mathbf{k})$: It is the difference in phase of the unkicked [Eq. (1.1)] and kicked [Eq. (1.8)] oscillator[9] after its state relaxed back to the limit-cycle.

Continuous Interaction. A simple example of continuous interaction is given by a periodically forced oscillator with

$$\Gamma(t, \mathbf{x}) = \mathbf{G}(\psi(t), \ \mathbf{x}) \ .$$

Here, $\psi(t) = \Omega t$ is the (2π-periodic) external phase with frequency Ω. After the application of the phase reduction procedure we arrive at

$$\dot{\theta} = \omega + K(\psi(t), \theta) \tag{1.12}$$

with a coupling function[8] $K(\psi, \theta) = (\nabla\theta, \mathbf{G}(\psi, \theta))$. The approximation is only good for a weak interactions. If the difference in frequencies $\omega - \Omega$ is small, the transversal variable $\Delta = \theta - \psi$ is slow. Averaging out the fast variable we obtain the equation for Δ in the standard Adler form [63]

$$\begin{aligned} \dot{\Delta} &= \omega - \Omega + q(\Delta) \ , \\ q(\Delta) &= \frac{1}{2\pi} \int_0^{2\pi} Q(\psi, \Delta + \psi) d\psi \ . \end{aligned} \tag{1.13}$$

If the average coupling function $q(\Delta)$ is bigger than the difference in frequencies, Eq. (1.13) has a fixed point; the phenomenon of *synchronization* sets in

[8]The vector of derivatives with respect to $\mathbf{x}_j$ is ∇, and with respect to $\mathbf{a}_k$, it is ∇_a.
[9]They should start with the same initial condition on the limit-cycle.

where Δ considered as an unwound variable remains bounded [63].

Synchronization can also occur for a pulse-like interaction (cf. Eq. (1.11)). However, it can never be present if oscillations are additionally forced by unbounded noise: Even for weak noise, phase slips, where $\Delta(t)$ grows by 2π, can occur with small probability.

1.3 Stochastic Description of Irregular Oscillations

Some autonomous irregular oscillations cannot be treated as a deterministic limit-cycle oscillator in an approximate way. The reason can be that random perturbations are not weak, and thus, the standard phase reduction gives a bad approximation. There are also systems where the random forcing induces oscillations in an excitable system which would equilibrate otherwise. Then, the approach cannot be applied because without a limit-cycle the foliation of the state space by a set of standard isophases is not possible: Phase simply cannot be defined[10].

The simplest system that shows noise-induced oscillations is the well-known stochastic *Adler equation* [29]

$$\dot{\theta}(t) = a + \cos\theta + \sigma\xi(t) \ , \tag{1.14}$$

It is a stochastic phase oscillator whose state is defined by a 2π-periodic phase variable θ (same class as Eq. (1.10)). Naturally, an oscillation is characterized by the growth of θ by 2π. For $|a| \leq 1$ for which the deterministic dynamics has a fixed point, the oscillator shows noise-induced oscillations. For $|a| > 1$ oscillations are noise-perturbed and a limit-cycle exists. For these, phase resetting curves and average coupling functions [Eq. (1.13)] can be derived perturbatively starting from the noise-free dynamics at $\sigma = 0$. However, this is not possible for noise-induced oscillations.

Even the notion of oscillation can be unclear in higher-than-one dimensions. Let us explain the difficulty by the example of the *FitzHugh-Nagumo model* that is a paradigmatic two-dimensional model of neuronal oscillations [6, 30, 66]:

$$\begin{aligned} \varepsilon\frac{dx}{dt} &= x - \frac{x^3}{3} - y \ , \\ \frac{dy}{dt} &= x + a + \sigma\xi(t) \ . \end{aligned} \tag{1.15}$$

The small parameter ε separates the time scales of the two variables x and y, and a governs the excitability of the model: It shows noise-induced oscillations

[10] As we have seen in the examples (cf. Fig. 1.2), this seems to be only true from the point of view of a theoretician.

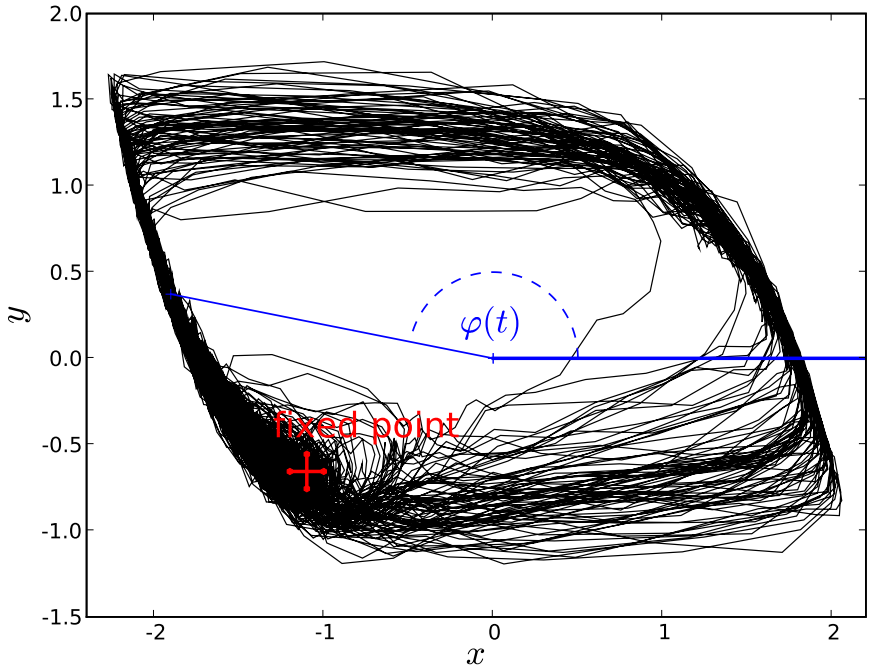

Figure 1.4: The noise-induced oscillations of the FitzHugh-Nagumo model [Eq. (1.15)] can fill the whole interior of the state space, here shown at parameters $a = 1.1$, $\sigma = 0.4$ and $\varepsilon = 0.1$. Therefore, it is not straightforward to distinguish between an oscillation and the dynamics in the vicinity of the fixed point (red cross). Possibly, one can define an arbitrary phase variable $\varphi(t) = \tan^{-1}(y/x)$. This is equivalent to a definition of oscillation.

for $a > 1$ and noise-perturbed ones for $a < 1$. For a small, but finite ε the system shows an imperfect canard [88]. Therefore, it can be unclear how to distinguish oscillations with small amplitude from the stochastic dynamics in the vicinity of the fixed point (cf. Fig. 1.4). One needs to find a – in this case – biophysical criterion: For a neuron embedded in a network of others, for example, an oscillation could be defined more clearly as the activity of the membrane potential that is strong enough to transmit information to another neuron. Let us, thus, assume that we have found a valid definition of oscillations. Then, a phase description still suffers from the problem of identifying the states of the same phase without any reference to a limit-cycle. If a stochastic phase variable could be defined by a phase reduction, the phase would still show noise-induced oscillations, such as oscillator (1.14) at $|a| \leq 1$, that do not allow for a perturbative characterization of interaction.

1.4 Description of Irregular Oscillations as Chaos

Autonomous irregular oscillations need not to be the result of random forcing. Under certain conditions, the state of a deterministic low-dimensional system,

such as a few global modes of a rotating fluid or the global modes of a laser, can show irregular oscillatory dynamics without randomness, where a state has a unique future. Such oscillations are modeled best with oscillators that show chaos [3, 16, 19, 25, 39, 53], of which some have been successfully characterized by a phase variable [7, 11, 57, 72].

The model with which we wish to describe such irregular oscillations shall obey a low-dimensional deterministic dynamics[11]

$$\dot{\mathbf{x}} = F(\mathbf{x}) \ . \tag{1.16}$$

The dynamics is said to be chaotic if two close typical states diverge exponentially on average (for a detailed introduction to continuous chaos, see Refs. [78, 19]). Because the states stay on the stable chaotic attractor – the invariant set of Eq. (1.16) – their distance must remain bounded. Therefore, the exponential divergence is only observable initially[12].

A well-known example of chaotic dynamics is the *Rössler oscillator* given by the equations [73]

$$\begin{aligned} \dot{x} &= -y - z \ ; \\ \dot{y} &= x + 0.15y \ ; \\ \dot{z} &= 0.2 + z(x - 10) \ . \end{aligned} \tag{1.17}$$

The oscillator was shown to model certain laser systems [19], but it was originally designed as a simplified model for the Lorenz system given by [49]

$$\begin{aligned} \dot{x} &= 10 \cdot (y - x) \ ; \\ \dot{y} &= 28 \cdot x - y - xz \ ; \\ \dot{z} &= -\frac{8}{3} \cdot z + xy \ . \end{aligned} \tag{1.18}$$

Both systems show a chaotic dynamics that allows for a definition of oscillation: The Rössler attractor[13] [of Eq. (1.17)] shows a ring-like structure that makes a definition of oscillation obvious. For example, the cylindrical coordinates

$$\varphi = \tan^{-1} \frac{y}{x} \ ; \quad \mathbf{a} = \left(\sqrt{x^2 + y^2}, z \right) \tag{1.19}$$

define an arbitrary phase variable $\varphi(t)$ that grows monotonically by 2π each time the trajectory cycles around the ring (cf. left plot of Fig. 1.5). As opposed to the Rössler attractor, the Lorenz attractor shows two centers of rotation (cf. right plot of Fig. 1.5). Therefore, an oscillation of the state seems to be ambivalent, similar to the case of stochastic oscillations (cf. Fig. 1.4). However, for many chaotic oscillators it may be uniquely characterized by means of their unstable periodic orbits.

[11] For spatially extended systems, the differential equation could describe only the few active modes. If many modes are active, a stochastic description can be more useful [31, 75].

[12] Each point on the invariant set contains an unstable direction in tangent space.

[13] The attractor of a dynamical system is the set of states that is invariant under the dynamics, and that attracts almost all trajectories in its vicinity.

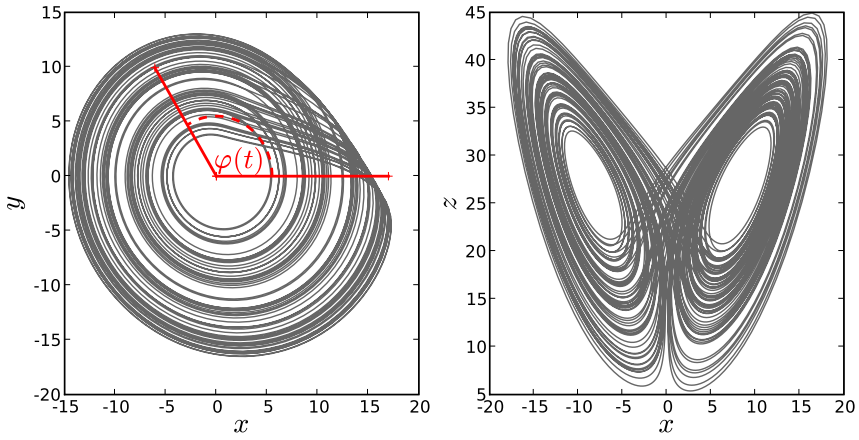

Figure 1.5: The Rössler attractor [Eq. (1.17)] shows a ring-like structure that allows for a natural definition of oscillation by an arbitrary phase variable $\varphi(t)$ [Eq. (1.19)] (left plot). The Lorenz attractor [Eq. (1.18)] on the other hand, shows two centers of rotation (right plot). Therefore, a definition of oscillation is not obvious for the Lorenz attractor.

Embedded in the chaotic attractor are an infinite number of *unstable periodic orbits* **(UPOs)** $\mathbf{x}_0(t+\tau) = \mathbf{x}_0(t)$, each one having a different period τ [44, 76]. The set of all UPOs can characterize many properties of chaos [4, 5], and here we use them to characterize chaotic oscillations. Each orbit has a certain *lap number* p of intersections with a Poincaré section of constant arbitrary phase φ. Considering the unwound[14] phase variable, it is given by

$$p = \frac{\varphi(\mathbf{x}_0(\tau)) - \varphi(\mathbf{x}_0(0))}{2\pi} \ . \tag{1.20}$$

With the lap number and the period we define the *oscillation period*

$$S = \frac{2\pi}{\nu} = \frac{\tau}{p} \ , \tag{1.21}$$

which will be comparable to the mean period of chaotic oscillations. Now, cylindrical coordinates $(\varphi, \mathbf{a})$ that characterize oscillations well should fulfill the conditions: The arbitrary phase variable $\varphi(t)$ has positive growth rate, and the lap number of each UPO is minimal. The Poincaré sections of constant arbitrary phase φ, called arbitrary Poincaré sections $I_0(\varphi)$, are parameterized by the amplitudes $\mathbf{a}$. We hope that such a characterization leads to a unique definition of chaotic oscillation. Arbitrary Poincaré sections of the Lorenz attractor that obey the conditions are illustrated in Fig. 1.6 (see Appendix C).

With the definition of oscillation by means of an arbitrary phase variable $\varphi(t)$ at hand, the mean frequency of chaotic oscillations can be computed from a typical chaotic trajectory ($\varphi(t)$ is unwound):

$$\omega = \lim_{t\to\infty} \frac{\langle \varphi(t) \rangle}{t} \ . \tag{1.22}$$

[14] "Unwound" means that φ is not taken modulo 2π, but it is extended to the real line.

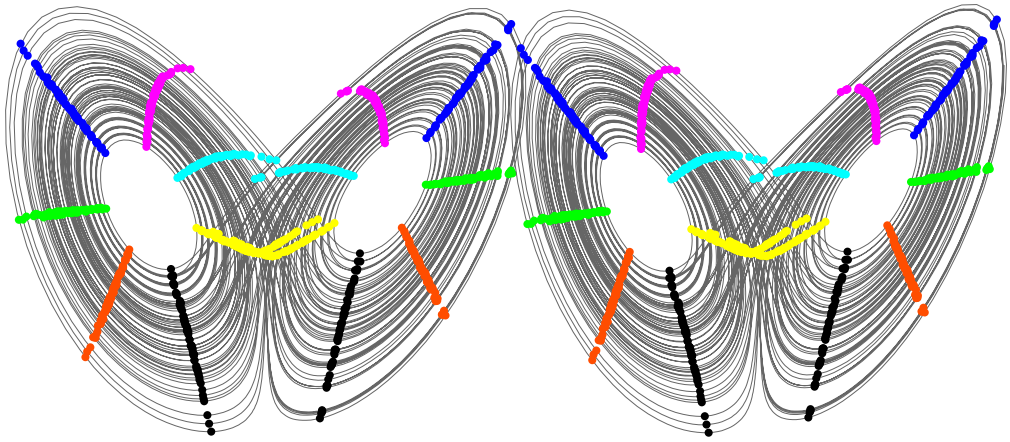

Figure 1.6: The stereogram of the Lorenz attractor [Eq. (1.18)] (gray line) illustrates that arbitrary Poincaré sections (color coded), marked by passages of the trajectory, are two-fold on the "wings" of the attractor (see instructions for use in Appendix C.1).

Because of the limit, the mean frequency is independent of the choice of the arbitrary phase.

The oscillation period of unstable periodic orbits [Eq. (1.21)] of chaotic oscillators usually does not coincide with the mean period of chaotic oscillations $T = 2\pi/\omega$. Yet, the trajectory comes infinitely close to each of the orbits in a quasi-random manner. The implications are that one observes a characteristic amount of phase diffusion of the phase $\varphi(t)$ for large times. It can be characterized by the phase diffusion coefficient

$$D = \lim_{t\to\infty} \frac{\langle [\varphi(t) - \omega t]^2 \rangle}{2t} \ . \tag{1.23}$$

Because of the large time limit the phase diffusion is independent of a particular choice of arbitrary phase as well.

For the Rössler oscillator [Eq. (1.17)], we located 80 p-orbits with $p \leq 10$ that have a finite, but narrow distribution of oscillation periods. Therefore, the oscillator has a non-vanishing phase diffusion coefficient [Eq. (1.23)]. However, it is very small. Because the exact frequency of the oscillator is not known, the diffusion must be computed by the Brownian bridge method described in Appendix B. From 50 independent trials, we obtained an estimation

$$\hat{D} = 8.8 \cdot 10^{-5} \pm \frac{3.95 \cdot 10^{-6}}{\sqrt{50}} \text{ rad s}^{-1} \ . \tag{1.24}$$

Because the diffusion is small compared to the mean frequency $\omega \approx 1.03$, the phase properties of the Rössler oscillator is well-represented by a deterministic phase equation as noted in Ref. [33]. This is not true for the Lorenz system that shows a considerably larger chaotic phase diffusion.

Chapter 2

Effective Description of Stochastic Oscillations

The difference in phase of two states of a deterministic phase oscillator[1] can depend on time. In a region of state space where the phase grows fast, the difference increases, while the states appear closer together in regions where the phase grows slowly. For deterministic phase oscillators, we know that phase differences depending on time are unphysical artifacts of the specific parameterization of oscillations [41]: The phase variable can always be re-parameterized by the transformation (1.2) based on the phase velocity. Because the transformed phase variable grows with constant phase velocity, phase differences are now constant. The transformation makes the arbitrarily parameterized phase variable invariant under both, time and initial parameterization. In this way, interaction functions can be also cast into an invariant form [40, 41]. A stochastic phase variable, on the other hand, cannot show a constant growth rate because of the random fluctuations. Still, a parameterization-independent representation, which we present in this chapter, would allow for an invariant characterization of interactions, as for the deterministic case. However, the matter is complicated by the fact that multiple definitions of average phase velocity are possible.

We address the problem by constructing two deterministic effective phase models that are based upon different definitions of average phase velocity of stochastic oscillations. The current model, which is based on the average time spent in an interval, is shown to exhibit the same mean frequency and invariant distribution density as the stochastic oscillations. The first passage model, which is based on an average velocity defined by mean first passage times, is shown to exhibit an invariant distribution density which instead corresponds to the, so called, mean first passage density of the oscillations. Based upon each of the models, the arbitrarily parameterized stochastic phase variable can be transformed to an invariant form. Dependent on the application, a specific effective phase model is suitable for an invariant phase description of interactions. The current model is easily extended for a characterization of continuous interactions as exemplified by periodically forced stochastic oscillations.

[1] A deterministic phase oscillator is governed by dynamics on the circle.

A pulse-like interaction on the other hand is described by the stochastic phase resetting curve that is correctly represented by the corresponding kicked first passage model. In this way, a theoretical description of interacting stochastic oscillations is obtained, which is shown to have far reaching implications for bivariate methods of data processing. In most examples of this chapter, an emphasis is made on noise-induced oscillations for which a perturbative approach is not applicable.

In this chapter, we use stochastic dynamics on a circle as our basic model of stochastic oscillations. They allow for a clear presentation of the theoretical framework because these, so called, stochastic phase oscillators are treatable analytically to a great extent. Furthermore, the term "protophase" is used in the rest of this chapter in order to differentiate between parameterization-dependent *protophases* and parameterization-independent (invariant) *phases*.

In the first section of this chapter, characteristic properties of stochastic phase oscillators are reviewed. In Sec. 2.2 and 2.3, we present the two models of effective phase dynamics – the *current model* and the *first passage model*. Their effective velocities are analysed in detail for certain asymptotic cases (Sec. 2.4). Thereafter, the theory is extended for a description of interactions of stochastic oscillations, where for simplicity, the discussion is confined to unidirectional interactions[2]. The current model is easily extended to describe the periodically forced stochastic phase oscillator, effectively (Sec. 2.5). The stochastic phase oscillator subject to a brief pulse is treatable within the framework of stochastic phase resetting that is presented in Sec. 2.6. Here, the first passage model applies.

2.1 Stochastic Phase Oscillators and their Effective Description

In this section, we present some well-known characteristic properties of stochastic phase oscillators in the context of noise-induced and noise-perturbed oscillations. The properties allow for a broad classification of the oscillator's dynamics. They will serve as a benchmark for the effective models. The section is concluded with a discussion on the notion of speed introducing the conceptual framework of this chapter.

Our basic model of stochastic oscillations is a stochastic phase oscillator that, for example, may have been obtained by the phase reduction method applied to noise-perturbed oscillations (cf. Sec. 1.2). The model attains states on the circle parameterized by a 2π-periodic random variable $\theta(t)$, called stochastic *protophase*. Let us consider the *unwound* protophase that is not taken modulo 2π: An *oscillation* is defined as the growth[3] of $\theta(t)$ by 2π.

[2]The surrounding exerts a continuous or pulse-like force on the oscillator.
[3]The protophase is always defined such that it grows with positive mean frequency

The protophase obeys the Langevin dynamics (in the Stratonovich interpretation [70])

$$\dot{\theta} = h(\theta) + g(\theta)\xi(t) \ , \tag{2.1}$$

where, in this work, $\xi(t)$ denotes δ-correlated Gaussian white noise: $\langle \xi(t)\xi(t')\rangle = 2\delta(t-t')$. If Eq. (2.1) is obtained by phase reduction, the *deterministic part* $h(\theta)$ and the *noise amplitude* $g(\theta)$ reflect to a certain degree a specific choice of parameterization of oscillations and are, thus, not *invariant*. If the deterministic part $h(\theta)$ is strictly positive, oscillator (2.1) can show *noise-perturbed* oscillations that persist with finite frequency if the noise amplitude goes to zero. However, if $h(\theta)$ has at least two zero crossings, oscillations cease as the noise amplitude vanishes: They are *noise-induced* [46].

A well-known example showing the most prominent features of stochastic oscillations is the stochastic *Adler equation* [29] (generalized theta model [15])

$$\dot{\theta}(t) = a + \cos\theta + \sigma\xi(t) \ . \tag{2.2}$$

For $|a| \leq 1$ it shows noise-induced oscillations, whereas for $|a| > 1$ oscillations are noise-perturbed. Furthermore, the Adler equation belongs to the subclass of stochastic phase models with *additive* noise, for which the noise amplitude $g(\theta)$ is a constant σ.

The most relevant quantities of oscillator (2.1) are accessible analytically. Its probability density $P(\theta,t)$ is governed by the Fokker-Planck equation associated to Eq. (2.1), which is given by [70]

$$\partial_t P = -\partial_\theta\left[hP\right] + \partial_\theta\left[g\partial_\theta\left[gP\right]\right] = -\partial_\theta J \ . \tag{2.3}$$

For the stationary probability density $P(\theta)$, the *probability flux* J is constant and we obtain the simpler equation

$$J = hP - g\partial_\theta\left[gP\right] \ . \tag{2.4}$$

It has the well-known solution [70]

$$P(\theta) = C\int_\theta^{2\pi+\theta} \frac{d\psi}{g(\theta)g(\psi)}\ \mathrm{e}^{-\int_\theta^\psi \frac{h(\varphi)}{g^2(\varphi)}\ d\varphi} \ , \tag{2.5}$$

where C is a *normalization constant* ensuring $\int_0^{2\pi} P(\theta)\ d\theta = 1$. If oscillations are noise-induced, the probability density becomes singular as the noise amplitude vanishes (left plot of Fig. 2.1).

Among the traditional quantities of stochastic phase oscillators are the mean frequency and the phase diffusion coefficient

$$\omega = \lim_{t\to\infty}\frac{\langle\theta(t)\rangle}{t} \ , \text{ and } \ D = \lim_{t\to\infty}\frac{\langle[\theta(t)-\omega t]^2\rangle}{2t} \ , \tag{2.6}$$

which are defined for the unwound protophase. They are expressed in terms of $h(\theta)$ and $g(\theta)$ through the well-known formulas [70, 47, 68, 48]

$$\omega = 2\pi J = 2\pi C\left[1 - \mathrm{e}^{-\int_0^{2\pi}\frac{h(\varphi)}{g^2(\varphi)}\ d\varphi}\right] \ , \text{ and} \tag{2.7}$$

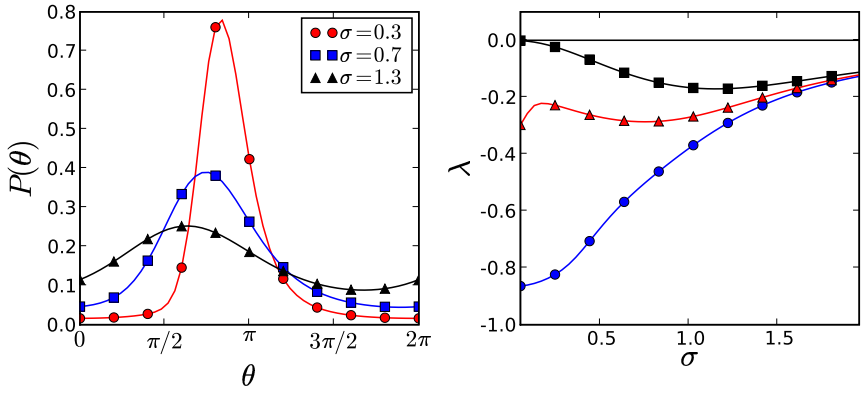

Figure 2.1: **Left plot**: The density $P(\theta)$ [Eq. (2.5)] of the Adler equation [Eq. (2.2)] becomes singular as the noise amplitude vanishes, if the oscillations are noise-induced (here shown for $a = 0.9$ and σ as indicated). **Right plot**: Dependent on a, the Lyapunov exponent λ [Eq. (2.9)] of the Adler equation as a function of the noise amplitude σ shows three characteristic dependencies, here shown for noise-induced oscillations at $a = 0.5$ (blue circles), and $a = 0.95$ (red triangles), and for noise-perturbed oscillations at $a = 1.5$ (black squares).

$$D = \frac{\frac{1}{2\pi}\int_0^{2\pi}\frac{d\psi}{g(\psi)}\left[\int_{\psi-2\pi}^{\psi}\frac{d\varphi}{g(\varphi)}\rho(\varphi,\psi)\right]^2\int_{\psi}^{\psi+2\pi}\frac{d\varphi}{g(\varphi)}\rho(\psi,\varphi)}{\left[\frac{1}{2\pi}\int_0^{2\pi}\frac{d\psi}{g(\psi)}\int_{\psi-2\pi}^{\psi}\frac{2d\varphi}{g(\varphi)}\rho(\varphi,\psi)\right]^3}\ , \tag{2.8}$$

where $\rho(\theta,\varphi) = \exp\left[-\int_\theta^\varphi \frac{h(\eta)}{g^2(\eta)}\,d\eta\right]$. For noise-induced oscillations the mean frequency converges to zero in the limit of vanishing noise amplitude (left plot of Fig. 2.2). If noise is additive, the mean frequency converges to a finite value in the limit $\sigma \to \infty$ (cf. Sec. 2.4). The quotient $\sqrt{D}/\omega$ is a measure for decoherence of oscillations and similar to the inverse of the Péclet number [47, 48]. For noise-induced oscillations, the well-known effect of coherence resonance is observable, where decoherence decreases for increasing noise amplitude [64] (right plot of Fig. 2.2). The effect is not observable for noise-perturbed oscillations. For a detailed discussion of coherence resonance the reader is referred to Ref. [46]. Unlike the Péclet number, the quotient diverges in the limit of weak noise.

Another interesting quantity that characterizes stochastic oscillations is the Lyapunov exponent λ associated to noise [24, 62, 71, 83]. It quantifies whether two copies of oscillator (2.1) under the influence of the same noise representation $\xi(t)$ will synchronize by stochasticity. For oscillator (2.1), λ is computed by [22, 71]

$$\lambda = \langle h'(\theta) + g''(\theta)g(\theta)\rangle\ . \tag{2.9}$$

If noise is additive, λ vanishes in the limit of large noise amplitude σ. In the limit $\sigma \to 0$, there are three cases (right plot of Fig. 2.1): For noise-perturbed oscillations, the Lyapunov exponent goes to zero as $\lambda \propto -\sigma^2$ [23]. For noise-induced oscillations, it converges to a finite negative value dependent on the

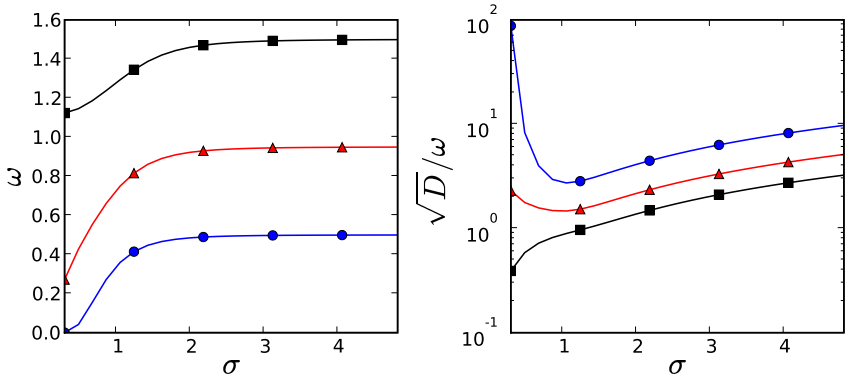

Figure 2.2: For noise-induced oscillations in the Adler equation [Eq. (2.2)] (red triangles: $a = 0.95$, and blue circles: $a = 0.5$), the mean frequency ω [Eq. (2.6)] goes to zero in the limit of small noise amplitude σ (left plot). The quotient $\sqrt{D}/\omega$ [Eq. (2.6)] as a function of σ (right plot) is a measure of decoherence, which has negative slope for noise-induced oscillations but not for noise-perturbed ones (black squares: $a = 1.5$).

quantitative stability of the oscillator's fixed point at $\sigma = 0$. Here, λ may as well show a local minimum as a function of σ (red triangles). It should be noted that the Lyapunov exponent of a stochastic phase oscillator is always negative whereas general stochastic oscillations may have a positive λ [22, 45]. Therefore, a phase reduction of such stochastic oscillations is not well-understood and it must be treated with care.

The dynamics of noise-induced oscillations can be quite close to that of noise-perturbed ones (cf. Ref. [64]) what suggests a unified theoretical description by a purely deterministic phase equation

$$\dot{\theta} = H(\theta) \tag{2.10}$$

to be possible. Generally, one cannot use the approximation $F(\theta) = h(\theta)$ by considering only the deterministic part $h(\theta)$ of oscillator (2.1) showing noise-induced oscillations because $h(\theta)$ has zero-crossings – Eq. (2.10) has stable fixed points and does not show oscillations. Instead, we have to construct an *effective phase model* using some criteria to determine $F(\theta)$. Generally, we demand that the effective phase model represents as many characteristic properties of stochastic oscillations as possible. Within this framework, one approach is presented based on the probability current. It allows for a construction of an effective phase model with the same mean frequency[4] (condition (i)) and the same invariant distribution density (condition (ii)) as the stochastic phase oscillator. Without violating these conditions, the phase diffusion coefficient (condition (iii)) can be modeled, too, by adding noise to Eq. (2.10) in a certain way. Another approach of effective modeling is based on first passage times.

[4]Then, it also shows the same mean period.

Roughly, the difference of these models lies in the definition of the local average speed (frequency) of stochastic oscillations: Given an interval of length $\Delta\theta$, the speed can be measured as the quotient of $\Delta\theta$ and the mean time Δt that oscillator (2.1) spends in this interval. This leads to the *current velocity* based on the probability current. Alternatively, the speed can be measured as the quotient of $\Delta\theta$ and the mean time required to reach the opposite boundary of the interval, which leads to the *first passage velocity*. For deterministic phase oscillators the two definitions of speed coincide, whereas for oscillations showing irregular features, there is a difference which is especially pronounced for noise-induced ones.

2.2 Current Model of Effective Phase Dynamics

In this section, an effective phase model of oscillator (2.1) based on the probability current is presented. It shows the same mean frequency and invariant distribution density as the oscillator. The current model finds its main application in Sec. 2.5, where an effective coupling function is constructed.

We construct the *current model* of oscillator (2.1) that obeys the deterministic phase equation

$$\dot{\theta} = H(\theta) \ . \tag{2.11}$$

Here, the mean time that oscillator (2.1) spends in an interval $[\theta, \theta + d\theta]$ leads us to a notion of speed. According to the invariant probability density, the mean time is defined as $dt = Pd\theta/J$. It follows, that the *current velocity* $H(\theta)$ is given by

$$H(\theta) = \frac{Jd\theta}{P(\theta)d\theta} = \frac{\omega}{2\pi P(\theta)} \ . \tag{2.12}$$

The same effective velocity is obtained by drawing a correspondence between the stationary Fokker-Planck equation (2.4) of oscillator (2.1) and the stationary Liouville equation $J = H(\theta)P(\theta)$ of the effective model [Eq. (2.11)][5].

Model (2.11) obeys conditions (i)[6] and (ii)[7] because it fulfills the stationary Liouville equation for $P(\theta)$ and it shows the correct period T:

$$-\partial_\theta \left[H(\theta)P(\theta)\right] = 0 \ ; \quad \int_0^{2\pi} \frac{d\theta}{H(\theta)} = T \ .$$

Using Eqns. (2.5) and (2.7), the current model of the Adler equation may be constructed and integrated numerically. A comparison of respective realizations $\theta(t)$ of Eqns. (2.11) and (2.2) shows that their observed dynamics is comparable even though the stochastic components are missing in the current model (top plot of Fig. 2.3).

[5]This is why we call it (probability) current velocity
[6]The frequency of the model is equal to the mean frequency of oscillations.
[7]The invariant distribution of the model is equal to the probability density of oscillations.

The current velocity $H(\theta)$ can be expressed in terms of $h(\theta)$ and $g(\theta)$. For this, Eq. (2.4) is divided by $P(\theta)$, and the result is compared to Eq. (2.12) yielding

$$H(\theta) = h(\theta) - \frac{1}{2}\partial_\theta \left[g^2(\theta)\right] - g^2(\theta)\partial_\theta \left[\ln P(\theta)\right] = h(\theta) - u(\theta) \ . \tag{2.13}$$

It consists of the deterministic contribution $h(\theta)$ and an osmotic contribution $u(\theta)$ that is especially pronounced for noise-induced oscillations (cf. bottom plot of Fig. 2.3). The current velocity corresponds to the point-wise average of central differences [34]. Therefore, it may be constructed from an observed (e.g., experimentally) time series $\theta_n = \theta(n\Delta t)$ by the simple averaging procedure

$$H(\theta) \approx \left.\frac{\langle \theta_{n+1} - \theta_{n-1} \rangle}{2\Delta t}\right|_{\theta_n = \theta} \ . \tag{2.14}$$

Meanwhile, forward differences $\theta_{n+1} - \theta_n$ provide the deterministic part $h(\theta)$ only: The reader is referred to Refs. [56, 65, 17, 34, 2] for details.

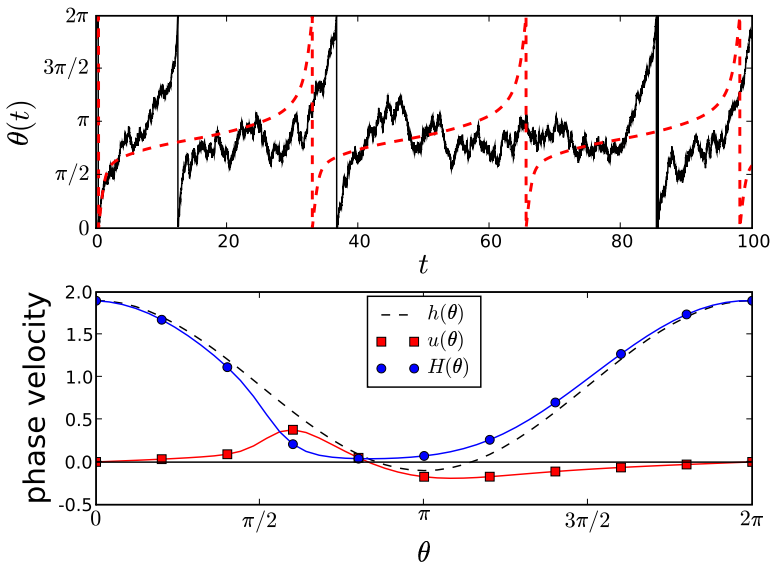

Figure 2.3: (top plot) The Adler equation [Eq. (2.2)] shows a realization (solid line) that is, even in the noise-induced case, strongly resembled by that of its current model [Eq. (2.11)] (red dashed line), here shown for $a = 0.9$ and $\sigma = 0.3$. For this, the osmotic contribution $u(\theta)$ to the current velocity is non-negligible as it accounts for the strict positivity of $H(\theta)$ (bottom plot, cf. Eq. (2.13)).

Having constructed the current model, we can transform its protophase θ to a uniformly rotating *phase* φ which has simple properties:

$$\dot{\varphi} = \omega \ ; \quad P(\varphi) = \frac{1}{2\pi} \ . \tag{2.15}$$

As it can be easily checked, the nonlinear transformation $\theta \to \varphi$ is given by

$$\varphi = S(\theta) = 2\pi \int_0^\theta P(\theta')\ d\theta' \ . \tag{2.16}$$

Herewith the parameterization-dependent differences in the protophase $\Delta\theta = \theta_2 - \theta_1$ can be transformed to the invariant differences in the phase (cf. Eq. (2.16))

$$\Delta\varphi = S(\theta_2) - S(\theta_1) = 2\pi \int_{\theta_1}^{\theta_2} P(\theta)\ d\theta \ . \tag{2.17}$$

Given a time series $\theta_n = \theta(n\Delta t)$ containing N data points, the transformation can be obtained numerically [41]. If one is not interested in the transformation $S(\theta)$ but in the transformed data $\varphi_n = S(\theta_n)$ only, one may alternatively evaluate

$$\varphi_n = \frac{2\pi}{N} \sum_{l=0}^{N-1} \Theta(\theta_n - \theta_l) \tag{2.18}$$

which is implemented quickly by sorting. ($\Theta(x)$ is the Heaviside function.)

Phase diffusion, mean frequency and probability density may be modeled simultaneously by the addition of δ-correlated ($\langle \eta(t)\eta(t') \rangle = 2\delta(t-t')$) additive noise $\sqrt{D}\eta(t)$ to the invariant phase dynamics (2.15):

$$\dot{\varphi} = \omega + \sqrt{D}\eta(t) \ . \tag{2.19}$$

Now, $\varphi(t)$ shows a phase diffusion constant D while preserving uniform density and mean frequency. Therefore, application of the inverse transformation $\theta = S^{-1}(\varphi)$ gives us the *stochastic current model*

$$\dot{\theta} = H(\theta) + \frac{\sqrt{D}}{\omega} H(\theta)\eta(t) \tag{2.20}$$

that fulfills conditions (i) and (ii) for any value of D. It may be chosen freely, and we chose it uniquely from condition (iii): The phase diffusion coefficients of the stochastic current model [Eq. (2.20)] and the stochastic phase oscillator [Eq. (2.1)] should be equal. This condition is fulfilled if coefficient (2.8) is used for D. The quotient $\sqrt{D}/\omega$ in front of the multiplicative noise, is exactly the quantity illustrated in the right plot of Fig. 2.2. In the limit of weak noise, the quotient diverges for noise-induced oscillations yielding an invalid model (cf. Eq. (2.40)), whereas for noise-perturbed oscillations $\sqrt{D}/\omega$ vanishes.

2.3 First Passage Model of Effective Phase Dynamics

In this section, an alternative effective phase model of stochastic oscillations is presented, which is based on first passage time statistics. The first passage

model predicts the correct stochastic phase resetting curve of stochastic oscillations as shown in Sec. 2.6.

As an alternative to the current model outlined in the last section, a velocity based on first passage time statistics of oscillator (2.1) shall lead us to the *first passage model*

$$\dot{\theta} = N(\theta) \ . \tag{2.21}$$

To determine $\dot{\theta} \approx \frac{\Delta\theta}{\Delta t}$ we interpret Δt as the average time which it takes to pass an interval of length $\Delta\theta$. More precisely, the *first passage velocity* is constructed using the mean first passage time $T(\alpha, \beta)$ which it takes for the stochastic phase of oscillator (2.1) to reach a boundary $\beta > \alpha$ starting at α. Its inverse is given by [36]

$$\frac{1}{N(\theta)} = \frac{dt}{d\theta} = \lim_{\varepsilon \to 0} \frac{T(\theta, \theta+\varepsilon) - T(\theta,\theta)}{\varepsilon} = \partial_\beta T|_{\alpha=\beta=\theta} \ . \tag{2.22}$$

Condition (i) is fulfilled by the first passage model[8]. However, condition (ii)[9] is generally not fulfilled as will be shown next.

The invariant distribution density of model (2.21), which we call *mean first passage density*, is given by

$$R(\theta) = \frac{\omega}{2\pi N(\theta)} \ . \tag{2.23}$$

It is also known as the *speed density* [36]. In order to obtain an equation for $R(\theta)$, the well-known equation for the mean first passage time of oscillator (2.1) has to be derived which we repeat following Ref. [18]. For an easier description of boundaries, the unwound stochastic protophase $\theta(t)$ is considered in the following. Consider the Fokker-Planck equation (2.3) with the sharp initial condition $P(\theta, 0) = \delta(\theta - \alpha)$. In this case Eq. (2.3) describes the conditional probability density $P(\theta, t|\alpha, 0)$. The boundary conditions

$$P(-\infty, t|\alpha, 0) = P(\beta, t|\alpha, 0) = 0 \tag{2.24}$$

are introduced[10], which correspond to the fact that states starting at α should only be considered as long as they do not reach the boundary β. Now, P has to be reinterpreted since the normalization condition does not hold anymore. The *no-passage probability* $G(\alpha, t)$ is defined as the probability that at time t boundary β is not reached when starting at α. It is given by

$$G(\alpha, t) = \int_{-\infty}^{\beta} P(\theta', t|\alpha, 0) d\theta' \ . \tag{2.25}$$

[8]The mean period of oscillator (2.1) is $T(\theta, 2\pi + \theta)$. Therefore, $\int_0^{2\pi} \frac{d\theta}{N(\theta)} = T$.

[9]The invariant distribution of the model is equal to the probability density of oscillations.

[10]We always assume that the oscillator shows a positive mean frequency. Therefore, we set the lower boundary to $-\infty$, and thus consider only passages of the boundary β. If the mean frequency is zero, the mean first passage time will diverge.

By a Kolmogorov backward expansion of $P(\theta', t|\alpha, 0)$, one finds that G obeys

$$\partial_t G = h(\alpha)\partial_\alpha G + g(\alpha)\partial_\alpha \left[g(\alpha)\partial_\alpha G\right] \ . \tag{2.26}$$

For $t \in [0, \infty)$ and $\alpha < \beta$, the probability density of first passage times is given by $g(\alpha, t) = -\partial_t G$. With respect to it, the mean first passage time is given by

$$T(\alpha, \beta) = \langle t \rangle = \int_0^\infty G(\alpha, t') \ dt' \ . \tag{2.27}$$

Integrating Eq. (2.26) over positive times, one obtains an equation for the mean first passage time

$$-1 = h\partial_\alpha T + g\partial_\alpha \left[g\partial_\alpha T\right] \ . \tag{2.28}$$

Because $\partial_\beta T|_{\alpha=\beta=\theta} = -\partial_\alpha T|_{\alpha=\beta=\theta} = 1/N(\theta)$, Eq. (2.28) may be rewritten for the mean first passage density $R(\theta)$ as

$$J = hR + g\partial_\theta \left[gR\right] \ . \tag{2.29}$$

This equation has the well-known solution

$$R(\theta) = C \int_{\theta-2\pi}^{\theta} \frac{d\psi}{g(\theta)g(\psi)} \mathrm{e}^{-\int_\psi^\theta \frac{h(\varphi)}{g^2(\varphi)} d\varphi} \tag{2.30}$$

with the same normalization constant C as in Eq. (2.5), and $J = \omega/2\pi$. Remarkably, Eq. (2.29) is similar to Eq. (2.4) except for a factor minus one. The equation provides an easily manageable analytic formula for the first passage velocity $N(\theta)$. Furthermore, it is seen that indeed condition (ii) is not fulfilled.

The mean first passage density has a direct meaning for a realization $\theta(t)$ of the stochastic protophase: Let t_n be the times of first passage, for which $\theta(t < t_n) < \theta(t_n)$ holds, where $\theta(t)$ is unwound. Connecting adjacent values of the point process $\theta_n = \theta(t_n)$ gives the smallest monotonous *envelope* $[\max_{t'<t} \theta(t')] \bmod 2\pi$ (left plot of Fig. 2.4). Each θ_n gives a starting point for a measurement of the passage time ending when $\theta(t)$ reaches $\theta_{n+1} = \theta_n + d\theta$. Although the trajectory of the corresponding time segment $\theta(t_n < t < t_{n+1})$ lies in an arbitrary region below θ_n, it is attributed to the interval $\theta_n < \theta < \theta_{n+1}$ for the mean first passage density $R(\theta)$. In fact, $R(\theta)$ is the probability density of the envelope. The probability density $P(\theta)$ and the mean first passage density $R(\theta)$ can be quite different (right plot of Fig. 2.4). Therefore, the current model and the first passage model are distinctly different from each other for general stochastic oscillations. The fact that $R(\theta)$ is the probability density of the envelope of $\theta(t)$ can be used for its numerical construction from data which is shown at the end of this section.

We would like to mention that going from the stochastic protophase $\theta(t)$ to its envelope, we achieve a monotonically growing protophase. Indeed, phase is often understood as a strictly monotonic variable, in some sense a "replacement" for a time variable. But for a stochastic oscillator one often observes

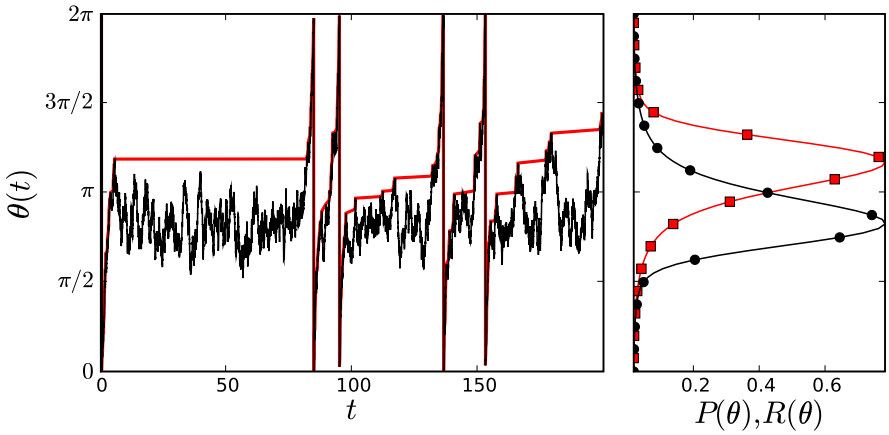

Figure 2.4: The protophase $\theta(t)$ (black solid line) of the Adler equation [Eq. (2.2)] and its *envelope* (red thick line) have similar long term dynamics (left plot). However, the invariant probability density $P(\theta)$ [Eq. (2.5)] (black circles) and the mean first passage density $R(\theta)$ [Eq. (2.30)] (red squares) are different (right plot), especially for noise-induced oscillations, here shown for $a = 0.9$ and $\sigma = 0.3$.

"reverse" variations. Thus, taking the envelope is a natural way to restore a monotonic function of time.

The first passage model [Eq. (2.21)] provides an effective phase dynamics of stochastic oscillations, which is alternative to the current model. It fulfills condition (i) in that it shows the same mean frequency as oscillator (2.1), but instead of modeling its probability density (condition (ii)), it preserves its mean first passage density (condition (iib)) which for deterministic oscillators, is equal to the invariant distribution density. Even for small noise amplitudes, the current model and the first passage model can be quite different if they describe noise-induced oscillations (cf. top plot of Fig. 2.5). For noise-perturbed oscillations the two velocities $H(\theta)$ and $N(\theta)$ converge to the deterministic part $h(\theta)$ as the noise amplitude vanishes (bottom plot of Fig. 2.5).

In the numerical example presented in Fig. 2.5, the current and the first passage velocities are mapped to each other by mirror symmetry. This is due to the fact that both $h(\theta)$ and $g(\theta)$ are symmetric in the Adler equation: If a stochastic phase oscillator has symmetric functions $h(\theta)$ and $g(\theta)$, the transformation $\theta \to -\theta$ maps Eq. (2.29) to Eq. (2.4). Their solutions are mapped to each other, too. Therefore, symmetry of h and g implies $N(\theta) = H(-\theta)$ as it is observed in Fig. 2.5.

As for the current model, a uniformly rotating invariant phase is constructed by the transformation (cf. Eq. (2.16))

$$\psi = Z(\theta) = 2\pi \int_0^\theta R(\theta')\, d\theta' \ . \tag{2.31}$$

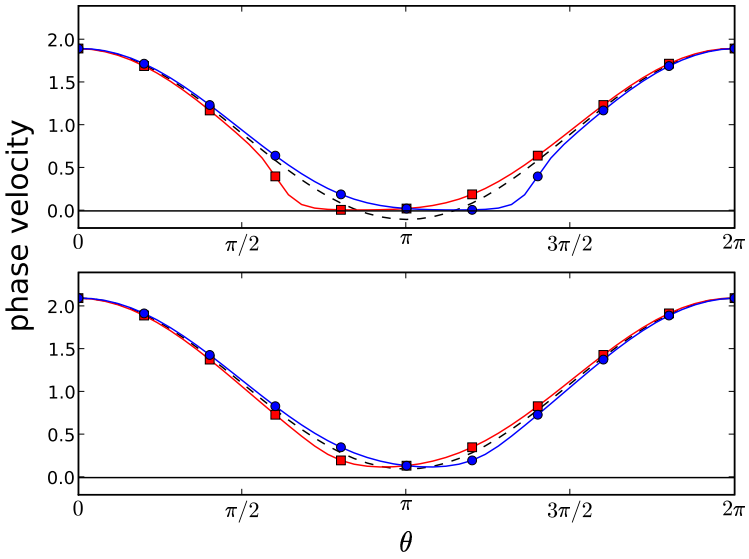

Figure 2.5: The current velocity [Eq. (2.12)] (red squares) and the first passage velocity [Eq. (2.22)] (blue circles) of the Adler equation [Eq. (2.2)] differ essentially for both, noise-induced (at $a = 0.9$, top plot) and noise-perturbed (at $a = 1.1$, bottom plot) oscillations, here shown for $\sigma = 0.2$. The difference in effective velocities is especially pronounced for noise-induced oscillations and does not disappear in the limit of vanishing noise, while both effective velocities converge to $h(\theta)$ (dashed line) if oscillations are noise-perturbed.

With $Z(\theta)$, differences in the protophase $\theta_2 - \theta_1$ are transformed to differences in the phase

$$\Delta\psi = Z(\theta_2) - Z(\theta_1) = 2\pi \int_{\theta_1}^{\theta_2} R(\theta)\, d\theta \ . \tag{2.32}$$

By adding effective noise to the dynamics of ψ, phase diffusion can be taken into account leading to (cf. Eqns. (2.19) and (2.20))

$$\dot{\theta} = N(\theta) + \frac{\sqrt{D}}{\omega} N(\theta)\eta(t) \ . \tag{2.33}$$

This stochastic first passage model fulfills conditions (i), (iib) and (iii).

Because the first passage model does not fulfill condition (ii)[11], an application of transformation (2.31) to the stochastic protophase $\theta(t)$ of oscillator (2.1) does not lead to a stochastic phase $\psi(t)$ that is uniformly distributed as it does for transformation (2.16). However, using Eq. (2.29), it is derived that the stochastic phase $\psi(t) = Z(\theta(t))$ shows a uniform ensemble velocity. To see this, let us consider any initial probability distribution $P(\theta, t)$. The

[11] Its probability density is $R(\theta) \neq P(\theta)$.

ensemble velocity is given by

$$\begin{aligned}\partial_t\langle\psi\rangle &= \int_0^{2\pi} Z(\theta)\partial_t P(\theta,t)d\theta \\ &= \int_0^{2\pi} P(\theta,t)\left[h(\theta)\partial_\theta Z(\theta) + g(\theta)\partial_\theta\left(g(\theta)\partial_\theta Z(\theta)\right)\right] \\ &= 2\pi\int_0^{2\pi} P(\theta,t)\left[h(\theta)R(\theta) + g(\theta)\partial_\theta\left(g(\theta)R(\theta)\right)\right] \\ &= \omega\ .\end{aligned} \tag{2.34}$$

Here, Eq. (2.3), Eq. (2.29) and the normalization condition of $P(\theta,t)$ was used. The property is important for stochastic phase resetting where the evolution of the mean phase is regarded conditional on fixed initial conditions.

The fact that $R(\theta)$ is the probability density of the envelope of a realization $\theta(t)$ of oscillator (2.1) can be used for an estimation of the transformation $Z(\theta)$ from sampled observations $\theta(n\Delta t)$ of stochastic oscillations. To construct the envelope, we need to find the times of first passage t_n for which the unwound realization has a history that is strictly smaller, i. e. $\theta(j\Delta t < t_n) < \theta(t_n)$. At these first passages $\theta_n = \theta(t_n)$, transformation (2.31) is estimated by

$$\psi_n = Z(\theta_n) = \frac{2\pi}{T}\sum_{\theta_j<\theta_n}\left(t_j - t_{j-1}\right)\ . \tag{2.35}$$

To find the transformation on the whole domain one can proceed by an appropriate interpolation of $Z(\theta_n)$, for example, via smoothing splines [86]. Note that Eq. (2.35) gives a biased estimator. This can be fixed by inserting a central difference scheme $(t_{j+1} - t_{j-1})/2$.

2.4 Asymptotic Properties of the Effective Velocity

In this section, the limiting cases of weak and strong additive noise are considered for the effective model. For the case of a vanishing noise amplitude in noise-induced oscillations, the effective velocity shows discontinuities. Furthermore, a formula for the estimation of mean frequency in the limit of strong noise is derived.

2.4.1 Singular Perturbation for Weak Noise

In the Fokker-Planck equation [Eq. (2.3)], the noise amplitude $g(\theta)$ appears in front of the derivative with the highest order in θ. Therefore, a perturbation expansion in $g(\theta)$ for a deterministic approximation of dynamics (2.1) might be singular. For a stochastic phase oscillator with additive noise

$$\dot\theta = h(\theta) + \sigma\xi(t)\ , \tag{2.36}$$

we show that a perturbation expansion becomes singular if oscillations are noise-induced. We discuss the case in which the deterministic phase description should model the probability density of the stochastic oscillations. The singularity that arises in the limit of weak noise $\sigma \to 0$ is discussed by a perturbation expansion starting from $\sigma = 0$, and starting from $\sigma > 0$ using the current model of effective phase dynamics. For the first passage model the situation is analogous as can be seen by the symmetry of Eqns. (2.4) and (2.29) (cf. Fig. 2.5). Furthermore, the results of this section generalize to stochastic phase oscillators with multiplicative noise[12] that is well-behaved.

For $\sigma = 0$, our considerations start with the arbitrary model $\dot{\theta} = h(\theta)$. Let us suppose that oscillator (2.36) shows noise-perturbed oscillations, i. e. $h(\theta)$ is strictly positive. Then, the invariant distribution density of the arbitrary model gives a proper zeroth order approximation to the probability density:

$$P(\theta) = \frac{C}{h(\theta)} + \mathcal{O}(\sigma) \ .$$

Better approximations can be obtained analytically by a Taylor expansion of $P(\theta)$ in σ. For the alternative case of noise-induced oscillations, we impose, without loss of generality, that $h(\theta)$ has zero crossings $\theta_\pm$. Then, the arbitrary model has a stable fixed point at θ_- as well as an unstable one at $\theta_+ > \theta_-$. Its distribution density is given by

$$P(\theta) = \delta(\theta - \theta_-) + \mathcal{O}(\sigma) \ . \tag{2.37}$$

It corresponds to the probability density of oscillator (2.36). However, higher order terms in σ that should lead to a smooth distribution density must necessarily be singular. One can see that a perturbation theory becomes singular for noise-induced oscillations. Note that in the limit $\sigma \to 0$, the mean first passage density also has a singular limit for noise-induced oscillations, which is located at the unstable fixed point. In the above example it is given by

$$R(\theta) = \delta(\theta - \theta_+) + \mathcal{O}(\sigma) \ . \tag{2.38}$$

For noise-perturbed oscillations the mean first passage density and the invariant probability density converge in this limit reflecting the fact that for deterministic self-sustained oscillators the quantities are synonymous.

Starting with the current model[13] of oscillator (2.36) computed for finite $\sigma \neq 0$, another view can be gained on the limit of weak noise $\sigma \to 0$. Using Eqns. (2.7) and (2.12), the current velocity is given by

$$H(\theta) = \frac{1 - \mathrm{e}^{-\frac{r(0,2\pi)}{\sigma^2}}}{\int_\theta^{\theta+2\pi} \frac{d\psi}{\sigma^2} \mathrm{e}^{-\frac{r(\theta,\psi)}{\sigma^2}}} \ , \ \text{with } r(\theta,\psi) = \int_\theta^\psi h(\varphi)\, d\varphi \ . \tag{2.39}$$

[12]The noise amplitude depends on the protophase.
[13]The derivation is analogous for the first passage model.

Let us assume without loss of generality that $r(0, 2\pi)$ is positive. In the limit of weak noise, the integral in the denominator of Eq. (2.39) is dominated by the minimum of $r(\theta, \psi)$ with respect to ψ. Using the method of stationary phase, the zeroth order expansion

$$H(\theta) = \mathcal{O}(\sigma) + \begin{cases} h(\theta) & : \text{ if } \operatorname{argmin}_\psi [r(\theta, \psi)] = \theta \\ 0 & : \text{ elsewise} \end{cases} \tag{2.40}$$

is obtained. Surprisingly, the limit of weak noise leads to a vanishing of current velocity in a finite interval around the fixed point θ_- and not just at this point.

In Fig. 2.6, the peculiar nature of $H(\theta)$ is illustrated for the Adler equation. If σ is small, the effective velocity becomes discontinuous for noise-induced oscillations (right plot of Fig. 2.6), whereas $H(\theta)$ converges to $h(\theta)$ for noise-perturbed ones (left plot of Fig. 2.6).

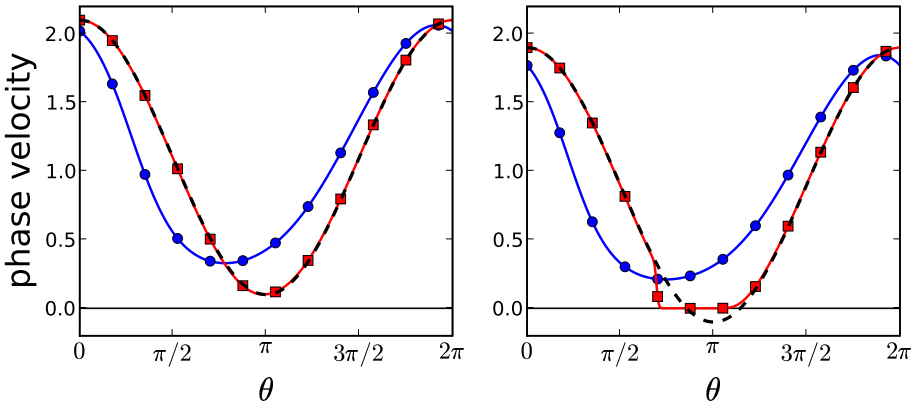

Figure 2.6: At different noise amplitudes, the current velocity $H(\theta)$ [Eq. (2.12)] of the Adler equation [Eq. (2.2)] shows qualitatively different behaviour dependent on the type of oscillations, here shown for a small ($\sigma = 0.1$, red squares) and a large ($\sigma = 0.7$, blue circles) value: For noise-perturbed oscillations ($a = 1.1$, left plot), $H(\theta)$ closely approximates the determinstic part $h(\theta)$ (black dashed line) at small σ, but for noise-induced oscillations ($a = 0.9$, right plot), $H(\theta)$ becomes discontinuous in the limit of vanishing noise (cf. Eq. (2.40)).

2.4.2 Estimating Frequency for Strong Noise

For strong noise, an estimation of the mean frequency can be troublesome if one has to rely on Monte-Carlo simulations. Here, we want to provide a formula that allows for an estimation of frequency at large noise amplitudes if an effective velocity at arbitrary σ is available. Still, only additive noise is considered, whereas here, the results do not generalize in any approximation.

The current velocity can be expressed as $H = h - \sigma^2 [\ln P]'$ (cf. Eq. (2.13)). Therefore, the integral over $H(\theta)$ from 0 to 2π does not depend on σ. To

evaluate the integral we consider the limit of strong noise $\sigma \to \infty$, for which $P(\theta) \to 1/2\pi$, and we obtain

$$\frac{1}{2\pi}\int_0^{2\pi} H(\theta)\, d\theta = \lim_{\sigma\to\infty} \omega = \omega_\infty \ . \tag{2.41}$$

The same result can be obtained for the first passage velocity. Thus for additive noise, the area under effective velocities is independent of the noise amplitude and proportional to the asymptotic mean frequency ω_∞.

2.5 Applications to Continuous Interaction

In this section, the current model of effective phase dynamics is extended to describe periodically forced stochastic oscillations that represent a simple example of continuously interacting stochastic oscillations. The current velocity is split into an autonomous part and an effective coupling function that allows for an invariant description of the interaction.

2.5.1 Construction of Effective Coupling

Performing a phase reduction of a stochastic oscillating system that is subject to a periodic forcing results in a stochastic phase oscillator with an additional term associated to the forcing. Therefore, our basic model [Eq. (2.1)] is extended by a coupling function that depends on the phase variable of the forcing $\psi(t)$. The model obeys the Langevin equation

$$\dot\theta = h(\theta) + g(\theta)\xi(t) + f(\psi(t),\theta) \ . \tag{2.42}$$

For deterministic oscillators, the coupling can lead to phase synchronization between ψ and θ [63]. However, the unbounded Gaussian noise prevents such a perfect synchronization. At most, phase slips[14] are exponentially rare. Again, the coupling function $f(\psi,\theta)$ is not invariant as it depends on the arbitrary parameterization of the protophase. Moreover, a quantification of coupling strength by a quotient f/h might not be well-defined if the unforced oscillations are noise-induced, because then, h has zero-crossings.

As a simple example, the *forced* stochastic *Adler equation*

$$\dot\theta = a + \cos\theta + \sigma\xi(t) + k\sin(\Omega t - \theta) \tag{2.43}$$

is considered. Its autonomous part is the Adler equation and the forcing phase[15] $\psi(t) = \Omega t$ grows uniformly. The chosen coupling tends to stabilize the phase difference $\Delta = \psi - \theta$ around $\Delta = 0$. The forced Adler equation is described by the stationary probability density $P(\theta,\psi)$ for which the Fokker-Planck equation is a partial differential equation. Unfortunately, it is not accessible analytically anymore. In numerical examples, we, therefore, computed

[14] During a phase slip, the phase difference grows by 2π.

[15] Being a phase, ψ describes states on a circle. Therefore, it is taken modulo 2π.

$P(\theta,\psi)$ by discretizing the stationary Fokker-Planck equation and solving it with a matrix inversion [67].

The θ-component of the stationary probability flux is given by[16] [70]

$$J = [h(\theta) + f(\psi,\theta) - g\partial_\theta g]\, P(\theta,\psi)\ . \tag{2.44}$$

The aim is to construct a forced effective phase model based on the probability current (cf. Sec. 2.2): The *forced current model*

$$\dot{\theta} = H(\theta,\psi) \tag{2.45}$$

depends on ψ as well. As prescribed by the autonomous case, a correspondence between the θ-component of the probability flux [Eq. (2.44)] and the θ-component of $J = H(\theta,\psi)P(\theta,\psi)$ (stationary Liouville equation) is drawn. This yields the current velocity

$$H(\theta,\psi) = \frac{J}{P} = h - g\partial_\theta g - g^2\partial_\theta \ln P + f\ . \tag{2.46}$$

In order to quantify the coupling effectively, we rewrite $H(\theta,\psi)$ as a sum of a ψ-independent *marginal current velocity* $H_m(\theta)$ and an *effective coupling* $F(\psi,\theta)$. The former is obtained in terms of the marginal probability density $P_m(\theta) = \int_0^{2\pi} P(\theta,\psi)d\psi$ by integrating Eq. (2.44) over ψ:

$$H_m(\theta) = \frac{\omega}{2\pi P_m(\theta)} = h - g\partial_\theta g - g^2\partial_\theta \ln P_m + \int_0^{2\pi} f\frac{P}{P_m}d\psi\ .$$

Rearranging $H = H_m + F$, we find the effective coupling

$$F(\psi,\theta) = f - \int_0^{2\pi} f\frac{P}{P_m}d\psi - g^2(\theta)\partial_\theta \ln\frac{P(\theta,\psi)}{P_m(\theta)}\ . \tag{2.47}$$

As for the current velocity, F may be decomposed into a deterministic part $\hat{f}$ and an osmotic part $\tilde{f}$, as given by

$$\begin{aligned} F(\psi,\theta) &= \hat{f}(\psi,\theta) - \tilde{f}(\psi,\theta)\ , \\ \hat{f}(\psi,\theta) &= f(\psi,\theta) - \int_0^{2\pi} f(\psi,\theta)\frac{P(\theta,\psi)}{P_m(\theta)}\ d\psi\ , \\ \tilde{f}(\psi,\theta) &= g^2(\theta)\partial_\theta \ln\frac{P(\theta,\psi)}{P_m(\theta)}\ . \end{aligned} \tag{2.48}$$

While the deterministic part contains information about the coupling function $f(\psi,\theta)$, the osmotic part is the result of statistical effects. It assures the lack of synchronization in the forced current model, as it is shown below.

To bring the forced current model into a standard form, we introduce a uniformly distributed phase φ by the transformation (cf. Eq. (2.16))

$$\varphi = S_m(\theta) = 2\pi\int_0^\theta P_m(\eta)d\eta\ . \tag{2.49}$$

[16] The forcing phase ψ might have a stochastic component correlated with the protophase θ. In this case, additional terms arise, but this is not discussed for simplicity.

Then we have[17] $P_m(\varphi) = 1/2\pi$. The transformation of the forced current model yields

$$\dot{\varphi} = \omega + 2\pi P_m(S_m^{-1}(\varphi))F(\psi, S_m^{-1}(\varphi)) = \omega + Q(\psi, \varphi) \; . \tag{2.50}$$

Eq. (2.50) provides the effective phase dynamics of a periodically forced stochastic phase oscillator in a standard form, with an effective coupling function Q that heavily depends on the noise intensity. Let us note that, corresponding to Eq. (2.48), the effective coupling function may be decomposed as $Q = \hat{Q} - \tilde{Q}$ into a deterministic and an osmotic contribution as well.

Now, it is possible to quantify the *local effect* of the forcing phase ψ on the state of the oscillator. As already noted, the naive quantity $f(\psi, \theta)/h(\theta)$ (cf. Eq. (2.42)), obtained from a perturbative approximation, might not be well-defined for noise-induced oscillations. Using the forced current model, a local effect is provided by $\kappa(\psi, \theta) = F(\psi, \theta)/H_m(\theta)$ for the protophase, and correspondingly $\kappa(\psi, \varphi) = Q(\psi, \varphi)/\omega$ for the phase.

The effective coupling function $Q(\psi, \varphi)$ can be estimated from an observation[18] φ_n, ψ_n by the pointwise average

$$\omega + Q(\psi, \varphi) \approx \left. \frac{\langle \varphi_{n+1} - \varphi_{n-1} \rangle}{2\Delta t} \right|_{\psi_n = \psi, \; \varphi_n = \varphi} \; . \tag{2.51}$$

However, we have seen that the coupling still incorporates statistical effects due to its osmotic part. From the perspective of bivariate signal analysis, the term $\hat{Q}$ contains physical information of the interactions of oscillations, whereas the osmotic term $\tilde{Q}$ may be viewed as a statistical artifact. In an experimental setup it might unfortunately not be easy to separate the deterministic from the osmotic contribution.

From a dynamical perspective, Eq. (2.50) is puzzling because it implies the appearance of synchronization which may not exist in stochastic systems (cf. Sec. 1.2.2). The riddle is resolved by the phenomenon of masking (see Sec. 2.5.2).

To give a first example of an effective coupling, the local effect computed in terms of the protophase $\kappa(\psi, \theta)$, and the phase $\kappa(\psi, \varphi)$ are compared for the forced Adler equation (see Fig. 2.7). The local effect provides information not only on the strength of coupling, but also where in state space the two phases interact the strongest. For example, $\kappa(\psi, \theta)$ is strongly localized in a neighborhood of the zero crossing θ_s with $h'(\theta_s) < 0$ for noise-induced oscillations. This means that this neighborhood is most sensitive to the applied coupling. However, the current velocity is slow in the neighborhood which is, therefore, significantly extended when transformed to the phase φ. Correspondingly, the sensitive neighborhood of θ transformed to the phase φ is stretched. In Fig. 2.7, this effect is illustrated with the forced Adler equation at parameter values $a = 0.9$ and $\sigma = 0.7$ for which it shows noise-induced oscillations. The coupling strength $k = 0.2$ was chosen bigger than the excitability threshold

[17] This definition of phase slightly differs from the one presented in Ref. [41].
[18] First, the transformation (2.49) has to be applied to obtain $\varphi_n = S_m(\theta_n)$.

but small enough to allow for an easy numerical computation. The forcing frequency $\Omega = 1$ was chosen to be faster then the mean frequency of the forced oscillator $\omega \approx 0.4$ to avoid masking (see Sec. 2.5.2). It is seen that $\kappa(\psi, \theta)$ is rather flat outside a neighborhood of θ_s, whereas for $\kappa(\psi, \varphi)$ the neighborhood is stretched (cf. right plot of Fig. 2.7). The described effect may not be as pronounced depending on the oscillator under consideration.

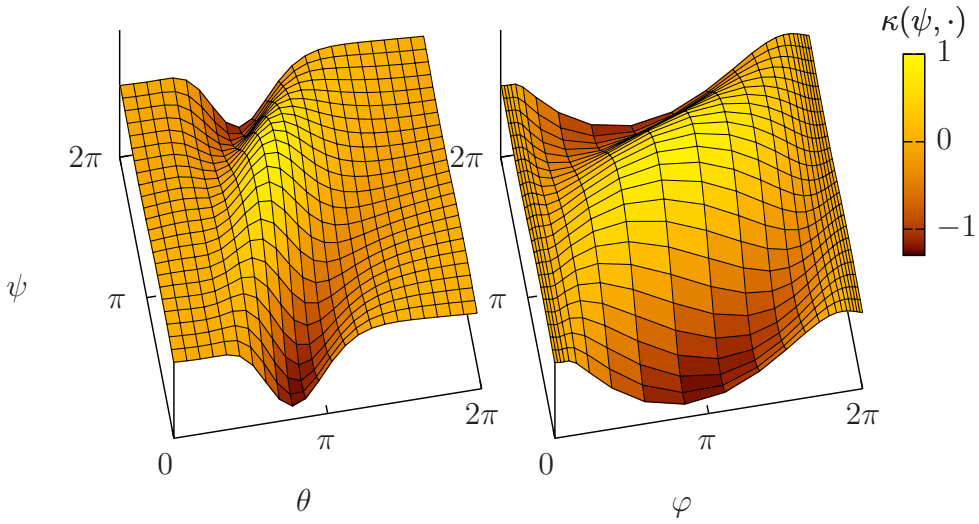

Figure 2.7: Compared to $\kappa(\psi, \theta)$ (left plot), the local effect $\kappa(\psi, \varphi)$ of the forced Adler equation [Eq. (2.2)] in terms of the phase φ (right plot) is stretched in regions of θ where the current velocity is small which is at $\theta \approx \pi$, here shown for $a = 0.9$, $\sigma = 0.7$, $k = 0.2$ and $\Omega = 1$ (cf. last paragraph of Sec. 2.5.1). Numerically, the coordinate θ was transformed to φ instead of the function.

2.5.2 Properties of Effective Coupling

Two phenomena of the effective coupling function are explained in the weak coupling limit. The first phenomenon is associated to noise-induced oscillations for which the weak coupling limit may not be applied if noise is also weak. The second phenomenon resolves the conceptual problem of effective synchronization implied by Eq. (2.50).

In the weak coupling limit, a separation of time scales exists. This can be utilized by averaging Eq. (2.50) over the external phase ψ. In this way, an equation for the phase difference $\Delta = \varphi - \Omega t$ is obtained in the standard Adler

form (cf. Eq. (1.13))

$$\begin{aligned} \dot{\Delta} &= \omega - \Omega + q(\Delta) \ , \\ q(\Delta) &= \frac{1}{2\pi} \int_0^{2\pi} Q(\psi, \Delta + \psi) d\psi \ . \end{aligned} \tag{2.52}$$

The function q is called *average effective coupling*. It also decomposes into a deterministic and an osmotic contribution $q = \hat{q} - \tilde{q}$:

$$\begin{aligned} \hat{q}(\Delta) &= \frac{1}{2\pi} \int_0^{2\pi} \hat{Q}(\psi, \Delta + \psi) d\psi \ , \\ \tilde{q}(\Delta) &= \frac{1}{2\pi} \int_0^{2\pi} \tilde{Q}(\psi, \Delta + \psi) d\psi \ . \end{aligned} \tag{2.53}$$

In the following, we show that $\hat{q}(\Delta)$ diverges in the limit of weak noise for noise-induced oscillations. Furthermore, we demonstrate how synchronization, implied in Eq. (2.52), is effectively avoided by an average masking of $\hat{q}(\Delta)$ by $\tilde{q}(\Delta)$ as the frequencies of oscillations and forcing converge.

Divergence For Small Noise

The deterministic part of the average effective coupling $\hat{q}(\Delta)$ is rewritten in terms of $\theta = S^{-1}(\Delta + \psi)$ as

$$\begin{aligned} \hat{q}(\Delta) &= \frac{1}{2\pi} \int_0^{2\pi} \hat{Q}(\psi, \Delta + \psi) \ d\psi \\ &= 2\pi \int_0^{2\pi} P_m^2(\theta) \hat{F}(S(\theta) - \Delta, \theta) \ d\theta \ . \end{aligned} \tag{2.54}$$

Note, that the marginal probability density is squared in this integral.

First, the limit of small noise is considered. Then, the osmotic term $\tilde{q}(\Delta)$ may be dropped. For noise-perturbed oscillations and small coupling the probability density has the limit $P_m(\theta) = C/h(\theta)$, leading to the average effective coupling

$$\lim_{\sigma \to 0} q(\Delta) = \frac{\omega^2}{2\pi} \int_0^{2\pi} \frac{\hat{F}(S(\theta) - \Delta, \theta)}{h^2(\theta)} \ d\theta \ . \tag{2.55}$$

For noise-induced oscillations, the limit [Eq. (2.55)] is not valid anymore. Therefore, let us again consider Eq. (2.54). Unless the coupling is strong enough to excite the stochastic phase oscillator, $P_m(\theta)$ will become bounded to a small interval around the fixed point of the autonomous oscillator as noise vanishes. The interval is proportional to the maximal amplitude of the coupling. Therefore, the integral over $P_m^2(\theta)$ will become large unless $\hat{F}(\psi, \theta)$ has special properties in this interval. For weakly coupled noise-induced oscillations it is therefore expected that

$$\max_{\Delta} \left[\lim_{\max g(\theta) \to 0} |q(\Delta)| \right] \to \infty \ . \tag{2.56}$$

For additive noise, let us also consider the limit $\sigma \to \infty$. The osmotic term $\tilde{q}(\Delta)$ vanishes which leads to the simple expression

$$\lim_{\sigma\to\infty} q(\Delta) = \frac{1}{2\pi}\int_0^{2\pi} \hat{F}(\theta-\Delta,\theta)\; d\theta \;. \tag{2.57}$$

The theory is illustrated with the forced Adler equation at small coupling strength $k = 0.01$ and by varying the noise amplitude σ. For such a weak coupling the difference between $P_m(\theta)$ and $P(\theta)$ [Eq. (2.5)] is small: The resulting error is of $\mathcal{O}(k^2)$. Therefore, $P(\theta)$ was used in the computation of the deterministic part of the average effective coupling $\hat{q}(\Delta)$. For noise-perturbed oscillations computed at $a = 1.1$ (left plot of Fig. 2.8), it was found that in the limit $\sigma \to 0$ the coupling converges to a finite function (cf. Eq. (2.55)) whereas for noise-induced oscillations at $a = 0.9$ (right plot of Fig. 2.8), the coupling diverged (cf. Eq. (2.56)). The result suggests that a weak coupling approximation should be considered with care if analyzing noise-induced oscillations in the limit of weak noise: Effectively, coupling may not be weak.

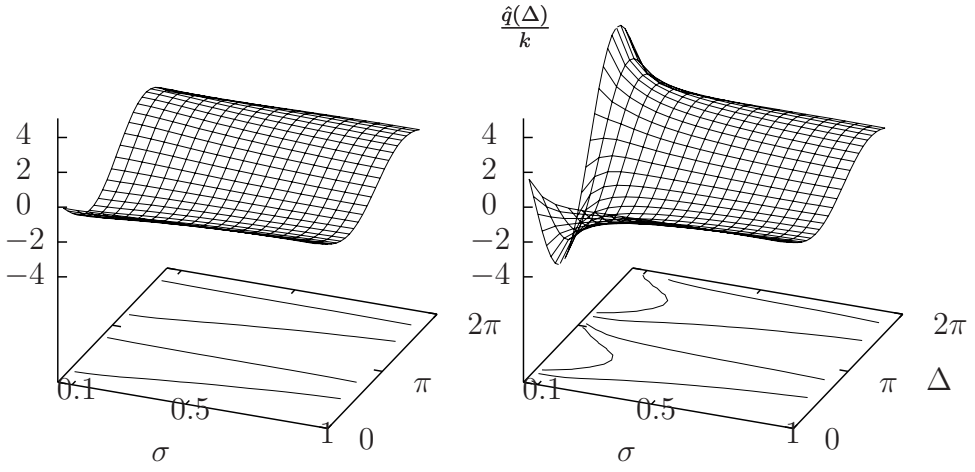

Figure 2.8: The deterministic normalized part of the average effective coupling $\hat{q}(\Delta)/k$ [Eq. (2.53)] of the forced Adler equation [Eq. (2.43)] converges as the noise amplitude σ vanishes for noise-perturbed oscillations ($a = 1.1$, left plot), and it diverges for noise-induced ones ($a = 0.9$, right plot), here shown for $k = 0.01$. (Contour lines are drawn for $|\hat{q}(\Delta)/k| = 1$ and 2 .)

Masking of Coupling

In Eq. (2.52), the implied synchronization of the effective phase model to the forcing phase is apparent (cf. Sec. 1.2.2). This is puzzling because stochastic phase oscillators cannot synchronize. As shown in this section, the riddle is resolved by the appearance of average detailed balance for the transversal variable $\Delta = \varphi - \psi$, that masks the average effective coupling function as the forcing frequency approaches the mean frequency.

Let us demonstrate the *masking of coupling* for a constantly growing forcing phase $\psi = \Omega t$. The Fokker-Planck equation of oscillator (2.42), given by

$$\partial_t P = -\partial_\theta \left[\left(H_m(\theta) + F(\psi, \theta) \right) P(\theta, \psi) \right] - \Omega \partial_\psi P(\theta, \psi) \ , \tag{2.58}$$

is transformed to the variables θ and $\Delta = S(\theta) - \psi$ as follows[19]: For some function $G(\Delta, \theta)$ the differential in the new variables is $dG = \partial_\Delta G d\Delta + \partial_\theta G d\theta$. Replacing the differential $d\Delta = 2\pi P_m d\theta - d\psi$, leaves us with the differential of $G(\theta, \psi)$ in the old variables $dG = \left(2\pi P_m \partial_\Delta G + \partial_\theta G \right) d\theta - \partial_\Delta G \ d\psi$. Thus, the partial derivative operators have to be replaced as

$$\begin{aligned} \partial_\theta &\to 2\pi P_m \partial_\Delta + \partial_\theta \ , \\ \partial_\psi &\to -\partial_\Delta \ . \end{aligned} \tag{2.59}$$

After the substitution in Eq. (2.58), we integrate over θ:

$$\begin{aligned} \partial_t P &= -\left[2\pi P_m(\theta) \partial_\Delta + \partial_\theta \right] \left[\left(H_m + F \right) P \right] + \Omega \partial_\Delta P \\ &= -\partial_\Delta \left[\left(\omega - \Omega + 2\pi P_m(\theta) F \right) P \right] - \partial_\theta \left[\left(H_m(\theta) + F \right) P \right] \ \Bigg| \int_0^{2\pi} d\theta \ \ , \\ \partial_t P_m(\Delta) &= -\partial_\Delta \left(\left(\omega - \Omega \right) P_m(\Delta) + 2\pi \int_0^{2\pi} P_m(\theta) F P d\theta \right) \\ &= -\partial_\Delta (J_\Delta) \ . \end{aligned}$$

In the small coupling limit the stationary probability density factorizes into the marginal densities: $P(\theta, S(\theta) - \Delta) = P_m(\theta) P_m(\Delta)$. Using the average probability flux of the transversal variable $J_\Delta = \frac{\omega - \Omega}{2\pi}$, we obtain:

$$\dot{\Delta} = \frac{\omega - \Omega}{2\pi P_m(\Delta)} = \omega - \Omega + q(\Delta). \tag{2.60}$$

With Eq. (2.60), we arrive at the same result for the average effective dynamics of Δ [Eq. (2.52)]. But now, the approximation used in Eq. (2.52) is understood better[20]. Furthermore, it can be easily seen that as ω approaches Ω the average effective coupling $q(\Delta)$ vanishes for all Δ because J_Δ vanishes exactly (detailed balance). In this way, synchronization is avoided.

[19] Actually, the procedure is standard.

[20] That is, the factorization of the joint probability density into marginals.

A similar derivation is possible for all types of (n, m)-relations of frequencies as in $n\omega = m\Omega$. Here, it can be shown that the (n, m)-th Fourier component of $Q(\psi, \theta)$ is missing through the mechanism of masking.

Let us present numerical evidence for the masking of coupling using the forced Adler equation (Fig. 2.9). The coupling strength $k = 0.01$ was chosen to be small compared to the mean frequency at $a = 1.5$ and $\sigma = 1$, and the average effective coupling $q(\Delta)$ was computed for different values of the forcing frequency Ω around the value of the mean frequency ω of the autonomous Adler equation. As Ω approaches ω, the deterministic and the osmotic parts of the average effective coupling exactly cancel. Therefore, the oscillator does not "feel" the forcing on average. Therefore, as $\omega - \Omega$ approaches zero, the function flattens. The contour lines of $q(\Delta; \Omega)$ as a function of two variables drawn for values close to zero illustrate the effect. Note that the masking of coupling is a general effect observable for forced and also bidirectional interacting stochastic phase oscillators. Moreover, it does not depend on the excitability property of the system, but only on the effective coupling strength. We also illustrate the effect of masking on the full effective coupling $Q(\psi, \varphi)$. For this, we compute $Q(\psi, \varphi)$ at an arbitrary value of the forcing frequency Ω and compare it to the case $\Omega = \omega$ where the masking is strongest. As seen from Fig. 2.10, the "resonant" $(1, 1)$-Fourier component in the coupling function is obviously missing, i. e. masked.

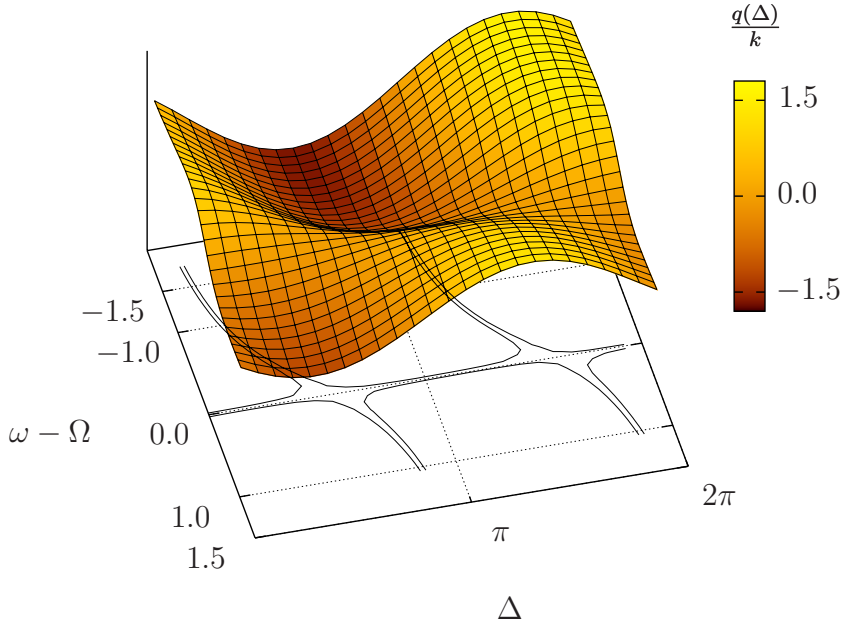

Figure 2.9: If the coupling is sufficiently weak, the normalized average effective coupling $q(\Delta)/k$ [Eq. (2.52)] of the forced Adler equation [Eq. (2.43)] vanishes as Ω approaches ω, here shown for $a = 1.5$, $k = 0.01$ and $\sigma = 1$. (Contour lines are drawn for $q(\Delta; \omega - \Omega)/k = \pm 0.05$ for illustration.)

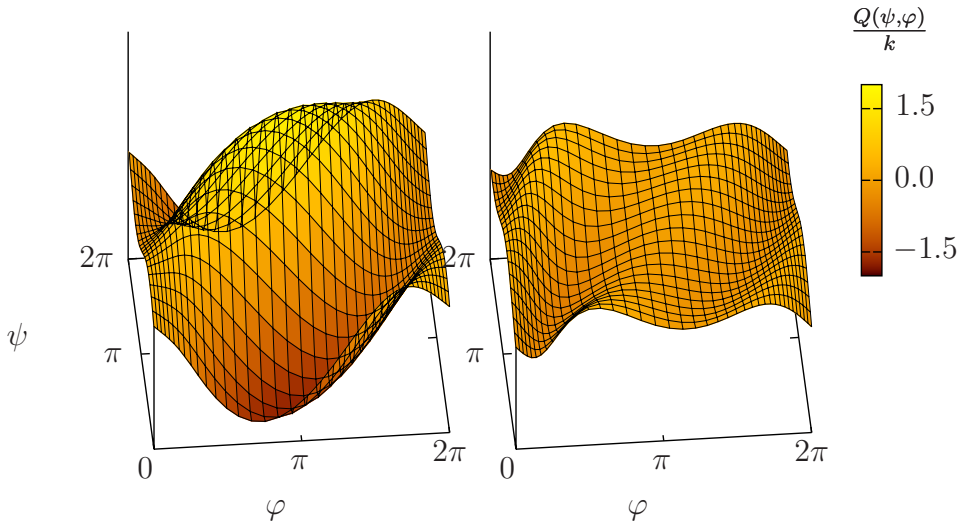

Figure 2.10: The normalized effective coupling $Q(\psi, \varphi)/k$ [Eq. (2.50)] of the forced Adler equation [Eq. (2.43)] shows a diagonal $(1, 1)$-Fourier mode at an arbitrary forcing frequency $\Omega = 2.5 \neq \omega$ (left plot). For $\Omega = \omega$ (right plot), the component is not visible anymore and the total power of the effective coupling is diminished, here shown for $a = 1.5$, $k = 0.01$ and $\sigma = 1.0$.

Let us comment on the not-so-weak coupling case, as well. In this case, the condition leading to Eq. (2.60) is not fulfilled. As a result, the coupling is not perfectly masked anymore. However, synchronization may still not be observable because a current-like model of high-dimensional oscillators has a Hamiltonian structure, as it was noted in Ref. [28].

After a throughout treatment of one-dimensional stochastic phase oscillators, we demonstrate how to construct an effective phase model for general stochastic oscillations which do not allow for an analytic treatment. To illustrate this construction, based on the observations of the oscillations, we take a noise-driven FitzHugh-Nagumo model as a paradigmatic example of an excitable system (cf. Sec. 1.3):

$$\begin{aligned} \epsilon \frac{dx}{dt} &= x - \frac{x^3}{3} - y \\ \frac{dy}{dt} &= x + a + \sigma\xi(t) + b\cos\Omega t \ . \end{aligned} \tag{2.61}$$

Together with a noisy force $\sigma\xi(t)$ that, for the chosen parameter values $a = 1.1$ and $\epsilon = 0.05$, induces oscillations, we have incorporated a periodic force $b\cos\Omega t$ for which we determine the effective phase coupling.

Although we do not have analytical expressions for the mean frequency

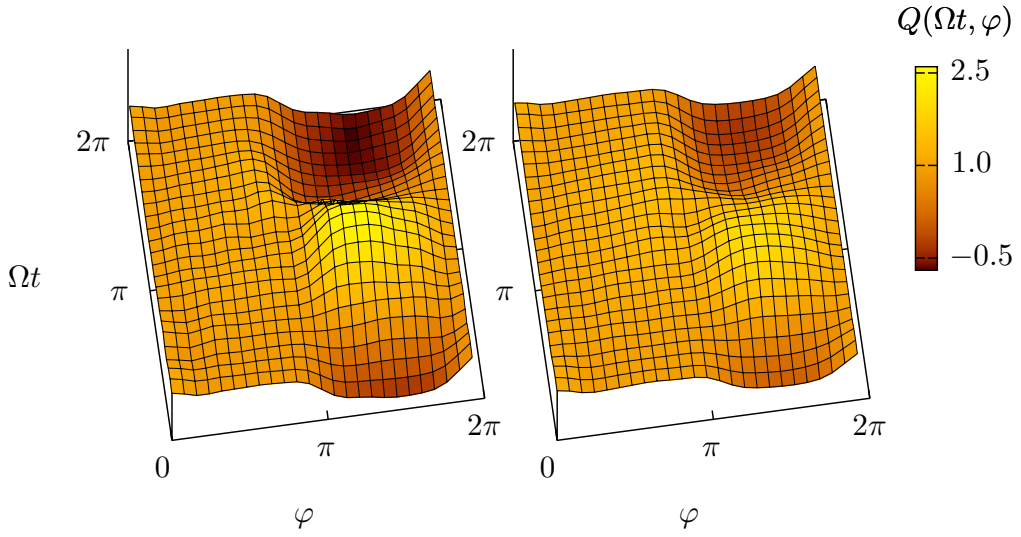

Figure 2.11: The estimated effective coupling $Q(\psi = \Omega t, \varphi)$ [Eq. (2.51)] of noise-induced oscillations of the forced FitzHugh-Nagumo model [Eq. (2.61)] depends on the noise amplitude σ, here shown for $a = 1.5$, $b = 0.1$, $\Omega = 1.3$, and for σ at $\sigma = 0.08$ (left plot: $\omega \approx 0.62$), and $\sigma = 0.11$ (right plot: $\omega \approx 0.95$). This could be due to the excitability (cf. Fig. 2.8) or frequency-induced masking (cf. Fig. 2.9).

and the probability density, these characteristics can be obtained from the observations $(x_n, y_n) = (x(n\Delta t), y(n\Delta t))$. After adopting the simplest choice for the protophase $\theta = \tan^{-1}(y/x)$, we performed a transformation to the phase φ according to Eq. (2.49). With long enough time series φ_n and ψ_n at hand, we determined the effective coupling function $Q(\psi, \varphi)$. For this we used a least squares fit to approximate the dependence of the central difference (2.51) on ψ and φ with a double Fourier series (see Ref. [41] for details). Both effects, the increase of effective coupling for vanishing noise and the masking of coupling, were observed in numerically obtained effective coupling functions for forced noise-induced oscillations of the FitzHugh-Nagumo model. In Fig. 2.11, we want to present an interesting case in order to illustrate certain pitfalls that may arise in the interpretation of effective coupling functions estimated from observed oscillations. Here, the effective coupling function was computed for two noise intensities corresponding to $\omega \approx 0.62$ and 0.95, whereas the forcing frequency was chosen as $\Omega = 1.3$. One can see in Fig. 2.11 that the amplitude of Q decreases with increasing noise intensity. The change in amplitude may have been related to a more pronounced masking of coupling induced by the frequency shift (cf. Fig. 2.9), or to the generic decrease in effective coupling for stronger noise (cf. Fig. 2.8). For an exploration of the extent to which the two effects participate, it is necessary to reconstruct the deterministic or osmotic part from data. However, this cannot be done reliably unless the correct states are identified to be in the same phase. For this, it is necessary to generalize the concept of standard isophases, a problem which we address in Chap. 3.

2.6 Stochastic Phase Resetting

In this section, a theory of phase resetting of stochastic phase oscillators is developed. The first passage model represents the phase resetting curve of the stochastic phase oscillator correctly, whereas the current model does not.

The theory of phase resetting is concerned with the response of regular oscillations to a brief pulse, a *kick*, applied at a certain protophase α with a certain strength and direction $\mathbf{k}$ (cf. Sec. 1.2.2). The freely rotating period T is compared to the period $T_{\mathbf{k}}(\alpha)$ wherein the kick is applied by computing the *phase resetting curve* [89, 10]

$$\mathrm{PRC}(\alpha, \mathbf{k}) = 2\pi \frac{T - T_{\mathbf{k}}(\alpha)}{T} \ . \tag{2.62}$$

It gives the shift in the uniformly rotating phase shown by the oscillations due to the kick. For example, Eq. (2.17) provides the phase resetting curve of the current model [Eq. (2.11)], whereas Eq. (2.32) provides it for the first passage model [Eq. (2.21)], if one sets $\theta_2 = \theta_1 + k$ for either[21]. Up to here, the quantities appearing in Eq. (2.62) are only well-defined for limit-cycle oscillations. We extend the applicability of Eq. (2.62) to the stochastic oscillations shown by stochastic phase oscillators (cf. Refs. [14, 55]), and discuss the results in terms of effective phase theory.

A kick applied at a time t' with scalar strength k, representing a brief pulse, is introduced to our basic model (2.1) by

$$\dot{\theta}(t) = h(\theta(t)) + g(\theta(t))\xi(t) + k\delta(t' - t) \ . \tag{2.63}$$

The *stochastic phase resetting curve* is computed by a comparison of the kicked and unkicked stochastic phase oscillator. For this, quantities appearing in Eq. (2.62) are interpreted as follows: Quantity T is given by the mean period of the unkicked oscillator. Quantity $T_k(\alpha)$ is computed for the kicked oscillator as the mean first passage time of the unwound protophase starting at $\theta = \alpha + k$ (value just after the kick) to reach the boundary $\theta = \alpha + 2\pi$.

The *kicked* stochastic *Adler equation*

$$\dot{\theta}(t) = a + \cos\theta + \sigma\xi(t) + k\delta(t' - t) \ . \tag{2.64}$$

serves as our basic model. Being infinitely fast, the *additive*[22] kick is applied numerically by shifting the state $\theta(t')$ by k.

By the above interpretation of Eq. (2.62), the stochastic phase resetting curve can be calculated using the mean first passage times $T(\alpha, \beta)$. From Eq. (2.28) it is deduced that $T(\alpha, \beta) + T(\beta, \delta) = T(\alpha, \delta)$. This is related to the Markov property of $\theta(t)$, and it allows us to express $T_k(\alpha)$ as

$$T_k(\alpha) = T - T(\alpha, \alpha + k) \ . \tag{2.65}$$

[21] For one-dimensional systems, the kick $\mathbf{k} = k$ is scalar.

[22] In the model, the phase sensitivity k does not depend on the protophase θ (cf. Sec. 1.2.2).

For Eq. (2.62), it follows that $\mathrm{PRC}(\alpha, k) = 2\pi T(\alpha, \alpha + k)/T$. This can be rewritten in terms of $R(\theta)$ using Eq. (2.23):

$$\mathrm{PRC}(\alpha, k) = 2\pi \int_{\alpha}^{\alpha+k} R(\theta)\, d\theta \ . \tag{2.66}$$

This is the exact formula for the stochastic phase resetting curve of a kicked general stochastic phase oscillator (2.1).

The theory is illustrated in Fig. 2.12, where we show the stochastic phase resetting curve $\mathrm{PRC}(\alpha)$ for noise-induced oscillations of the kicked Adler equation with a small pulse strength $k = \pi/16$. For weak noise, the oscillator becomes very sensitive at certain protophases were the first passage velocity is slow. For example at $\sigma = 0.1$ (squares), a kick with strength $k = \pi/16$ applied to the protophase θ can have almost a 16-fold effect on the phase φ. On the other hand, $\mathrm{PRC}(\alpha)$ is negligibly small at protophases α were the dynamics is fast. For neuronal oscillators the corresponding states are said to lie in the *refractory period* [32].

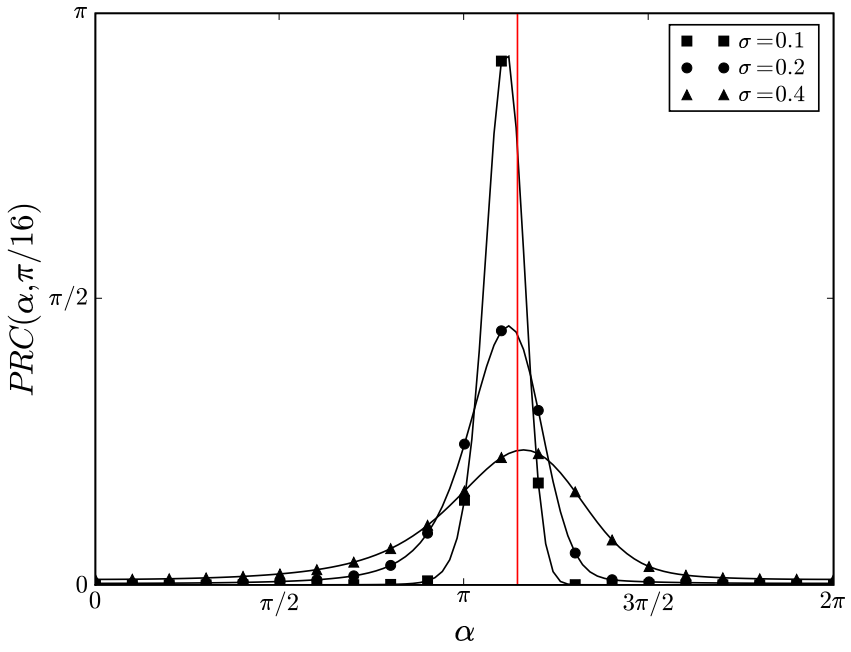

Figure 2.12: For noise-induced oscillations of the kicked Adler equation [Eq. (2.64)], the stochastic phase resetting curve $\mathrm{PRC}(\alpha, k)$ [Eq. (2.66)] is heavily dependent on the noise amplitude σ (values as indicated). For weak noise (squares), $\mathrm{PRC}(\alpha, k)$ is maximal if the pulse just suffices to kick the oscillator beyond the unstable fixed point (red vertical line), here shown for $a = 0.9$ and $k = \pi/16$.

Let us discuss how the stochastic phase resetting curve [Eq. (2.66)] is represented by the effective phase models. It is easily seen that the phase resetting

curve

$$\Delta\varphi(\alpha,k) = 2\pi \int_{\alpha}^{\alpha+k} P(\theta)\, d\theta \tag{2.67}$$

derived for the current model [Eq. (2.11)] does not correspond to that of the stochastic phase oscillator, whereas the phase resetting curve

$$\Delta\psi(\alpha,k) = 2\pi \int_{\alpha}^{\alpha+k} R(\theta)\, d\theta \tag{2.68}$$

derived for the first passage model [Eq. (2.21)] yields the correct formula. Let us explain why the current model fails: In Sec. 2.2, it was seen that the current velocity is constructed as "$H = J/P$" which leads to the stationary solution (2.12). However, the stationary state is broken in the phase resetting procedure, because the time evolution of $\theta(t)$ starts from the definite value $\theta = \alpha + k$. Consider for example the moment right after the resetting of an oscillator with additive noise, where $P(\theta, t') = \delta(\theta - \alpha - k)$. The probability flux is calculated by integrating Eq. (2.4), and one obtains $2\pi J(\alpha + k) = h(\alpha + k)$ which does not coincide with the stationary flux $\omega/2\pi$. Deviations to the stationary solution (2.12) are most prominent in the excitable regime where $2\pi J(\alpha + k) = h(\alpha + k) < 0$. In this case, the time-dependent current model

$$\dot{\theta} = \frac{J(\theta,t)}{P(\theta,t)} \tag{2.69}$$

has non-monotonic dynamics. Therefore, it does not yield a good phase description.

The phase resetting curve of stochastic phase oscillators can be understood in a more intuitive way. Again, the basic idea is that a pulse kicks the system from a phase θ_1 to a phase $\theta_2 = \theta_1 + k$. Let us compute the time-dependent ensemble average of unwound protophases $\Theta_{1,2}(t) = \langle\theta(t)\rangle$ with respect to the two probability densities $P_{1,2}(\theta, t = 0) = \delta(\theta_{1,2} - \theta)$ (with and without kick). Asymptotically, the densities assume the same stationary state leading to a constant average velocity $\lim_{t\to\infty}\langle\dot{\theta}(t)\rangle = \omega$. Thus in the limit $t \to \infty$, the phase difference $\Delta\Theta(t) = \Theta_2(t) - \Theta_1(t)$ is a constant, and it is equal to the corresponding value of the phase resetting curve $\mathrm{PRC}(\theta_1, k)$.

To give a numerical example, two groups, each containing 1000 realizations of the Adler equation at $a = 0.95$ and $\sigma = 0.2$, with one group starting at $\theta_1 = \theta_+ - 0.2$ and the other at $\theta_2 = \theta_+ + 0.2$. Here, θ_+ is the unstable fixed point $a = -\cos\theta_+$. For each group an average over realizations was performed to obtain the average dynamics $\Theta(t) = \langle\theta(t)\rangle$. While asymptotically uniformly rotating (cf. top plot of Fig. 2.13), initially, $\Theta(t)$ has systematic non-uniformities such that the initial phase difference $\Delta\Theta(0) = \theta_2 - \theta_1$ widens (cf. bottom plot of Fig. 2.13). Asymptotically, it reaches the value $\Delta\psi = Z(\theta_2) - Z(\theta_1)$ as correctly predicted by the stochastic phase resetting curve [Eq. (2.66)] and the first passage model [Eq. (2.68)]. Let us note that the result is in line with the constant ensemble velocity of the stochastic phase $\psi(t) = Z(\theta(t))$ (cf. Eq. (2.34)).

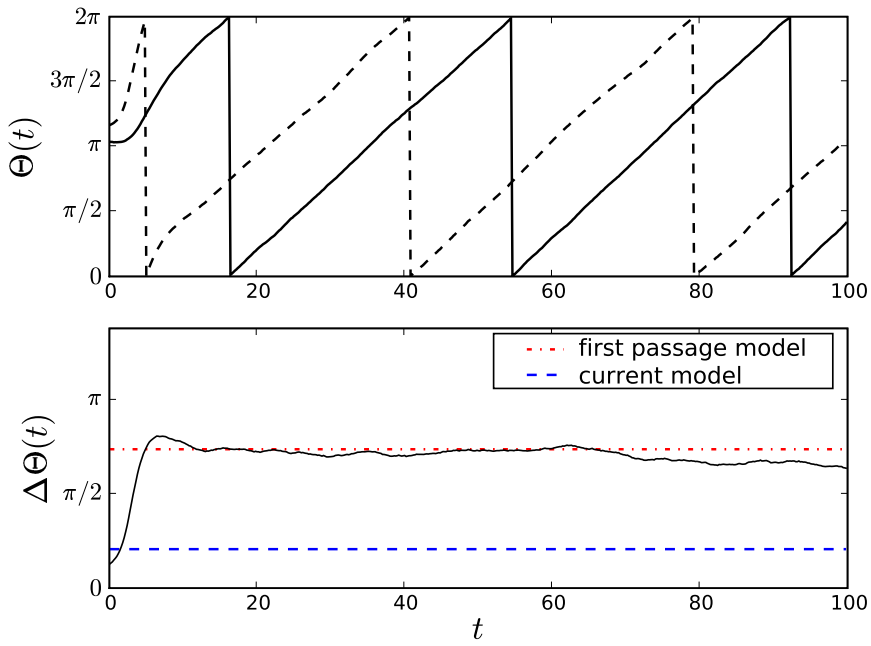

Figure 2.13: Two trajectories of $\Theta(t)$, each one averaged over 1000 realizations of the Adler equation [Eq. (2.2)] (and then taken modulo 2π), were computed starting at two distinct initial conditions $\theta_{1,2} = \theta_+ \pm 0.2$ (top plot, $+$: dashed, $-$: solid), here shown for $a = 0.95$ and $\sigma = 0.2$. They showed after an initial non-uniformity a constant growth rate, such that the initial phase difference $\Delta\Theta(0) = \theta_2 - \theta_1$ widens (bottom plot, solid line) to the value $\mathrm{PRC}(\theta_1, 0.4) = \Delta\psi(\theta_1, 0.4)$ [Eq. (2.68)] (red dotted line) as predicted by the first passage model [Eq. (2.21)]; the corresponding prediction of the current model [Eq. (2.67)] (blue dashed line) is not correct.

2.7 Conclusions

In summary, two useful formulations of the effective phase theory for an invariant description of stochastic oscillations were presented each one relying on different definitions of phase velocity. While the concept of average time spent in an interval led to the current model, a velocity definition based on mean first passage times led to the first passage model. For noise-perturbed oscillations, it was shown that respective effective velocities converge as noise vanishes, whereas for noise-induced oscillations, they do not. The current model could be extended to characterize continuous interactions effectively, as exemplified with the periodically forced stochastic phase oscillator. The first passage model, on the other hand, was shown to exhibit the correct phase resetting curve in reaction to a brief pulse.

We showed that the current model exhibits the same mean frequency and invariant distribution density as the stochastic oscillations. The first passage model, on the other hand, exhibits the correct mean first passage density in place of the distribution density. While for deterministic oscillations the two

densities are equal, for stochastic oscillations they can differ, especially for noise-induced ones. Therefore, the two effective models provide different definitions of an invariant phase of stochastic oscillations, while for deterministic oscillations the invariant phase remains unambiguous.

In the characterization of interactions, we were able to characterize periodically forced stochastic oscillations by an effective coupling function between the phase of oscillations and the phase of the forcing. While it has been previously shown how such coupling functions can be estimated from observed oscillations [40], we now extended the understanding of the properties of coupling functions by the analytical analysis of the periodically forced stochastic phase oscillator. Importantly, it was shown that the effective coupling function heavily depends on both, the frequencies of oscillation and the noise amplitude. Particularly for noise-induced oscillations, the effective coupling function diverges as noise-vanishes because the oscillator becomes increasingly more sensitive to external forces in the region of excitability. Furthermore, we found that the effective coupling function can be heavily masked dependent on the relative frequencies of the forcing and the forced oscillations (cf. Fig. 2.10). The result implies that a detection of directional coupling from observed oscillations can be biased which can lead to faulty conclusions on the coupling structure.

On the other hand, we also characterized the response of stochastic oscillations to a brief pulse by the stochastic phase resetting curve. It was found that the curve heavily depended on the noise amplitude as well, especially for noise-induced oscillations (cf. Fig. 2.12). Furthermore, we found that the first passage model has the same phase resetting properties as the stochastic oscillations, as opposed to the current model. Therefore, it is possible to estimate the stochastic phase resetting curve from observed oscillatory data by using formula (2.35).

Chapter 3

Phase Reduction of Irregular Oscillations

The standard procedure of phase reduction follows the criterion that *states are in the same phase if they become indistinguishable in the course of time*. For two states of a limit-cycle oscillator, this is exactly the cases if they collapse to the same state on the limit-cycle, which leads to the concept of standard isophases (cf. Sec. 1.2). The limit-cycle's foliation of standard isophases has been used to derive the reduced stochastic dynamics of noise-perturbed limit-cycle oscillations. It should be noted, however, that this is clearly a perturbative approach because the full stochastic dynamics may not anymore obey the criterion of standard phase reduction. This is most obvious for irregular oscillations that underlies no limit-cycle, such as chaotic or noise-induced oscillations.

Therefore, we propose a generalization of standard isophases without any reference to a limit-cycle, that is also based on the criterion of distinguishability: A generalized isophase is defined as a Poincaré section, such that all return times to the section are constant. For stochastic oscillations, this condition is formulated in an average sense leading to the notion of average isophases. They allow for a phase reduction of noise-induced, noise-perturbed and non-Markovian oscillations in a unified way. Average isophases can also be estimated from observed oscillations, which is illustrated with a signal of regular human respiration. The treatment of chaotic oscillations is more problematic: It is argued that generalized isophases exist neither exactly due to chaotic phase diffusion, nor optimally due to unstable periodic orbits. Therefore, isophases can only be obtained approximately which breaks their strict invariance. However, we demonstrate by the example of Rössler's oscillator, that good approximate isophases still lead to a qualitatively better phase description.

In the first section of this chapter, the generalized concept of standard isophases is introduced together with a numerical scheme for their construction from observed oscillations. In Sec. 3.2, the average isophases of noise-perturbed, noise-induced and non-Markovian oscillations are discussed by considering modified versions of the Landau-Stuart oscillator. The applicability of the numerical scheme is demonstrated by a signal of regular human respi-

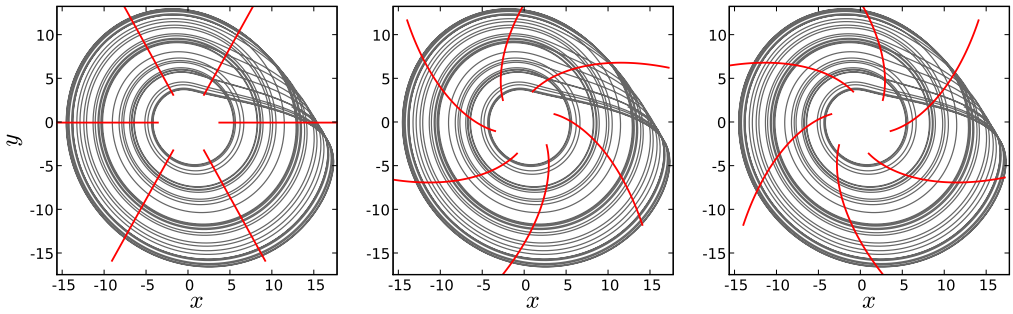

Figure 3.1: Each of three variants of a family of Poincaré sections (red lines) yield the same definition of oscillation for the Rössler oscillator [Eq. (1.17)] (grey trajectories). But their respective phase definitions do not coincide because different sets of states are identified to be in the same phase.

ration. In Sec. 3.3, generalized isophases of chaotic oscillations are discussed in detail: The relationship between the isophases, chaotic phase diffusion, unstable periodic orbits, and their Floquet multipliers is explained. At the end of the section, certain aspects of the phase reduced dynamics of the Rössler oscillator are discussed.

3.1 Concepts of Generalized Isophases

In this section, the concept of standard isophases, applicable for limit-cycle oscillators, is generalized for an application to irregular oscillations. The generalized isophases can be estimated from observed oscillations by a numerical scheme that is presented thereafter. Furthermore, other possible routes to a phase reduction of irregular oscillations are discussed.

A definition of irregular oscillations shown by the trajectory of a system corresponds to a 2π-periodic family of Poincaré sections $J(\varphi)$: The trajectory completes one oscillation if it consecutively passes all sections of the family. To all states that lie on the same Poincaré sections, the same value of phase φ is assigned. With a definition of phase, the mean frequency [Eq. (1.22)] and phase diffusion coefficient [Eq. (1.23)] may be computed as well. In Fig. 3.1, three variants of a family of Poincaré sections for the Rössler oscillator are illustrated. Even though their associated mean frequencies and diffusion coefficients are equal, their corresponding sections clearly identify different states to be in the same phase. Therefore, an additional condition is needed to define the phase in a non-arbitrary and invariant way. For this, we demand that the dynamics of the phase variable should be in a certain sense independent of the amplitudes $\mathbf{a}$ parameterizing the Poincaré sections. If the amplitude dynamics is dissipative, states in the same phase will become indistinguishable in the course of time and the criterion that is stated above is fulfilled. Starting from a family of arbitrary Poincaré sections, the arbitrary phase dynamics may still

depend on the amplitudes. Then, one needs to find a phase correction $\Delta(\mathbf{x})$ that eliminates this dependence via the transformation

$$\theta = \varphi - \Delta(\mathbf{x}) \ . \tag{3.1}$$

Each of this sections $I(\theta)$ of constant θ, called generalized isophases, is defined according to the following condition: The return times of $I(\theta)$ must be equal to some characteristic period[1] T_{char}. The definition avoids any reference to a limit-cycle or a coordinate system. More precisely, we compute the time interval $T(\mathbf{x})$ that is needed, starting at a state $\mathbf{x} \in I(\theta)$, to return to $I(\theta)$ after one oscillation was performed, and we compare $T(\mathbf{x})$ to T_{char}. A family of *generalized isophases* $I(\theta)$ obeys the condition:

$$\text{For each } \mathbf{x} \text{ in } I(\theta): \ T(\mathbf{x}) = T_{\text{char}} = \frac{2\pi}{\omega_{\text{char}}} \ . \tag{3.2}$$

The dynamics of $\theta(t)$ is invariant under any nonlinear transformations of state space because return times do not depend on the specific coordinate system. If we are dealing with a limit-cycle oscillator, conditions (1.3) and (3.2) define the same isophases on its basin of attraction. Our strategy for a construction of generalized isophases is to find a *phase correction* $\Delta(\mathbf{x})$ such that $I(\theta)$ fulfills condition (3.2).

To give an analytically tractable example of generalized isophases, let us consider the *unstable Landau-Stuart oscillator* governed by

$$\dot{r} = r(r^2 - 1); \ \dot{\varphi} = \alpha - \kappa r^2 \ . \tag{3.3}$$

It is exactly solvable: For the initial conditions $r(0) = R$ and $\varphi(0) = \Phi$, it has the well-known solutions

$$\begin{aligned} r(t) &= \left[1 + \frac{1 - R^2}{R^2} \mathrm{e}^{2t}\right]^{-1/2} \ , \\ \varphi(t) &= (\alpha - \kappa)t - \kappa \ln r(t) + \Phi + \kappa \ln R \ . \end{aligned} \tag{3.4}$$

Oscillator (3.3) shows an unstable periodic orbit (UPO) with frequency $\omega = \alpha - \kappa$. Depending on the initial conditions, its state performs oscillations for $R < 1$, or it diverges in finite time for $R > 1$. For the corresponding stable oscillator, the non-isochronicity parameter κ quantifies how much isophases curve in phase space leading to an amplitude dependence of φ (see Sec. 1.2.1). We will see that this is also true for the generalized isophases of oscillator (3.3).

As the characteristic period we chose that of the UPO: $T_{\text{char}} = \frac{2\pi}{\omega}$. In order to obtain a phase that rotates independent of r, we set $\theta = \omega t + \Phi + \kappa \ln R$. Inserting θ into Eq. (3.4), we find that generalized isophases $I(\theta)$ are solutions to the equation

$$\theta = \varphi + \kappa \ln r \ . \tag{3.5}$$

[1] If return times are not constant the set cannot be invariant. Furthermore, the criterion may be formulated also using the characteristic frequency $\omega_{\text{char}} = 2\pi/T_{\text{char}}$.

For each $(\Phi, R) \in I(\theta)$ the return time of $\theta(t)$ is constantly equal to T_{char} because $\theta(t)$ rotates independent of the state. Therefore, condition (3.2) is fulfilled. Furthermore, the phase correction [Eq. (3.1)] is given by $\Delta(r) = -\kappa \ln r$. As for the stable Landau-Stuart oscillator [Eq. (1.5)], it is governed by the non-isochronicity parameter κ as well, but the correction has the opposite sign. Therefore, we must conclude that the shape of a generalized isophase has no immediate implications on the amplitude dependence of frequency (cf. Sec. 1.2.1).

Alternatively, one may think of the unstable Landau-Stuart oscillator as a seldom visited part of state space of a bigger system that has a different characteristic frequency $\frac{2\pi}{T_{\text{char}}} = \omega_0 = \omega + \Delta\omega$. Now, T_{char} is different from the period of the UPO. Therefore, condition (3.2) cannot be fulfilled on the orbit's states. To fulfill the condition for states off the orbit, we now seek a phase with the dynamics $\dot{\theta} = \omega_0$. Therefore, we rewrite Eq. (3.4) in terms of $\omega_0 t$:

$$\varphi(t) = \omega_0 t + \Phi + \kappa \ln R - \kappa \ln r - \Delta\omega t(r) \ . \tag{3.6}$$

Here, we need to rewrite time as a function of radius. We get

$$t(r) = \frac{1}{2} \ln |r^2 - 1| - \ln r + \ln \frac{R}{\sqrt{1 - R^2}} \ . \tag{3.7}$$

After the substitution, a uniformly rotating phase is given by $\theta = \omega_0 t + \Phi + \kappa \ln R + \Delta\omega \ln(\sqrt{1 - R^2}/R)$. Comparing the result with Eq. (3.1), the phase correction is given by

$$\Delta(r) = -(\kappa - \Delta\omega) \ln r - \frac{\Delta\omega}{2} \ln |r^2 - 1| \ . \tag{3.8}$$

While condition (3.2) is fulfilled at all states, but those of the orbit, the phase correction diverges as $\ln |1 - r|$ in the limit $r \to 1$. Thus, the generalized isophase winds itself infinitely often around the limit-cycle (cf. Fig. 3.2). As we will see in Sec. 3.3, the divergent behaviour of phase correction is a generic property to UPOs that has implications for approximations of the generalized isophases of chaotic oscillations.

From the example we have seen that generalized isophases may not exist everywhere. In fact, it is given evidence in Sec. 3.3 that for chaotic oscillations the isophases may exist nowhere. In this case, condition (3.2) can only be fulfilled in an approximate way. Formally, a (small) *recurrence error* $\varepsilon(\mathbf{x})$ modifies the condition that characterizes an *approximate isophase*:

$$\text{For each } \mathbf{x} \text{ in } I(\theta) : \ T(\mathbf{x}) = T_{\text{char}} + \varepsilon(\mathbf{x}) \ . \tag{3.9}$$

In the example, the singularity of the phase correction [Eq. (3.8)] can be fixed in an arbitrary way by allowing a non-zero recurrence error for states close to the limit-cycle. For states $\mathbf{x}_0$ on the period T orbit, the recurrence error is bounded by the inequality (Ineq.)

$$|\varepsilon(\mathbf{x}_0)| \geq |T - T_{\text{char}}| \ . \tag{3.10}$$

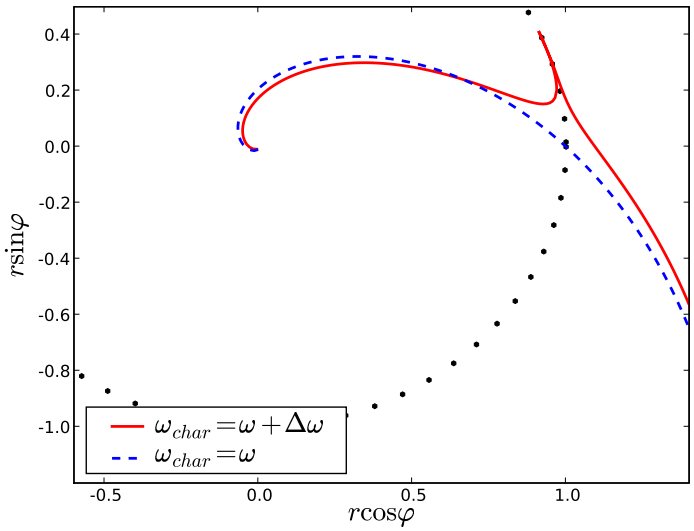

Figure 3.2: The unstable Landau-Stuart oscillator [Eq. (3.3)], here shown for $\alpha = 2$ and $\kappa = 1$, has a generalized isophase $I(0)$ [Eq. (3.5)] similar to that of the usual Landau-Stuart oscillator [Eq. (1.5)] if the frequency of the unstable periodic orbit is chosen as characteristic (blue dashed line): $\omega_{\text{char}} = \omega = 1$. If ω_{char} is shifted by $\Delta\omega = 0.1$, the phase correction [Eq. (3.8)] shows a singularity at $r = 1$ where the isophase (red solid line) winds itself infinitely often along the limit-cycle (black dots).

A *good* approximate isophase has a recurrence error close to the bound (3.10).

For stochastic oscillations, the return time of a Poincaré section is defined as the time interval which it takes the phase variable to grow[2] by 2π. In this way multiple crossings of the section are avoided. The return time, interpreted as a first passage time, is a random variable and therefore, not suitable for condition (3.2). Therefore, the average of the return time $\langle T(\mathbf{x})\rangle$ conditional on the initial state $\mathbf{x}$ is used in the characterization of *average isophases* $I(\theta)$:

$$\text{For each } \mathbf{x} \text{ in } I(\theta): \ \langle T(\mathbf{x})\rangle = T_{\text{char}} = \frac{2\pi}{\omega_{\text{char}}} \ . \tag{3.11}$$

As the characteristic period one uses the mean period of stochastic oscillations.

3.1.1 Obtaining Generalized Isophases from Data

Starting point of an iterative construction of generalized isophases is a suitable vector time series $\mathbf{x}_j = \mathbf{x}(j\Delta t)$ with N data points, which is obtained by numerical simulation or by embedding observed oscillations [35]. One needs to find a transformation to cylindrical coordinates $\mathbf{x}_j \to (\varphi_j, \mathbf{a}_j)$, such that φ_j grows by 2π in the course of one oscillation – i. e. the coordinates define a family of arbitrary Poincaré sections. For example, the cylindrical coordinates (1.19) of the Rössler oscillator are well-suited for the construction.

[2]Phase is always chosen such that it grows.

As a zeroth order approximation $\theta_j^{(0)}$ to a good phase that rotates independent of amplitudes, we can chose the arbitrary phase φ of the cylindrical coordinates. Accordingly, the Poincaré section $I_0(\theta^{(0)})$ approximates the generalized isophase. For each value $\theta_j^{(0)}$ of the unwound phase, the return time $T_0(\mathbf{x}_j) \approx l(j)\Delta t$ of $I(\theta_j^{(0)})$ is estimated, for which $\theta_{l(j)+j}^{(0)} - \theta_j^{(0)} \approx 2\pi$. The return time will not yet fulfill condition (3.2). Using a sequence of phase corrections $\Delta_m(\mathbf{x})$ a better phase

$$\theta_j^{(m)} = \varphi_j - \Delta_m(\mathbf{x}_j) \tag{3.12}$$

is computed. The return time $T_m(\mathbf{x})$ to the corresponding section $I_m(\theta^{(m)})$ should fulfill condition (3.2) with increasing accuracy. Setting $\Delta_0(\mathbf{x}) = 0$, the next approximate phase correction $\Delta_{m+1}(\mathbf{x})$ is, therefore, computed from the mth using the nonlinear iteration scheme

$$\Delta_{m+1}(\mathbf{x}) = \Delta_m(\mathbf{x}) + \frac{k}{2}\,\omega_m(\mathbf{x})\,[T_m(\mathbf{x}) - T] \ . \tag{3.13}$$

In this formula, differences in return times are transformed to differences in phase with the local frequency

$$\omega_m(\mathbf{x}_j) \approx \frac{\theta_{j+1}^{(m)} - \theta_{j-1}^{(m)}}{2\Delta t} \ . \tag{3.14}$$

Furthermore, a parameter $k \in (0, 1)$ controls the speed of convergence of the algorithm. After a sufficient large number M of iterations, $I_M(\theta^{(M)})$ should fulfill condition (3.2) up to a wanted accuracy.

To be able to fulfill the approximate condition [Eq. (3.9)] for chaotic oscillators or the average condition [Eq. (3.11)] for stochastic oscillators, the numerical scheme must be modified in the same way: The return times of $\theta^{(m)}$ are replaced by *average return times*

$$T_m(\mathbf{x}) \approx \Delta t \langle l(j) \rangle|_{\mathbf{x}_j = \mathbf{x}} \tag{3.15}$$

that are averaged over a neighborhood of $\mathbf{x}$. For chaotic oscillations, the average prevents the recurrence error of the mth iteration $\varepsilon_m(\mathbf{x})$ from becoming an increasingly complex function (see Sec. 3.3).

For stochastic oscillations, one should additionally perform an, at least, point-wise average of the local frequency [Eq. (3.14)]. But for some cases, this is not enough because the average local frequency may not point in the direction of growth of phase for some states (cf. Sec. 3.2). As a consequence, the next phase correction Δ_{m+1} would be worse than the previous one. This is fixed by using the mean frequency ω:

$$\Delta_{m+1}(\mathbf{x}) = \Delta_m(\mathbf{x}) + \frac{k}{2}\,\omega\,[T_m(\mathbf{x}) - T] \ . \tag{3.16}$$

Typically, k has to be chosen smaller in this equation than in Eq. (3.13) because this scheme has worse convergence properties.

The local average can be implemented by demanding certain smoothness conditions for $T_m(\mathbf{x})$ using, for example, smoothing splines, finite polynomials or kernel functions [67]. In this work, we use standard smoothing splines to approximate a generalized isophase parameterized by a single amplitude for which $\Delta(a)$ is a scalar function [12]. To find a global phase correction $\Delta(\varphi, \mathbf{a})$ for all states, we use polynomial basis functions: For each of the amplitudes $\mathbf{a}_j$ we use the powers $\mathbf{a}_j^n$, and for the phase variable φ we use trigonometric polynomials $(\exp i\varphi)^n$. For example in $1+2$ dimensions[3], where we can write $\mathbf{x} = (\varphi, r, h)$, the phase correction is defined by the coefficients c_{mnl}:

$$\Delta(\varphi, r, h) = \sum_{m=0}^{N_r} \sum_{n=0}^{N_h} \sum_{l=0}^{N_\varphi} c_{mnl}\ r^m h^n \mathrm{e}^{il\varphi}\ . \tag{3.17}$$

The coefficients are computed via a linear least squares fit [67].

3.1.2 Other Routes to an Invariant Phase

Before we proceed to discuss generalized isophases of stochastic and chaotic oscillations, we wish to mention other routes towards a definition of optimal phase, that do not rely on the statistics of return times, but on the average speed of phase. This is reminiscent of the difference in definitions of the current model and the first passage model of effective phase dynamics presented in the previous chapter.

The invariant phase of limit-cycle oscillators has the special property of constant growth $\dot{\theta} = \omega$. In Ref. [40], the usefulness of the approach in data processing was discussed, and we want to repeat the main theoretical issues: In order to generalized the condition to irregular oscillations of a state $\mathbf{x}(t)$, we demand for the dynamics of its phase $\theta(\mathbf{x}(t))$ to grow with the mean frequency ω:

$$\left\langle \frac{d}{dt}\theta\left(\mathbf{x}(t)\right)\right\rangle\Big|_{\mathbf{x}(t)=\mathbf{x}} = \omega\ . \tag{3.18}$$

In order to proceed, let us be specific in considering a stochastic oscillator governed by the Langevin equation [70]

$$\dot{\mathbf{x}} = F(\mathbf{x}) + G(\mathbf{x})\xi(t)\ . \tag{3.19}$$

Performing the derivative leads to

$$\left\langle \frac{d}{dt}\theta(\mathbf{x}(t))\right\rangle\Big|_{\mathbf{x}(t)=\mathbf{x}} = \langle(\dot{\mathbf{x}}(t), \nabla)\,\theta(\mathbf{x})\rangle|_{\mathbf{x}(t)=\mathbf{x}} = \omega\ , \tag{3.20}$$

The equation can be treated numerically by parameterizing $\theta(\mathbf{x})$ as in Eq. (3.1) and estimating the time derivatives of $\mathbf{x}$. Here, we wish to discuss two possible ways to interpret the appearing average:

[3]This is a regular cylinder with an angle (phase variable) φ, a height h and a radius r.

In a perturbative approach, the time derivative $\dot{\mathbf{x}}$ is replaced by the deterministic part $F(\mathbf{x})$ [82, 90]. The resulting isophases are given by their deterministic counterpart: They are standard isophases. This approximation can only work for noise-perturbed oscillations (see Sec. 1.2.2). However, if the system under considerations shows noise-induced oscillations, standard isophases do not exist. In such cases the approach must fail to give arbitrary results.

Motivated by the results of Sec. 2.2, $\dot{\mathbf{x}}$ can be replaced by the multidimensional current velocity $\mathbf{v}(\mathbf{x})$ from the stationary Fokker-Planck equation associated to Eq. (3.19). This is equivalent to the theoretical description of Eq. (3.19) via an effective model $\dot{\mathbf{x}} = \mathbf{v}(\mathbf{x})$. The velocity can even be estimated component-wise, and efficiently from observed oscillations by [34]

$$\mathbf{v}_k(\mathbf{x}) = \lim_{\tau \to 0} \left. \frac{\langle \mathbf{x}_k(t+\tau) - \mathbf{x}_k(t-\tau) \rangle}{2\tau} \right|_{\mathbf{x}(t)=\mathbf{x}} . \tag{3.21}$$

For one-dimensional stochastic phase oscillators this approach leads to reasonable results (cf. Eq. (2.14)), but for higher-dimensional systems this approach fails: In Ref. [28], it has been pointed out that, for example, a two-dimensional effective model underlies a Hamiltonian structure. Therefore, isophases still cannot be found.

3.2 Average Isophases of Stochastic Oscillations

In this section, average isophases of stochastic oscillations are presented. First, we outline certain convergence properties of the scheme (3.13) by a noisy Landau-Stuart oscillator. Then, we discuss the isophases of noise-perturbed, noise-induced and non-Markovian oscillations by other modifications of the Landau-Stuart oscillator. Furthermore, the benefit of average isophases for the analysis of observed irregular oscillations is demonstrated by the example of regular human respiration.

Let us start with a somewhat degenerate example of noise-perturbed oscillations for which noise does not change isophases. The Landau-Stuart oscillator [Eq. (1.4)] is perturbed by multiplicative Gaussian noise $\xi(t)$, with the property $\langle \xi(t)\xi(t') \rangle = 2\delta(t-t')$, interpreted in the Stratonovich sense [70]:

$$\dot{\Psi} = (1+i\alpha)\Psi - (1+i\kappa)|\Psi|^2\Psi + \sigma\Psi\xi(t) . \tag{3.22}$$

In polar coordinates $\Psi = r\mathrm{e}^{i\theta}$, the dynamics transforms to

$$\dot{r} = r(1-r^2) + r\sigma\xi(t) , \quad \dot{\varphi} = 1 + \kappa(1-r^2) , \tag{3.23}$$

where we set $\alpha = 1+\kappa$ to ensure that $\varphi(t)$ has a positive mean frequency[4].

For the deterministic system at $\sigma = 0$, the standard isophases are defined by the transformation to the phase $\theta = \varphi - \kappa \ln r$. Taking the time derivative for $\sigma \neq 0$ yields the dynamics

$$\dot{\theta} = 1 + \sigma\kappa\xi(t) . \tag{3.24}$$

[4] An oscillation is defined by the growth of $\varphi(t)$ by 2π.

From this, two insights are gained: The noise induces an effective diffusion in the system's phase dynamics of amplitude $D = \kappa^2\sigma^2$. Furthermore, the mean return time is independent of r, and therefore, the average isophases of oscillator (3.23) are equal to the deterministic ones[5]: The phase correction is $\Delta(r) = \kappa \ln r$.

Knowing the exact phase correction, we examined the convergence of scheme (3.16) applied to time series $\Psi_n = \Psi(n\Delta t)$ of oscillator (3.23). Here, we were interested in the interplay of the damping parameter k of the scheme [Eq. (3.13)] and the non-isochronicity parameter κ. It was found that for larger κ, the scheme became less stable, and therefore k had to be chosen smaller to ensure convergence. Furthermore, The optimal value of k, qualified by a fast convergence, was smaller for a larger non-isochronicity.

The scheme was started with the polar (cylindrical) coordinates (φ, r). To measure the distance between the mth approximate phase correction and the theoretical expectation an error function was defined:

$$E_m(k,\kappa) = \sqrt{\int_{r_0}^{r_1} \frac{\left[\Delta_m(r) - \kappa \ln r\right]^2}{r_1 - r_0}\, dr}\ , \tag{3.25}$$

The limits of integration $r_0 = \min_n r_n + 0.1$ and $r_1 = \max_n r_n - 0.1$ were chosen arbitrarily in the range of the available time series $r_n = |\Psi_n|$, because elsewhere the estimation was not expected to be good. In Fig. 3.3, a comparison of $E_3(k,\kappa)$ as a function of k is presented for two values $\kappa = 1$ and $\kappa = 3$, calculated for $\sigma = 0.2$. In addition, the values of $E_0(\kappa)$ are drawn (horizontal lines). If $E_m(k,\kappa) > E_0(\kappa)$, the scheme was said to diverge. From the figure, it is seen that for stronger non-isochronicity (red curve) k has to be chosen smaller to assure convergence. Let us note that the scheme [Eq. (3.13)] can be made arbitrarily stable by choosing a sufficiently small value of k.

3.2.1 Noise-induced and Noise-perturbed Oscillations

To analyse a simple example of noise-induced oscillations, the Landau-Stuart oscillator [Eq. (3.23)] was modified to

$$\dot{r} = r(1 - r^2) + r\sigma\xi(t)\ , \quad \dot{\varphi} = \alpha + \cos\varphi - 5r^2\ . \tag{3.26}$$

First, let us discuss its deterministic dynamics for $\sigma = 0$: The nullcline of the radius variable is given by the circle $r = 1$. If it intersects the nullcline of phase, which is the circle

$$r_f(\varphi) = \sqrt{\frac{\sin\varphi + \alpha}{2}}\ , \tag{3.27}$$

[5]Notably, we have found a non-trivial stochastic oscillator for which average isophases are degenerate in the sense that noise does not change them.

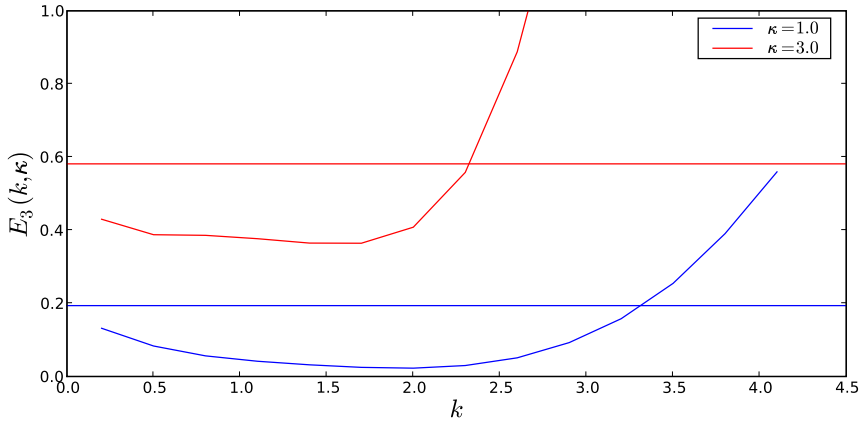

Figure 3.3: The error function $E_3(k, \kappa)$ [Eq. (3.25)] (here for $\kappa = 1$ and 3, curved lines) illustrates that for stronger non-isochronicity (larger κ), k has to be chosen smaller to assure convergence. (Divergence is indicated by a crossing of the horizontal line corresponding in color.) This one marks the value $E_0(\kappa)$ of the initial error. The estimation of phase correction was performed using time series of length $T = N\Delta t = 10^5 \cdot 0.05$ s and $N_r = 2$ (cf. Eq. (3.17)).

the dynamics (3.26) has two fixed point (cf. dashed lines in left plot of Fig. 3.5). This is true for $|\alpha - 5| < 1$. If noise is then switched on by choosing a $\sigma \neq 0$, the state can perform noise-induced oscillations[6] (see top left plot of Fig. 3.4). Noise-perturbed and noise-induced oscillations differ in frequency and coherence of oscillations, yet, their stereotypical excursions can be quite similar (cf. top plots of Fig. 3.4).

Let us describe our expectations on average isophases by the example of noise-induced oscillations of oscillator (3.26). We divide a noise-induced oscillation in a phase of excursion at $\varphi(t) \approx \pi$ and a phase of relaxation at $\varphi(t) \approx 0$. Noise excites the phase of relaxation to perform an excursion with varying amplitudes ($r(t)$ during the excursion). However, The information on the amplitude of excursion is gradually lost during the relaxation. If the return time is dominated by the period of relaxations, we can expect for the excursion, that the isophases have a tendency to be aligned along the radial direction. For the relaxation, the non-isochronicity will be stronger. Estimated average isophases of oscillator (3.26) confirm this qualitative description (see left plot of Fig. 3.5): The non-isochronicity[7] at the excursions is small compared that of the relaxation. The same qualitative behaviour is observed for noise-perturbed oscillations (cf. right plot). Apparently, the effect of noise is stronger if the dynamics is slow leading to a loss of information on the previous amplitude of the previous oscillation. We conclude from the example that average isophases apply to noise-induced and noise-perturbed oscillations in a unified way.

With the example of oscillator (3.26), we wish to explain why the scheme

[6]Oscillations are characterized through a growth of $\varphi(t)$ by 2π.
[7]The non-isochronicity is the radius dependence of phase.

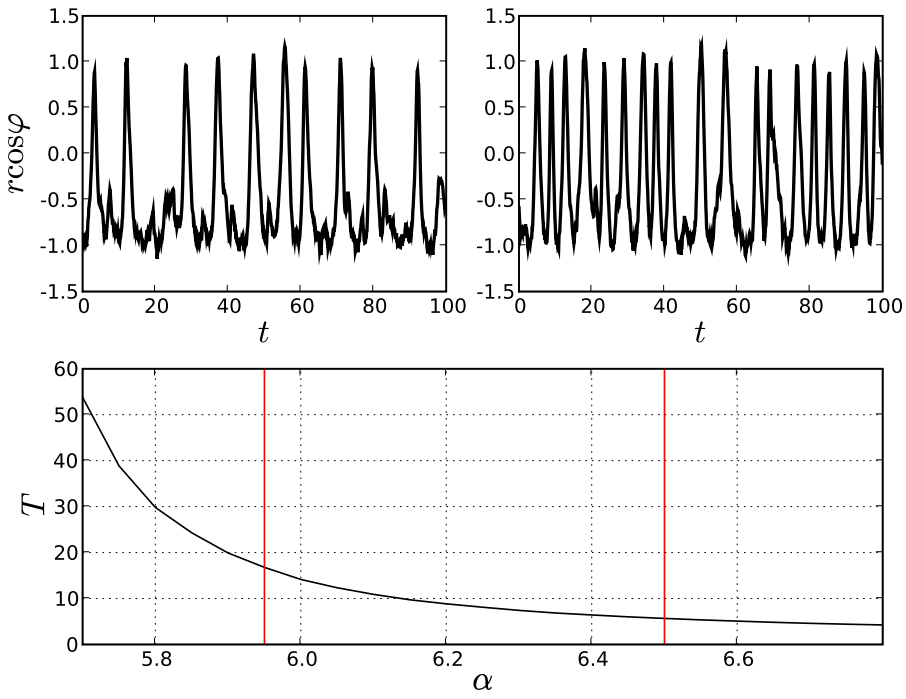

Figure 3.4: The modified Landau-Stuart oscillator [Eq. (3.26)] for $\sigma = 0.1$ and $\alpha = 5.95$ shows incoherent stereotypical noise-induced oscillations (top left plot). Noise-perturbed oscillations ($\alpha = 6.5$) are more coherent (top right plot). For both cases, the mean period T is positive (bottom plot).

(3.13) had to be modified for an application to stochastic oscillations: For radii greater then that of the circular nullcline of $r(t)$, the stationary probability current in the direction of the phase variable J_φ of oscillator (3.26) changes directions. While J_φ points into the direction of growing phase φ within the circle, it points in the opposite direction outside of it. Therefore, a locally averaged frequency [Eq. (3.14)] will not convert differences in average return times into differences in phase variable because the average has the wrong sign. To account for this, it is essential to use Eq. (3.16), where the mean frequency with the correct sign is used for all states, rather than Eq. (3.13).

3.2.2 Non-Markovian Oscillations

The definition of average isophases is applicable to non-Markovian oscillations as well. If, for example, there exist hidden variables, the corresponding average return times are computed according to the marginal probability density. This is always possible as long as variables of the system are accessible, that show the oscillations. Then, the isophases are optimal only for the given set of variables. Incorporating different variables will result in different average isophases because other marginal densities are used.

To illustrate the argument, white noise in the Landau-Stuart oscillator

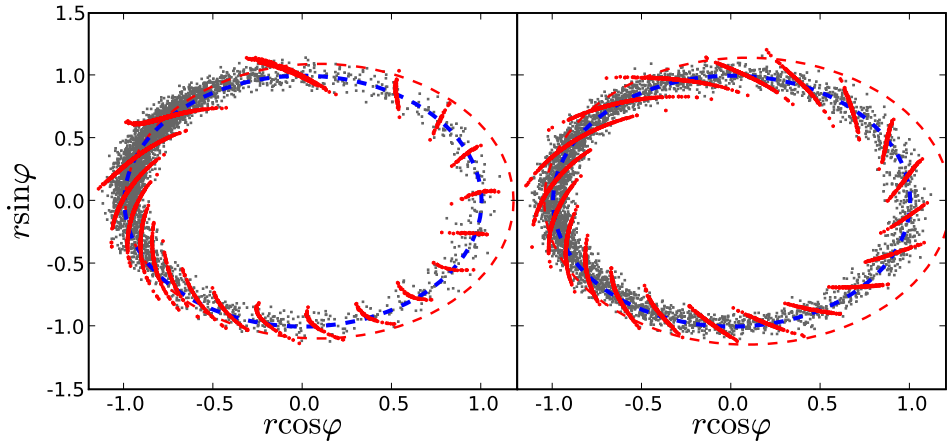

Figure 3.5: Average isophases (red lines) of oscillator (3.26), estimated with the scheme (3.16), depend on the separation of time scales of excursion and relaxation phase, here shown for $\sigma = 0.1$. As the time scales separate (from right: $\alpha = 6.5$; to left: $\alpha = 5.95$), the excursions of different radius can hardly be distinguished by their return times, and the isophases in the excursion align along the radial direction. Dashed lines mark the nullclines of the radial (blue line) and angular (red line) dynamics. The conditions of estimation were (left; right): $N\Delta t = 5\cdot 10^6\cdot 0.1$; $10^6\cdot 0.1$, $M = 40$; 35, $k = 0.02$, $N_r = 2$ and $N_\theta = 5$.

[Eq. (3.23)] is replaced by an Ornstein-Uhlenbeck process ζ that has an exponential auto-correlation function [51]. The full system is described by the three-dimensional Langevin equations[8]

$$\begin{aligned} \dot{r} &= r(1-r^2) + r\sigma\zeta \ , \quad \dot{\varphi} = 2 - r^2 \ , \\ \dot{\zeta} &= \frac{-\zeta}{\gamma} + \frac{1}{\sqrt{\gamma}}\xi(t) \ . \end{aligned} \tag{3.28}$$

But we still want to regard only the radius variable r and the phase variable φ to obtain average isophases. Without ζ, variables (φ, r) are non-Markovian[9].

Let us discuss the limiting cases of small and large time scale γ on which correlations of ζ decay. For $\gamma = 0$, we have seen that average isophases are given by the deterministic ones. This is different for $\gamma \neq 0$. Let us consider the dummy variable $\psi = \varphi - \ln r$. Its dynamics is given by

$$\dot{\psi} = 1 - \sigma\zeta \ ; \quad \dot{\zeta} = -\frac{\zeta}{\gamma} + \frac{1}{\sqrt{\gamma}}\xi(t). \tag{3.29}$$

We see that the mean period of oscillations (here parameterized through ψ) is $T_{\text{char}} = 1$ because the mean of ζ is zero. Still, ψ does not provide a phase because r and ζ are correlated. We can integrate Eq. (3.29) and obtain

$$\psi(t) - \psi(0) = t + \sigma\gamma\left[\zeta(t) - \zeta(0)\right] \ . \tag{3.30}$$

[8] $\langle \xi(t)\xi(t')\rangle = 2\delta(t-t')$.

[9] However, (φ, r) are proper cylindrical coordinates still describing what we mean by oscillation.

By requirement, we do not have information on ζ and we need to express it in terms of r to obtain average isophases. Therefore, we first average Eq. (3.30). To obtain $\zeta(r)$ we need to make an adiabatic approximation by setting $\dot{r} = 0$, in which r is enslaved by ζ. We get $\sigma\zeta(r) = r^2 - 1$. Substituting this together with the point-wise averaged good phase $\theta = t$ to Eq. (3.30) we obtain the result

$$\theta = \varphi - \ln r - \gamma \left(r^2 - 1\right) \ . \tag{3.31}$$

Here, an addition term appears in the phase correction $\Delta(r) = \gamma\,(r^2 - 1)$ proportional to the time scale of $\zeta(t)$.

In Fig. 3.6, numerical estimates of the average isophases are compared to the analytical result [Eq. (3.31)] for different values of γ. As we already know, the average isophase is equal to the standard one for $\gamma = 0$ (cf. Eq. (3.31)). For other values of γ in an intermediate range, the approximate formula (3.31) seems be a good approximation as well as seen for $\gamma = 0.5$ and $\gamma = 5$ despite of an irrelevant phase shift (red line). However, the average isophase is not valid anymore if the state is perturbed away from its equilibrium. For example, a kick applied in the radial direction is not well described by the average isophase because after the kick the hidden variable ζ is biased compared to its equilibrium according to the new radius.

We conclude that a valid phase description of non-Markovian oscillations is possible by using average isophases.

3.2.3 Average Isophases of Regular Respiration

In the following, we apply the method of average isophases to one of the datasets of regular respiration described in Ref. [61]. The Approach can lead to a novel classification of breathing patterns as well as to a definition of phase and associated quantities, that depends less on the choice of arbitrary phase. The breathing period based on the average isophase is compared to the standard marker-based breathing period from Ref. [61].

Scalar Respiratory Signal

We obtained datasets of respiratory signals of the "fantasia database" described in Ref. [61], and accessible on `www.physionet.org` [21]. It is described that using a belt around the breast, two-hour-measurements of a continuous signal of relative change in lung volume sampled at 250 Hz were taken (see Ref. [61] for details). Here, the data from subject `f1o06` were analysed.

Preprocessing and Embedding of Data

By visual inspection, *episodes of regular respiration* could be identified as stereotypical oscillations interrupted by episodes of irregular respiration (top left plot of Fig. 3.7). In addition, unidentified high frequency components were present in the data (top right plot). In a first step, the former difficulty was overcome by a visual preselection of time segments containing episodes of regular respiration. For this, periods of irregular respiration where avoided with a

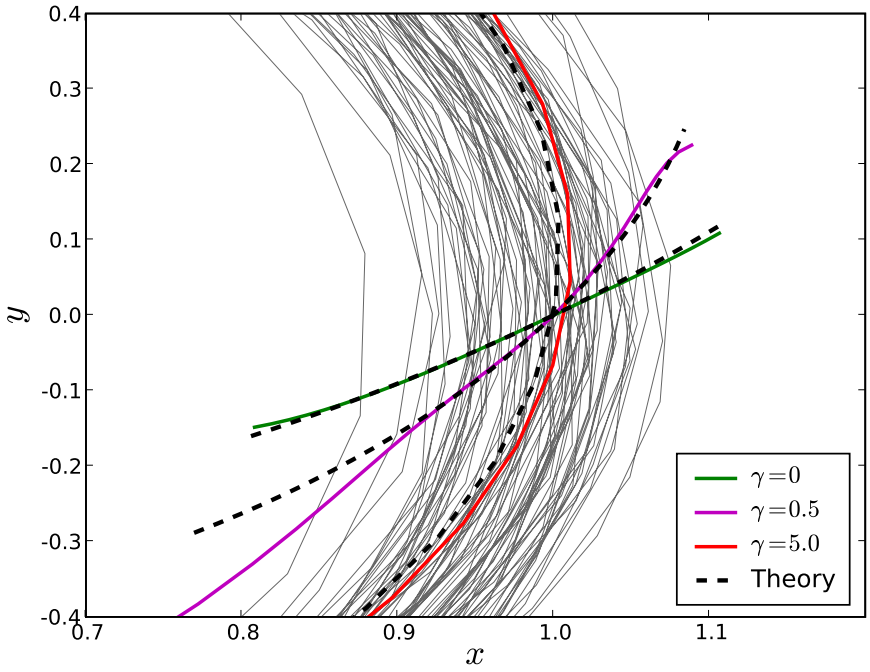

Figure 3.6: Estimated average isophases of oscillator (3.28) (colored solid lines) depend on the correlation time γ of the colored noise. The approximate formula [Eq. (3.31)] (dashed lines) works good in the whole range of γ (approximating dashed and solid lines are correspondent). The shown trajectory was computed for $\gamma = 0.5$ (gray line bundle). The conditions of estimation were: $N\Delta t = 10^5 \cdot 0.1$, $M = 10$, $k = 0.5$, and $N_r = 9$.

safety margin of 80 seconds. Thereafter, the high frequency components were filtered by applying a $(50, 50, 2)$-Savitzky-Golay filter[10] [67]. In this way 14 scalar time segments of regular respiration x_n sampled for $\Delta t = 0.004$ seconds were obtained, each containing between 10 and 100 breaths.

Different embedding techniques may be successfully applied to the preprocessed data. For example in Ref. [77], a (non-local) delay embedding in four dimensions was performed which made a description of respiration by a deterministic model possible. In favor of an easy interpretation, a differential embedding was chosen in this study [35]. Using the same Savitzky-Golay filter, the normalized first and second derivatives $\dot{x}_n$ and $\ddot{x}_n$ were estimated from data. From an inspection of the embedded data it was concluded that the regular part of dynamics is effectively two-dimensional (bottom plots of Fig. 3.7). In the $(\dot{x}, x)$ projection, the trajectory attained a broad band of states encircling a center of rotation (left plot), whereas the second derivative $\ddot{x}_n$ was linear anti-correlated to x_n (right plot). Therefore, the second derivative was

[10] A (n_l, n_r, m)-Savitzky-Golay filter uses n_l (n_r) data points to the left (right) of the central point to fit a polynomial of degree m. The polynomial is used to correct the center.

not used for the computation of average isophases.

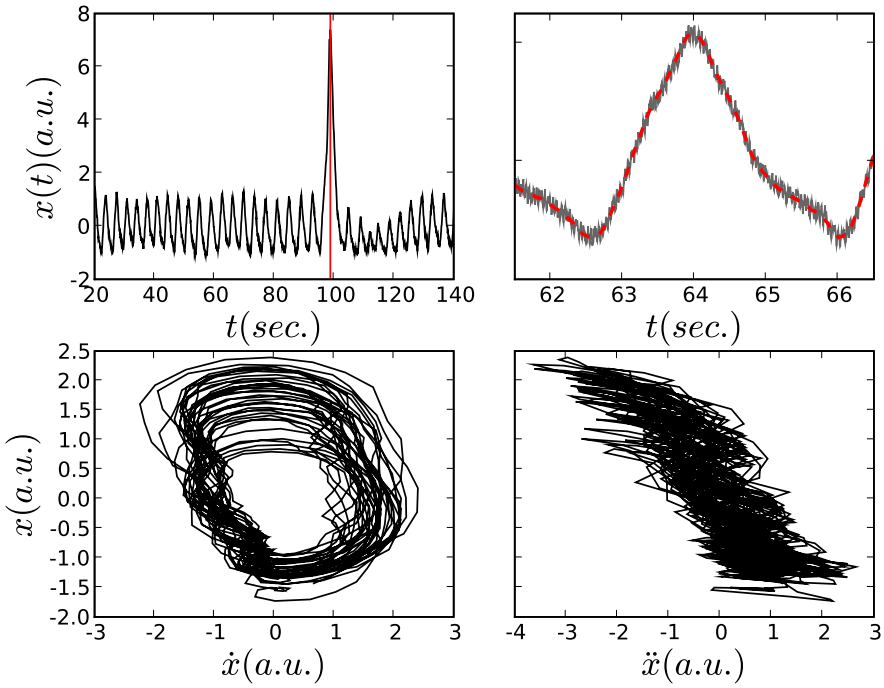

Figure 3.7: **Top plots:** Time segments of respiratory data were preprocessed by excluding irregular breaths (left: red vertical line), and measurement noise was removed by application of $(50, 50, 2)$-Savitzky-Golay filter (right: grey to red dashed line). **Bottom plots:** The embedding in the state space $(\dot{x}, x)$ reveals irregular oscillations (left), while the state space $(\ddot{x}, x)$ shows linear anti-correlation (right). (a. u.: arbitrary units)

Construction of Average Isophases

After finding a suitable embedding, polar coordinates were chosen by $\varphi_n = \tan^{-1}(x_n/\dot{x}_n)$ and $r_n = \sqrt{x_n^2 + \dot{x}_n^2}$. They serve as a starting point for the estimation of average isophases by the scheme (3.13). For each preprocessed and embedded time segment of regular respiration, the isophases were estimated and compared. During the iterative estimation, the convergence was checked visually. Convergence was reached after $M \approx 50$ iteration steps at $k = 0.05$. Another problem posed the polynomials used for an estimation of return times $T_m(\varphi, r)$. To allow for sufficient smoothing we fixed the parameters $N_\varphi = 3$ and $N_r = 2$. We also inspected the estimation upon changing these parameters in a certain range to validate the robustness of each fit. For datasets containing at least 50 oscillations it was found that the isophases did not change qualitatively.

Dependent on the time segment, estimated average isophases demonstrated characteristic patterns that could be ordered in two groups (cf. Fig. 3.8). These

groups (A: plots (a,b) and B: plots (c,d)) differed by form and skewness of the isophases. Unlike for example the heart beat, the timing and depth of respiration, that shape the isophase, are under the control of the conscious mind. Therefore, the pattern of the isophases observed in groups A and B is unexpectedly coherent. This coherence provides evidence for the applicability of the approach. Moreover, more valuable information might be hidden in the classification.

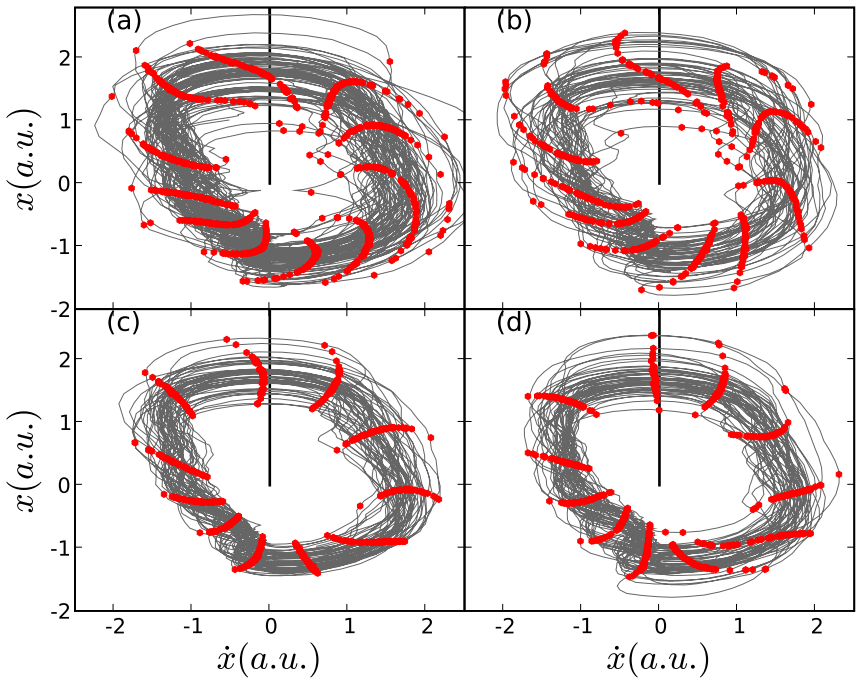

Figure 3.8: Time segments of regular respiration (gray line) containing 89 (a), 53 (b), 52 (c) and 51 (d) oscillations together with estimated average isophases $I_M(\theta)$ (red dots) illustrate similarity in groups A (a,b) and B (c,d). The begin of respiratory cycles as defined in Ref. [61] (black vertical line) can be different from the corresponding isophase $I_M(\pi/2)$ as seen in group A. The conditions of estimation were: $\Delta t = 0.004$ s, $M = 50$, $k = 0.05$, and $N_r = 2$, $N_\theta = 3$. (a. u.: arbitrary units)

Distribution of Inter-breath Intervals

In Ref. [61], fractal scaling properties of human respiratory dynamics was studied by performing detrended fluctuation analysis of time series of inter-breath intervals. Such a breathing period was measured as the time between two markers defined as local maxima of the respiratory signal. In our context, the breathing period is defined as the time it takes for the phase to grow by 2π. Therefore, let us interpret the marker-based approach in the context of phase dynamics. A local maximum is defined by the conditions $\dot{x} = 0$ and $\ddot{x} < 0$.

Therefore, the marker-based breathing period is equivalent to the return time of the Poincaré section $I_0 = I_0(\pi/2) = \{x > 0,\ \dot{x} = 0\}$ (cf. Fig. 3.8).

The estimation presented in Fig. 3.8 suggested the possibility of an optimal definition of breathing period using average isophases. Therefore, we compared two calculations of the breathing period, one using the section I_0 and the second one using the corresponding estimated average isophase $I_M = I_M(\pi/2)$ (cf. Fig. 3.8). For the comparison, we computed return times T_k of the respective sections I_k and compared them. The comparison shown in Fig. 3.9, demonstrates that although the two periods strongly correlated, for group A there were also significant deviations between them. Contrary, for group B the periods are almost indistinguishable which was expected from the similarity of the respective Poincaré sections (see especially plot (d) of Fig. 3.8).

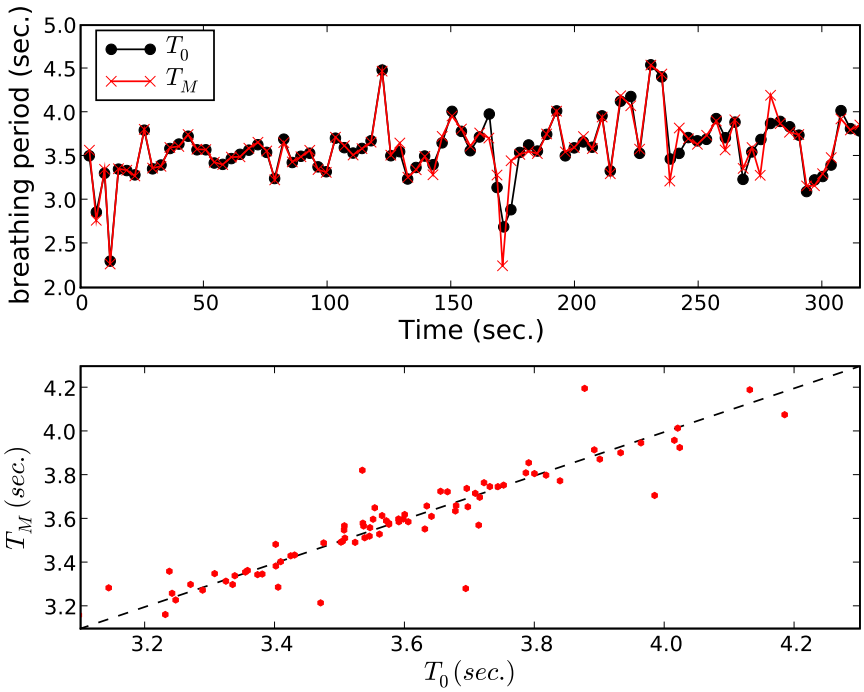

Figure 3.9: The breathing period T_0, computed as in Ref. [61], shows strong correlations to the return times T_M of the corresponding average isophase (shown for the same data as in Fig. 3.8 (a)).

Comparing the breathing periods of a marker-based technique with those computed from estimated average isophase, certain quantitative deviations were observed (cf. Fig. 3.9). These deviations are intrinsic errors generated by the arbitrary choice of markers: Other arbitrary markers would yield different deviations. In contrast, the isophases are invariant up to statistical fluctuations. Therefore, the method may lead to a better definition of breathing period.

3.3 Generalized Isophases of Chaotic Oscillations

In this section, we discuss the possibility and value of generalized isophases of chaotic oscillators [Eq. (1.16)]. The isophases only exist for certain subsets of the chaotic attractor, namely embedded **unstable periodic orbits (UPOs)** and their unstable manifold. For a typical chaotic trajectory that shows chaotic oscillations, the isophases can only be approximated due to UPOs and chaotic phase diffusion (cf. condition (3.9)). With better approximations of the generalized isophase it winds itself around all UPOs (cf. Fig. 3.2). Evidence for this intimate relationship is provided in various ways including a comparison of good approximate isophases and the isophases of UPOs by means of their Floquet multipliers. After we have seen that states can only be characterized to be approximately in the same phase, it is shown that the isophases are still compatible with the criterion of phase reduction if phase diffusion is weak. Therefore, the corresponding phase variable can be described by a simple phase equation driven by correlated noise. This is illustrated by a numerical estimation of chaotic phase diffusion based on the stochastic phase dynamics, that corresponds well to the estimate (1.24).

Let us suppose, we had found a family of generalized isophases $I(\theta)$ on the chaotic attractor, that obeys condition (3.2), exactly. In this case, the characteristic period is the mean period of a typical chaotic trajectory: $T_{\text{char}} = T$. The associated unwound phase variable $\theta(t)$ obeys $\theta(t + T_{\text{char}}) = \theta(t) + 2\pi$. Using this property to compute the chaotic phase diffusion [Eq. (1.23)], we obtain

$$D = \lim_{n\to\infty} \frac{\langle [\theta(nT_{\text{char}}) - 2\pi n]^2 \rangle}{2nT_{\text{char}}} = 0 \ , \ \text{for } n \in \mathbb{N} \ . \tag{3.32}$$

By this simple calculation, it is seen that the family does not exist if the chaotic oscillations show a non-zero phase diffusion.

3.3.1 Generalized Isophases of Unstable Periodic Orbits

Embedded in the chaotic attractor are an infinite number of **unstable periodic orbits (UPOs)** $\mathbf{x}_0(t + \tau) = \mathbf{x}_0(t)$, each one having a different period τ (cf. Sec. 1.4). With an arbitrary phase φ of the chaotic oscillator, that is unwound, a *lap number* and an *oscillation period*

$$p = \frac{\varphi(\mathbf{x}_0(\tau)) - \varphi(\mathbf{x}_0(0))}{2\pi} \ , \text{ and } S = \frac{2\pi}{\nu} = \frac{\tau}{p} \tag{3.33}$$

may be assigned to the UPO (cf. Sec. 1.4). Furthermore, a point set $I(\theta)$, called *orbit phase set*, that obeys condition (3.2) with characteristic period S is obtained: If one fixes a zero phase by assigning $\theta(\mathbf{x}_0(0)) = \theta$, $I(\theta)$ is given by

$$I(\theta) = \{\mathbf{x}_0(nS) \mid n = 0, \ldots, p-1\} \ . \tag{3.34}$$

It fulfills condition (3.2) for all points of the orbit. Furthermore, one may demand that the *orbit phase* $\theta(t)$ grows uniformly: $\dot{\theta} = \nu$. Then, $\theta(t)$ is

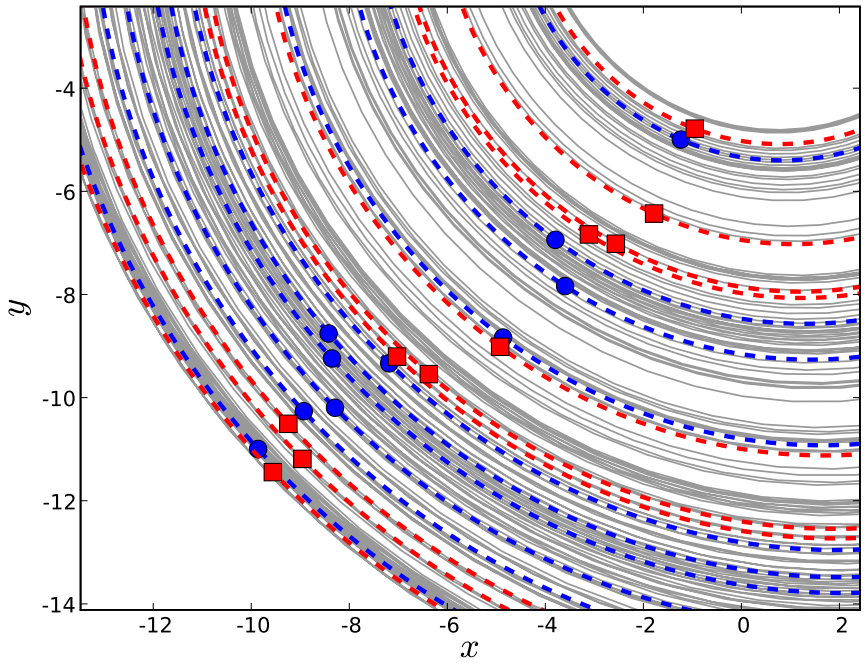

Figure 3.10: The orbit phase sets [Eq. (3.34)] of two $p = 10$ UPOs (red and blue dashed lines) of the Rössler oscillator [Eq. (1.17)] were computed and the arbitrary phase shift of each was chosen such that the orbit phase sets $I(4\pi/3)$ (red squares and blue circles) of the orbits coincided the most. The sets approximately describe the same curve in state space.

uniquely defined. In Fig. 3.10, the orbit phase set for $\theta = 4\pi/3$ of two UPOs with lap number $p = 10$ are plotted. Since the orbits do not share any states, the zero phases can be chosen separately. For example, it can be chosen such that orbit phase sets coincide the most for each value of θ, as shown in the figure.

The definition of orbit phase set [Eq. (3.34)] can be extended to the unstable manifold $W^u(\mathbf{x}_0)$ of the UPO $\mathbf{x}_0(t)$ by considering the time reversed dynamics: Asymptotically, each state $\mathbf{x}(t) \in W^u(\mathbf{x}_0)$ shares its past with a certain state $\mathbf{x}_0(t)$ on the UPO:

$$\lim_{t \to -\infty} ||\mathbf{x}(t) - \mathbf{x}_0(t)|| = 0 \ . \tag{3.35}$$

Then, $\mathbf{x}$ is assigned the same phase as $\mathbf{x}_0$: $\theta(\mathbf{x}) = \theta(\mathbf{x}_0)$. This is similar to the construction of standard isophase (cf. condition (1.3)). This, so called, *orbit isophase* $I(\theta) \subset W^u(\mathbf{x}_0)$ fulfills the condition of generalized isophases [Eq. (3.2)] for $T_{\text{char}} = S$.

The mean period T of a typical chaotic trajectory does not usually coincide with the oscillation period of one of the unstable periodic orbits. Therefore, it is useful to discuss the case of an orbit isophase $I(\theta) \subset W^u(\mathbf{x}_0)$ fulfilling condition (3.2) for $T_{\text{char}} = T$, as well. For a three-dimensional chaotic oscillator, for which $W^u(\mathbf{x}_0)$ is two-dimensional, the situation is equivalent to the

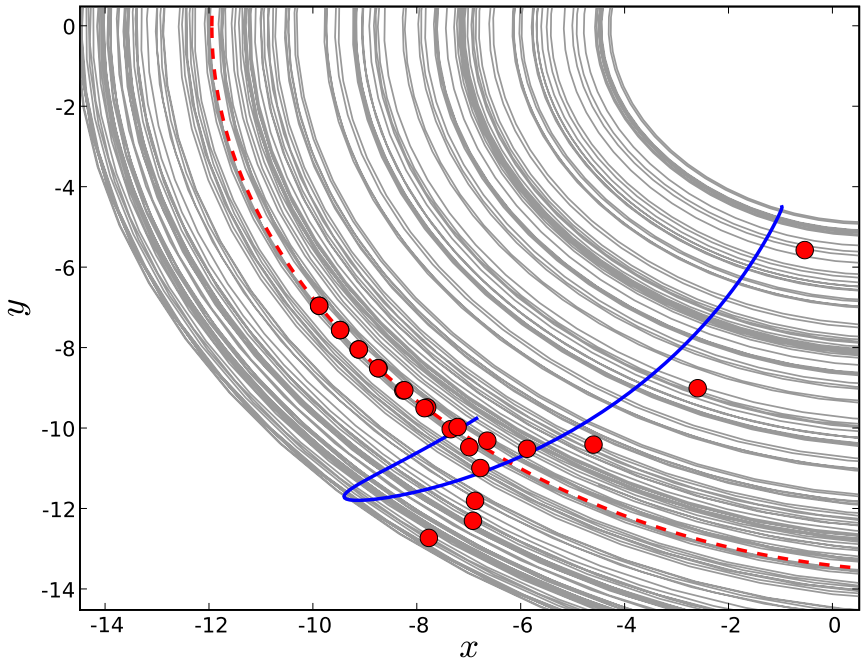

Figure 3.11: For a UPO of the Rössler oscillator [Eq. (1.17)], the orbit phase set [Eq. (3.34)] can be extended to the unstable manifold in two ways: One can use as the orbit's period S as characteristic (blue line), or the mean period (red circles) of the chaotic attractor that is shown grey lines, here shown for the 1-orbit. Using the mean period leads to a divergence of the phase correction as for oscillator (3.3) (cf. Fig. 3.2).

unstable Landau-Stuart oscillator for which it was shown that a generalized isophase winds itself infinitely often as it approaches the orbit (cf. Fig. 3.2).

Let us consider the simplest UPO of the Rössler oscillator that has a lap number $p = 1$. Its oscillation period is $S \approx 6.024$ whereas the mean period of a typical trajectory is $T \approx 6.073$. Numerically, we calculate the orbit isophase $I(\theta)$ for a single value of θ. For $T_{\text{char}} = S$, the orbit isophase $I(\theta)$ is a smooth curve that even resembles to a certain extent the orbit phase sets of UPOs with large lap number (cf. Fig. 3.10 and 3.11). For $T_{\text{char}} = T$ (red circles in Fig. 3.11), the orbit isophase winds itself around the UPO as expected (cf. Fig. 3.2).

3.3.2 Approximate Isophases

Generalized isophases of chaotic oscillations would wind themself around all **unstable periodic orbits (UPOs)**. Therefore, they can only be obtained in an approximate way by fulfilling condition (3.9) with a small but finite recurrence error $\varepsilon(\mathbf{x})$. The characteristic period is now the mean period of a typical chaotic trajectory. How small may the recurrence error be? Because

of the UPOs, we can give certain bounds to $\varepsilon(\mathbf{x})$: For each state $\mathbf{x}_0$ of such an UPO with oscillation period S, we obtain the inequality

$$|\varepsilon(\mathbf{x}_0)| \geq |S - T| \ . \tag{3.36}$$

This gives a lower bound for the recurrence error at each state of an UPO. A *good* approximate isophase has a recurrence error close to the bound (3.36).

The numerical scheme for an estimation of generalized isophases [Eq. (3.13)] is iterative providing increasingly better approximations of condition (3.2). In the light of the weakened condition (3.9), the recurrence error $\varepsilon_m(\mathbf{x})$ of the mth iteration decreases with each further step. From the examples discussed in Fig. 3.2 and 3.11, it is expected that, as the recurrence error approaches its natural bound [Ineq. (3.36)], the arc length – in state space – of the approximate isophase diverges as it winds itself around numerous UPOs. To verify this idea, a sequence of approximate isophase I_m starting at the arbitrary Poincaré section $I_0(4\pi/3)$ [Eq. (1.19)] was computed for the Rössler oscillator using smoothing splines (cf. Sec. 3.1.1). The results are shown in Fig. 3.12. For each iteration, the arc length a_m of I_m in the boundaries of the attractor was monitored. In addition, the standard deviation of return times $\hat{\varepsilon}_m^2 = \langle T_m^2(\mathbf{x})\rangle - T^2$ was monitored as a measure of $\varepsilon_m(\mathbf{x})$. It was seen that a_m diverges as $\hat{\varepsilon}_m$ gets smaller (black dashed line in left plot). More precisely, the point of divergence was estimated to be at a finite value of $\hat{\varepsilon}_m$ as expected from the lower boundary of recurrence error [Ineq. (3.36)]. This could be verified further, by the standard deviation of oscillation periods of a set of 80 UPOs computed for the Rössler oscillator: The value of the standard deviation (red vertical line) appears to be close to the limit point $\lim_{m\to\infty} \hat{\varepsilon}_m$. The observation gives evidence that a smooth approximate isophase is torn apart by quasi-randomly distributed UPOs in the attractor as the approximation gets better (cf. Fig. 3.13). The isophases computed via smoothing splines were also compared [Fig. 3.13] to the corresponding member of a family of approximate isophases $I(\theta)$ of the Rössler oscillator, that were modeled with polynomial basis functions marked as a blue square in Fig. 3.12, and drawn as a blue line in Fig. 3.13. This "blue" approximate isophase is similar to the green one obtained via smoothing splines. But because smoothing splines allow for more discontinuity, the corresponding isophases are longer (cf. right plot of Fig. 3.13).

The example illustrates that Ineq. (3.36) implies how good approximate isophases can be. However, the merit of a better approximation does not become apparent. By the example of the Rössler oscillator [Eq. (1.17)], we want to give numerical evidence for the qualitative advantage of better approximate isophases, too: The key property of generalized isophases is the decoupling of the phase dynamics from the amplitudes. Of course this decoupling is broken in the approximation (3.9), but the amplitude dependence becomes less regular and may be treated as a random distortion to the phase dynamics.

The approximate decoupling of phase and amplitude dynamics becomes most apparent for systems with weak phase diffusion. Then, the states on a good approximate isophase will keep their information in phase longer then

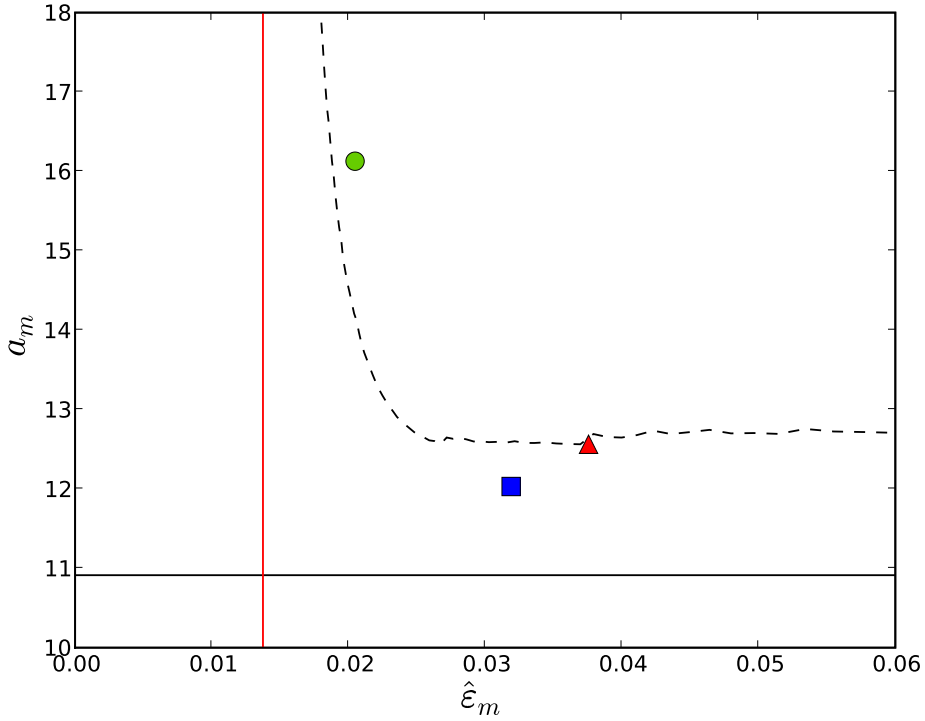

Figure 3.12: The arc length a_m as a function of $\hat{\varepsilon}_m$ (dashed line) of a sequence of approximate isophases $I_m(4\pi/3)$ of oscillator (1.17) diverges as the approximation approaches the bound (3.36) set by UPOs (red vertical line). The black horizontal line marks the arc length of the arbitrary Poincaré section $I_0(4\pi/3)$ [Eq. (1.19)]. The sequence of approximate isophases was computed using smoothing splines, whereas the one marked in blue is a member of the family presented in Fig. 3.17. This one is shorter because polynomials of a global model [Eq. (3.17)] allow for less irregularity than smoothing splines. In this sense, they are more efficient.

their amplitude information. This is illustrated in Fig. 3.14, where states starting (for $t = 0$) at the arbitrary Poincaré section $I_0(4\pi/3)$ [Eq. (1.19)] (top plots) and at a good approximate isophase $I_M(4\pi/3)$ (bottom plots) are computed at $t = 10 \cdot T$. One can see that the broadening along the direction of phase is less pronounced for the approximate isophase. More importantly, differences in amplitude are not systematically transfered into differences in phase, but seem to become distributed quasi-randomly along the approximate isophase as a result of the stretching and folding mechanism.

3.3.3 Connection to Floquet Multipliers

The relationship between **unstable periodic orbits (UPOs)** and the approximate isophases of chaotic oscillations can be strengthened by taking into ac-

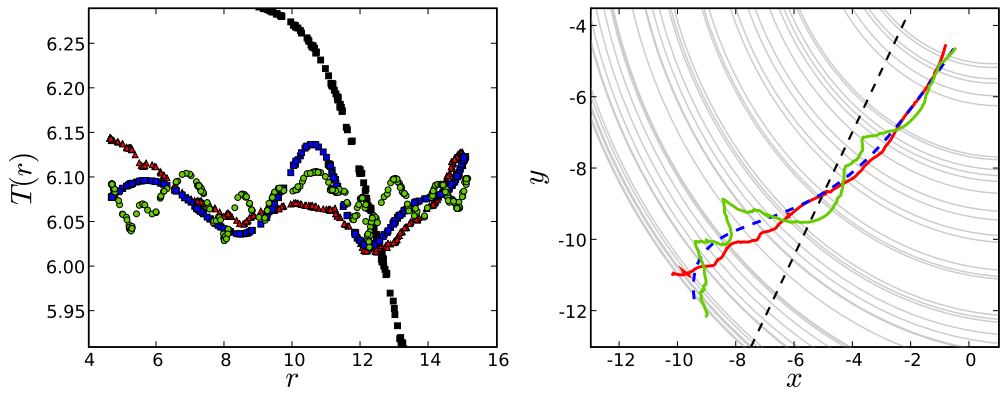

Figure 3.13: Good approximate isophases [Eq. (3.9)] of the Rössler oscillator [Eq. (1.17)] (colors as in Fig. 3.12) have a narrower distribution of return times as $I_0(4\pi/3)$ marked in black (left plot). However, they are less continuous as well (right plot). Approximate isophases computed using smoothing splines (red and green) can be less smooth than those modeled by polynomials [Eq. (3.17)] (blue).

count the stability of UPOs through their unstable Floquet multiplier (cf. Appendix A). It is expected that the isophase fulfills Ineq. (3.36) with better accuracy for UPOs that are visited more often because they are less unstable. To illustrate this with the Rössler oscillator [Eq. (1.17)], a measure of distance of a p-orbit $\mathbf{y}$ to the good approximate isophase $I(4\pi/3)$ (green circle in Fig. 3.12) was introduced. The p common states of the approximate isophase and the orbit $\mathbf{y}_j \in I(4\pi/3)$ ordered by the orbit's time evolution were computed. Now, we considered the states $\mathbf{y}_j^J$ of the orbit phase set $J(\alpha) \ni \mathbf{y}_0$, where the states $\mathbf{y}_j^J$ were ordered by the orbit's time evolution as well, starting with $\mathbf{y}_0^J = \mathbf{y}_0$. Therefore, each $\mathbf{y}_j^J$ approximated $\mathbf{y}_j$. Now, α was varied in a certain range[11] to minimize the euclidean distance

$$d = \sqrt{\sum_{k=0}^{p-1} \frac{||\mathbf{y}_k^J - \mathbf{y}_k||^2}{p-1}} \ . \tag{3.37}$$

The minimized distance d measured how well an orbit phase set is approximated by the approximate isophase. The measure was calculated for the 80 available UPOs together with their Floquet multipliers. It was found that orbits showing a larger distance had a tendency to be less stable (right plot of Fig. 3.15). Visually, it was observed that all analysed UPOs were well approximated. For illustration, a 10-orbit and a 9-orbit from the lower and upper range of d are displayed in state space together with the approximate isophase as well as their respective orbit phase sets (left plot).

It seems that the orbit isophase of an UPO with a high lap number approximates a good approximate isophase, well. However, the observed relationship

[11] The numerical optimum was always within a view degrees of the starting value.

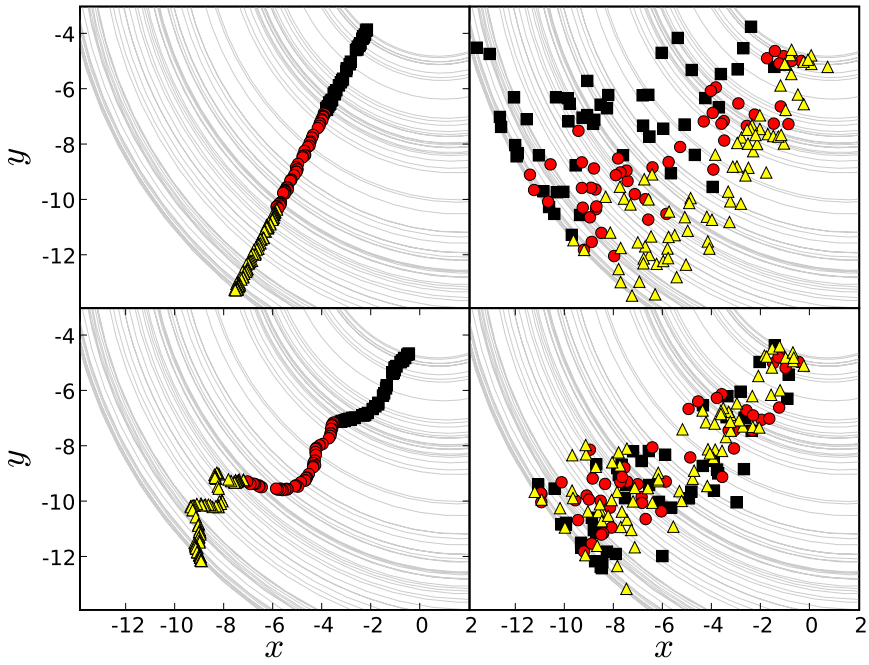

Figure 3.14: Initial states (marked as symbols) on the arbitrary Poincaré section $I_0(4\pi/3)$ [Eq. (1.19)] (upper left plot) and approximate isophase $I_M(4\pi/3)$ (lower left plot, marked by a green circle in Fig. 3.12) are computed at $t = 10{\cdot}T$ (10 average rotations), here shown for the Rössler oscillator [Eq. (1.17)]. States on the good approximate isophase shows less diffusive broadening in direction of the phase than the arbitrary Poincaré section after 10 average rotations (corresponding left plots). Moreover, states of different amplitude become indistinguishable only for the good approximate isophase as seen by the mixing of colors.

displayed in the right plot of Fig. 3.15 is not clear enough to draw any precise conclusion.

3.3.4 Correlation and Phase Diffusion

After we have identified the states of chaotic oscillations that are approximately in the same phase, we present correlation properties of the reduced phase dynamics by means of the frequency fluctuations of the approximate phase variable.

Let us first consider the frequencies ω_n with which a typical chaotic trajectory returns to an arbitrary Poincaré section $J(\varphi)$. The return frequency obeys the *return frequency relation*

$$\omega_{n+1} = M(\omega_n) \ . \tag{3.38}$$

In general $M(\omega_n)$ is not a function because one ω_n may have several outcomes. The distribution of states in the *frequency state space* (ω_n, ω_{n+1}) will be fractal

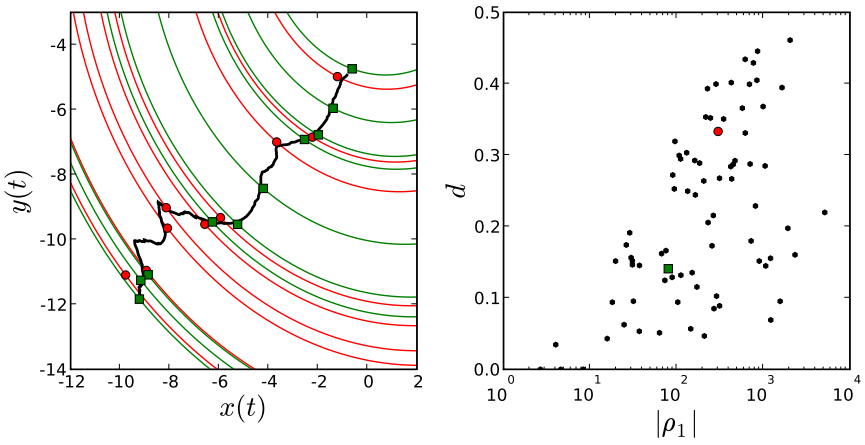

Figure 3.15: **Left plot:** The good approximate isophase [Eq. (3.9)] (black line), marked as a green circle in Fig. 3.12, of the Rössler oscillator [Eq. (1.17)] resembles the phase shift adjusted orbit isophases [Eq. (3.34)] with varying accuracy, here shown for a 9-orbit (red circles) and a 10-orbit (green squares). **Right plot:** A distance measure d [Eq. (3.37)] quantifies this accuracy. Weak correlations to the instability of the UPOs measured by the Floquet multiplier $|\rho_1|$ are observable, here shown for 80 p-orbits with $p \leq 10$.

with a dimension less than one, as shown for the section $I_0(4\pi/3)$ [Eq. (1.19)] of the Rössler oscillator in the left plot of Fig. 3.16. However, for a good approximate isophase $I(\theta)$ [Eq. (3.9)], the return frequency relation acquires a special shape: Let us consider a p-orbit with oscillation period S and an intersection $\mathbf{x} \in I(\varphi)$. The frequency of return will be close to $2\pi/S$ in the vicinity of $\mathbf{x}$ (cf. Ineq. (3.36)). Thus, each intersection lies close to the diagonal of the frequency state space in a random way (cf. right plot of Fig. 3.16).

The return frequency to a good approximate isophase may be described as a correlated random process. However, this does not tell us how fluctuations are distributed among the phases of oscillation. For this, we considered a long enough typical trajectory of the Rössler oscillator. Via the cylindrical coordinates (1.19), we obtained the approximate phase variable $\theta_n = \theta(n\Delta t)$ of a family of approximate isophases (blue square in Fig. 3.12 and Fig. 3.17). In order to eliminate "deterministic" non-uniformities of the dynamics, θ_n was adjusted using Eq. (1.2). Then, the numerical derivative[12] $\dot{\theta} \approx (\theta_{n+1} - \theta_{n-1})/2\Delta t$ was estimated. It serves as an estimate of the phase velocity that fluctuates around its mean value ω (cf. Fig. 3.18). We compared the phase velocity $\dot{\theta}$ to that of the arbitrary phase variable φ [Eq. (1.19)]. While fluctuations in the arbitrary phase velocity $\dot{\varphi}$ depended on φ, the fluctuations of $\dot{\theta}$ were almost uniformly distributed and, notably, sometimes larger than that of the arbitrary phase. Similar results are reported in Ref. [40]. We conclude that approximate isophases do not only eliminate the amplitude dependence of the phase veloc-

[12] $\Delta t = 0.01$ was chosen small enough.

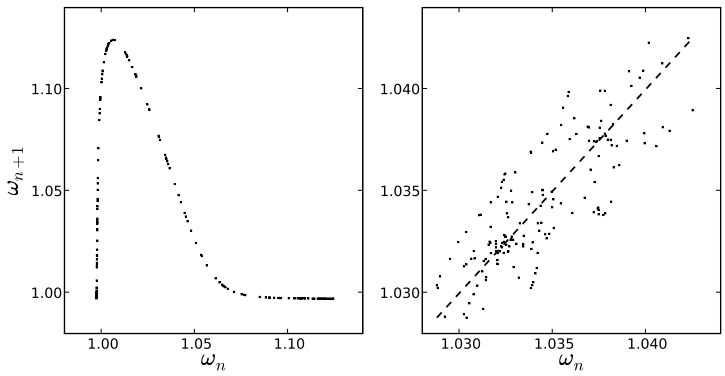

Figure 3.16: The return frequency relation [Eq. (3.38)] of the Rössler oscillator [Eq. (1.17)] for the arbitrary Poincaré section $I_0(4\pi/3)$ [Eq. (1.19)] can be described as a chaotic map (left), whereas a good approximate isophase $I(4\pi/3)$ [Eq. (3.9)] (green circle in Fig. 3.12) has a random nature (right plot). Close passages of unstable periodic orbits should lie on the diagonal (dashed line in right plot).

ity, but they also flatten the phase dependence on its velocity fluctuations. We suspect that the dependence will get less pronounced for better approximate isophases.

From Fig. 3.16 and 3.18, it becomes apparent that the new quality of good approximate isophases is a uniformly random influence of amplitudes on the phase dynamics rather then a phase dependent low-dimensional deterministic one. Therefore, we model chaotic oscillations by the stochastic phase equation

$$\dot{\theta} = \omega + \eta(t) \ ; \ \ \theta(t) = \omega t + \int_0^t \eta(t') \ dt' \ . \tag{3.39}$$

Here enters their mean frequency ω and an additive effective noise term $\eta(t)$ that represents the uniform fluctuations in phase velocity (cf. Fig. 3.18).

The stochastic phase description Eq. (3.39) holds best for good approximate isophases. Therefore, we consider a single approximate isophase that, as it was shown, could be obtained with good accuracy (cf. Fig. 3.12). To draw a connection to the phase diffusion coefficient [Eq. (1.23)], a coarse-grained variable

$$\Delta\theta_n = \int_{t_n}^{t_{n+1}} \eta(t') \ dt' \tag{3.40}$$

is computed, and the equation is rewritten as $\Delta\theta_n = T_n(\omega_n - \omega)$. Let us note that $\Delta\theta_n$ can be defined for both, an arbitrary phase $\varphi(t)$ and a phase $\theta(t)$ parameterizing a good approximate isophase. Now, a relation between

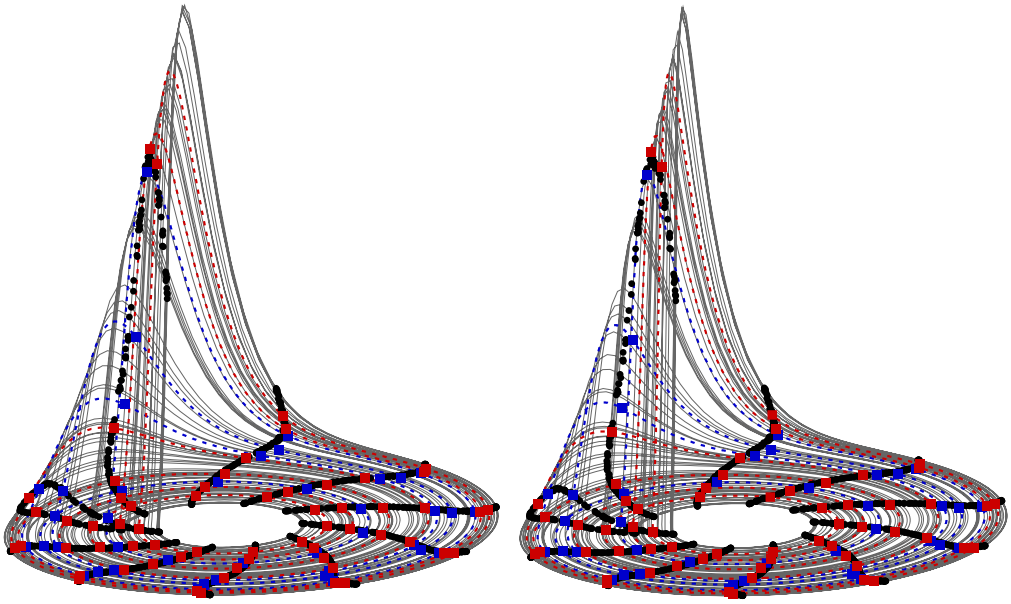

Figure 3.17: Stereogram of Rössler's attractor (grey line) together with return points to chosen members $I(\theta)$ of a family of approximate isophases (black dots) correspond well to a family of orbit phase sets (blue and red squares) of a 4-orbit and a 6-orbit (dashed lines). The conditions of estimation were: $N\Delta t = 10^5 \cdot 0.2$ s, $M = 30$, $k = 0.2$, $N_\varphi = 4$, $N_r = 4$ and $N_h = 1$. (See instructions for use in Appendix C.1.)

effective noise and phase diffusion coefficient is obtained:

$$\begin{aligned} D &= \frac{1}{2T} \sum_{q=-\infty}^{\infty} K_q \ , \\ K_q &= \langle \Delta\theta_0 \Delta\theta_q \rangle \ . \end{aligned} \tag{3.41}$$

The formula allows us to compute an estimate of the phase diffusion coefficient from the correlations of frequency fluctuations.

The stochastic phase description [Eq. (3.39)] was tested for the Rössler oscillator [Eq. (1.17)], where a good approximate isophase (green circle in Fig. 3.12) was used to compute ω_n. We computed the coarse-grained autocorrelation function K_q for recurrence data $\Delta\theta_n$ (see top left plot of Fig. 3.19). For this, we used time series of approximately 8000 returns. Then, Eq. (3.41) was evaluated to estimate the phase diffusion coefficient D. The estimation was performed in 50 independent trials yielding on average

$$\hat{D} = 8.395 \cdot 10^{-5} \pm \frac{2.427 \cdot 10^{-5}}{\sqrt{50}} \text{ rad s}^{-1} \ . \tag{3.42}$$

The estimate is close to the value [Eq. (1.24)] obtained via the Brownian bridge method. To illustrate how the procedure depends on the goodness of the approximate isophase, we compared the result with an estimate obtained for

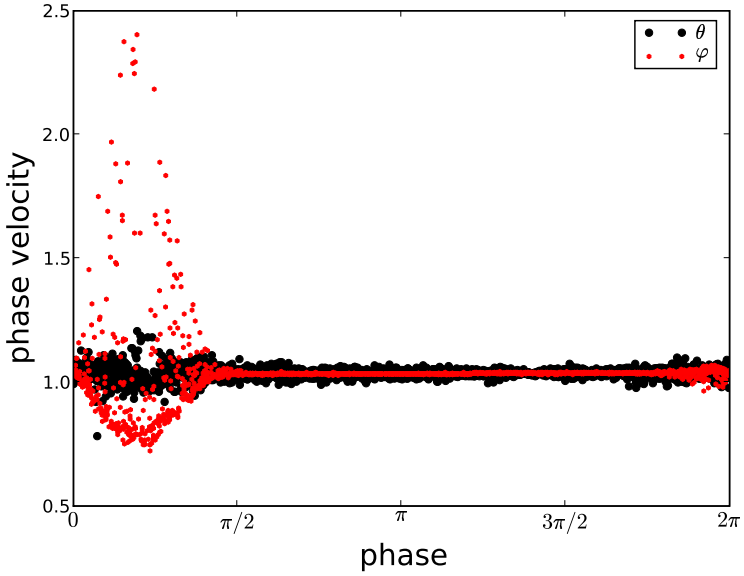

Figure 3.18: The phase velocity $\dot{\theta}$ of the family of approximate isophases $I_M(\varphi)$ that is shown in Fig. 3.12 of the Rössler oscillator [Eq. (1.17)] shows fluctuations that are distributed more uniformly than the velocity $\dot{\varphi}$ of the family of arbitrary Poincaré sections $I_0(\varphi)$ [Eq. (1.19)].

the arbitrary Poincaré section $I_0(4\pi/3)$ [Eq. (1.19)]. For this, the procedure was performed exactly as for the approximate isophase yielding an estimate $\hat{D} \approx 0.003 \pm 0.0001$ rad s^{-1} which is two orders of magnitude to large.

It seemed that the coarse-grained variable $\Delta\theta_n$, computed from the approximate isophase of the Rössler oscillator [Eq. (1.17)], showed a strong oscillatory component which was also manifest in its autocorrelation function by a negative deflection at about $q = 7$ (cf. top plots of Fig. 3.19). We found that, the phenomenon was present to a varying extent using different approximate isophases. Though robust in this sense, it cannot be ruled out that the observed oscillatory component is an artefact of the construction algorithm used to obtain the approximate isophases.

3.4 Conclusions

In summary, we generalized the concept of standard isophases for an application to chaotic and stochastic irregular oscillations. For stochastic oscillations, the generalized isophases were defined in an average sense. They allowed for a generalized method of phase reduction with which noise-perturbed, noise-induced, and non-Markovian oscillations are treatable in a unified way. Furthermore, an algorithm for the estimation of the isophases from observed oscillations was proposed, and it was successfully applied to signals of regular human respiration. For chaotic oscillations, generalized isophases could only

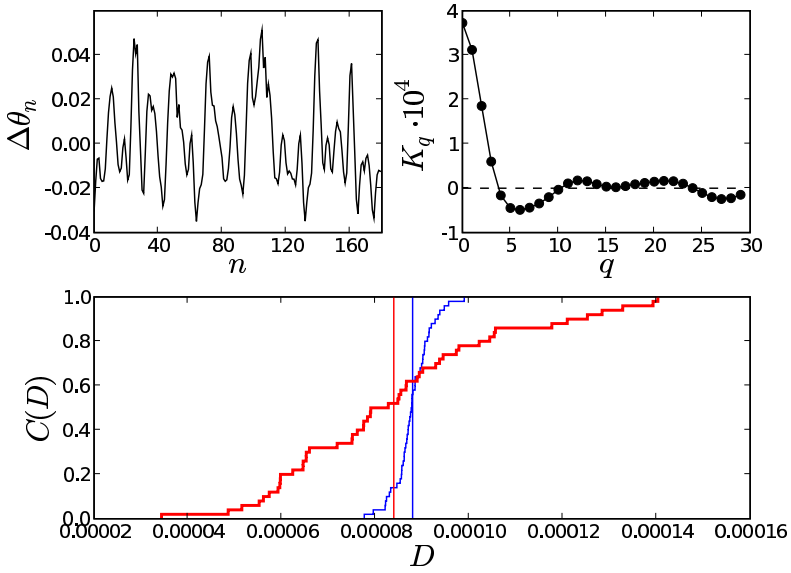

Figure 3.19: The coarse-grained variable $\Delta\theta_n$ [Eq. (3.40)] (top left plot) shows oscillatory fluctuations that are reflected in its autocorrelation function K_q [Eq. (3.41)] by a negative deflection (top right plot). **Bottom plot:** Cumulative probability distributions of 50 estimates of the phase diffusion coefficient, computed from Eq. (3.41) (red line), and using the Brownian bridge method (Appendix B) (blue line) show comparable mean values (red vertical lines). The distribution of the former (red) values is broader because less data was used.

be defined in an approximate way. Still, good approximate isophases of the Rössler oscillator led to a qualitatively better phase reduction in which chaos was treatable as a uniformly random perturbation to the phase dynamics.

In order to obtain a reduced phase dynamics of irregular oscillations, states of the same phase have to be identified along certain Poincaré sections. For weakly perturbed limit-cycle oscillators standard isophases allow for an invariant identification because they are based on the limit-cycle. But whenever a stable limit-cycle is absent or cannot be inferred, the theory of generalized isophases is needed. Because the definition of the isophases is solely based on their return times, they remain invariant under coordinate transformations, even without the presence of a limit-cycle.

The return times of generalized isophases are constructed to be constant on average for stochastic oscillations, and approximately constant for chaotic oscillations. Therefore, the phase variable will return to the isophase independent[13] of the initial state. On the other hand, the information contained in the amplitude variable that makes states of the same phase distinguishable

[13]The independence is either on average for stochastic oscillations or approximatively for chaotic ones.

will decay due to dissipation. Therefore, all states starting on the same generalized isophase become indistinguishable in the course of time, again in an average or approximate sense. Importantly, an application of the theory to quasi-periodic oscillations will not fulfill this criterion, because for these, the amplitude information will not decay.

The theory was shown to be applicable to non-Markovian stochastic oscillations. However, the claimed invariance of a generalized phase reduction of such oscillations has to be weakened: For a certain set of variables, the average isophases will not depend on the coordinate system. But taking into account additional variables can lead to a different identification of states. This observation is particularly important for the construction of isophases from observed oscillations: In the example of regular human respiration, the second time derivative could have possibly contained additional information that would have influenced the shape of estimated isophases if the derivative had been taken into account.

Generalized isophases of chaotic oscillations can neither be obtained exactly because of phase diffusion, nor optimally because of the **unstable periodic orbits (UPOs)**: An increasingly better approximation of an isophase becomes singular at all UPOs, whereas the best isophase (which is singular) is bounded by the diversity of their oscillation periods. However, UPOs can have a constructive role as well. A comparison of orbit phase sets with approximate isophases yields a good correspondence (cf. Fig. 3.17). Therefore, the orbit phase sets can possibly be used to infer a good approximate isophase. It should be noted, however, that for less phase-coherent chaotic oscillators, such as the Lorenz system, the relationship between orbit phase sets and approximate isophases is less pronounced (see Appendix C).

Chapter 4

Summary and Outlook

The goal of this work was the construction of an invariant phase description of stochastic and chaotic irregular oscillations and their interaction with the surrounding. For this it was necessary to interrelate different phase values of stochastic oscillations to each other. Furthermore, those states of irregular oscillations had to be identified that are in the same phase. We interrelated different phase values using the phase velocities of two deterministic effective phase models of the stochastic oscillations. This allowed us to invariantly characterize periodic forcing as well as pulse-like interactions. On the other hand, we identified all states of the same phase by a criterion that generalizes the concept of standard isophases. In this way, a phase value could be uniquely attributed to each state of all types irregular oscillations in a unified way. Together, the concept of generalized isophases and the effective phase theory provide a unified and invariant description of irregular oscillations that can be easily adopted as a method of data processing.

The periodic forcing and the pulse-like interaction of stochastic oscillations were characterized by an effective coupling function and a stochastic phase resetting curve, respectively. The main feature of both characterizing functions is that they intrinsically depend on the observed regime and on the noise amplitude, especially for noise-induced oscillations. Thus, characterizing functions obtained from one observation cannot be used for a prediction of the dynamics at other noise amplitudes. As a drastic example, the effective coupling function is heavily biased if the mean frequencies of stochastic oscillations and forcing are close. Importantly, the phenomenon can lead to a faulty detection of coupling from observed oscillations. Let us note that the periodically forced case was treated in this work for simplicity. The effective phase theory can be easily extended for a description of arbitrary coupled ensembles of stochastic oscillations.

In order to perform a phase reduction of irregular oscillations, states were identified to belong to the same isophase if they become indistinguishable in the course of time. This criterion provides a direct generalization of standard isophases, but without making any reference to a stable limit-cycle. In addition, the corresponding phase reduction does not depend on the specific coordi-

nate system because generalized isophases are intrinsically invariant. Generalized isophases are defined for stochastic oscillations in an average sense. Here, a unified reduction of noise-induced, noise-perturbed, and non-Markovian oscillations is possible. For chaotic oscillations, the isophases can only be obtained approximately because of chaotic phase diffusion and unstable periodic orbits. Even though this breaks the strict invariance of the phase reduction, good approximate isophases provide a qualitatively better phase dynamics for which chaos enters the dynamics as additive correlated noise.

Under the discussed constrains, the phase description of irregular oscillations allows for a characterization of their interactions with the surrounding that does neither depend on the observed variables nor on the parameterization of oscillations.

Generalized isophases can possibly provide a refined understanding of emergent behaviour of weakly coupled oscillating systems. For example, a theoretical phase description of weakly coupled limit-cycle oscillators can be extended to ones of greater complexity, such as stochastic or chaotic oscillators. In this way, more realistic models of natural systems are treatable. However, from our current point of view, the phase description of irregular oscillations finds its greatest field of application in the analysis of observed biophysical oscillations. For example, the continuous coupling of phase variables extracted from different brain areas has been mostly studied in the context of linear oscillations, even though there is growing evidence for inherent nonlinearities. We believe that this is mainly due to a lack of theoretical understanding of oscillations that show big irregularities, such as those observable in the brain or the cardiovascular system. We hope that the results presented in this work will help to set a new methodology in the studies of biophysical oscillations. Another field of application is neuronal dynamics, where a growing interest is observed in the phase resetting properties of few and many neuronal oscillators. Many treatments rely on a perturbative approach that assumes a stable limit-cycle. However, fluctuating forces as well as excitability are ubiquitously observed properties in single and multiple neuronal systems. Therefore, a certain indecisiveness lies in the treatment which, we hope, the stochastic theory of phase resetting can repair. However, the fluctuating forces observed in many neuronal systems show correlations beyond the validity of the white noise approximation. Even though it was shown, that the phase reduction of non-Markovian oscillations is possible, the loss of information through hidden variables can bias a description of phase resetting beyond its merit. Therefore, the presented methods should be processed further for a specific experimental setup.

Appendix A

Stability of Unstable Periodic Orbits

The stability property of an unstable periodic orbit $\mathbf{x}_0(t+\tau) = \mathbf{x}_0(t)$ of a chaotic system [Eq. (1.16)] is of special importance for the theoretical description of chaos. A linearization of Eq. (1.16) around the orbit yields

$$\dot{\delta} = df\left(\mathbf{x}_0(t)\right)\delta, \tag{A.1}$$

where $\delta(t)$ is a tangent vector. According to Floquet theory there exists a principal fundamental matrix solution $\Phi(t) = P(t)\exp\left[tA\right]$ where $P(t)$ is τ-periodic and A is a constant matrix. The stability of $\mathbf{x}_0(t)$ is determined by the *Floquet multipliers* ρ_j that are the eigenvalues of $\Phi(\tau)$. If $|\rho_j| < 1$ holds for all j the orbit is stable. If for the kth Floquet multiplier $|\rho_k| > 1$ the orbit is unstable in the kth direction determined by the eigenvector to ρ_k. The unstable periodic orbits embedded in a chaotic attractor have stable directions through which the trajectory approaches them and unstable directions through which it absents itself.

Appendix B

Estimation of Phase Diffusion

An estimation of the phase diffusion coefficient [Eqns. (1.23) and (2.6)] of irregular oscillations is not straightforward because their mean frequency ω might not be known exactly. Let us consider the case, where ω needs to be estimated as well. In this case a Brownian bridge process is constructed with which the diffusion coefficient can be inferred.

Starting point of the analysis is a set of N_{avg} sampled realizations of an arbitrary phase variable $\varphi_n = \varphi(n\Delta t)$ each containing N data points. The observation time is $T = N\Delta t$. For each unwound realization, the mean frequency is estimated by

$$\hat{\omega} = \frac{\varphi_{N-1} - \varphi_0}{T} \ . \tag{B.1}$$

The difference $\delta_n = \varphi_n - \hat{\omega} n\Delta t$ is a realization of a *Brownian bridge process* because it fulfills the conditions

$$\begin{aligned} \delta_0 = \delta_{N-1} &= 0 \ , \\ \langle \delta_n \rangle &= 0 \ , \\ \Delta_n = \langle \delta_n^2 \rangle &= c\frac{2t_n(T-t_n)}{T} \ , \end{aligned} \tag{B.2}$$

if T is big enough[1]. Then, the coefficient of variance c is an estimate of the diffusion coefficient D. The computation of c is done by a linear least-squares fit to the data Δ_n which has to be computed as an average over the realizations of the Brownian bridge.

The method was tested using realizations of the Adler equation [Eq. (2.2)] at different parameters, for which estimates of the diffusion coefficient could be compared to the analytic formula (2.8). In conclusion, a smaller diffusion coefficients demands for more realizations, whereas longer correlations as well as inhomogeneities of oscillations in φ ask for more oscillations per realizations in order to have a faithful estimate of D.

An illustration of the method is given in Fig. B.1 using the Adler equation [Eq. (1.14)]. The dependence on T was analyzed in detail for the above example. The coefficient $c = \hat{D}$ was computed with $N_{\mathrm{avg}} = 200$ as a function of the mean number of oscillations in the realizations, which is proportional to

[1] Time has to be chosen the bigger the more correlations exist in the phase dynamics.

T. To obtain a statistical ensemble each calculation was performed 50 times. It was seen that as the number of oscillations per realization increased the systematic error decreased whereas the statistical error remained independent of T (bottom plot of Fig. B.1). The statistical variation from a single estimation as shown in the top plot of Fig. B.1 was also analyzed via bootstrapping techniques [13]. However, the resultant deviation was two orders of magnitude smaller then the one obtained across different calculations.

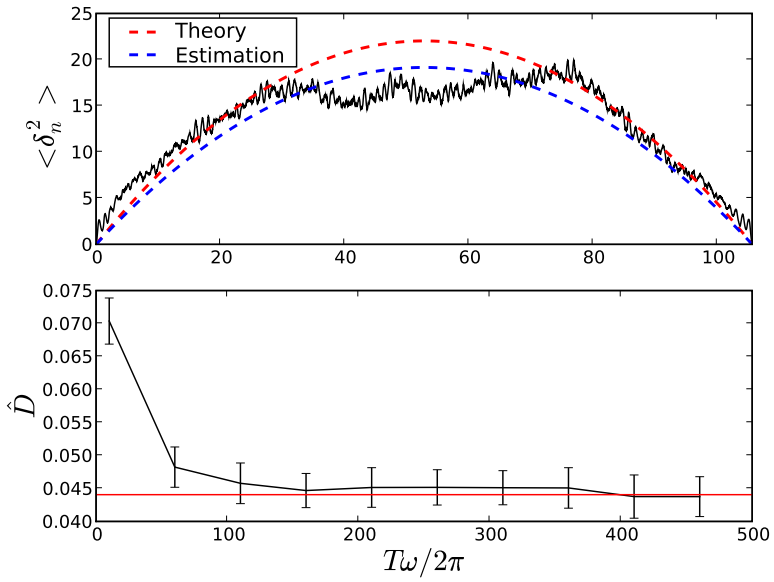

Figure B.1: For a good estimation of the phase diffusion coefficient $\hat{D} = c$ [Eq. (B.2)] of the Adler equation [Eq. (1.14)] by the Brownian bridge method, enough oscillations on average (the number is $T\omega/2\pi$) for each of the $N_{\text{avg}} = 200$ realizations have to be ensured (bottom plot), here shown for $a = 1.2$ and $\sigma = 0.1$. Then, $\langle\delta_n^2\rangle$ is well represented by the theoretical curve [Eq. (B.2)] (top plot), here shown for 150 oscillations on average.

B.1 Phase Diffusion Coefficient of the Rössler Oscillator

The phase diffusion coefficient [Eq. (1.23)] of the Rössler oscillator [Eq. (1.17)] is computed using the Brownian bridge method (cf. Appendix B). Due to long correlations present in the arbitrary phase variable $\varphi(t) = \tan^{-1}(y(t)/x(t))$ [Eq. (1.19)], we used $N_{\text{avg}} = 650$ representations containing 16400 oscillations for the average in Eq. (1.23) (cf. Fig. B.2 for an illustration). The calculation was performed 50 times yielding estimate

$$\hat{D} = 8.8 \cdot 10^{-5} \pm \frac{3.95 \cdot 10^{-6}}{\sqrt{50}} \text{ rad s}^{-1} \, . \tag{B.3}$$

Furthermore, the numerical cumulative distribution function C of $\hat{D}$, computed from the 50 calculations, was compared to a Gaussian (see bottom plot of Fig. B.2). The Kolmogorov-Smirnov statistics had a value of $0.65/\sqrt{50}$ (red vertical line), and thus, gaussianity seemed to be a good assumption (cf. Fig. B.2).

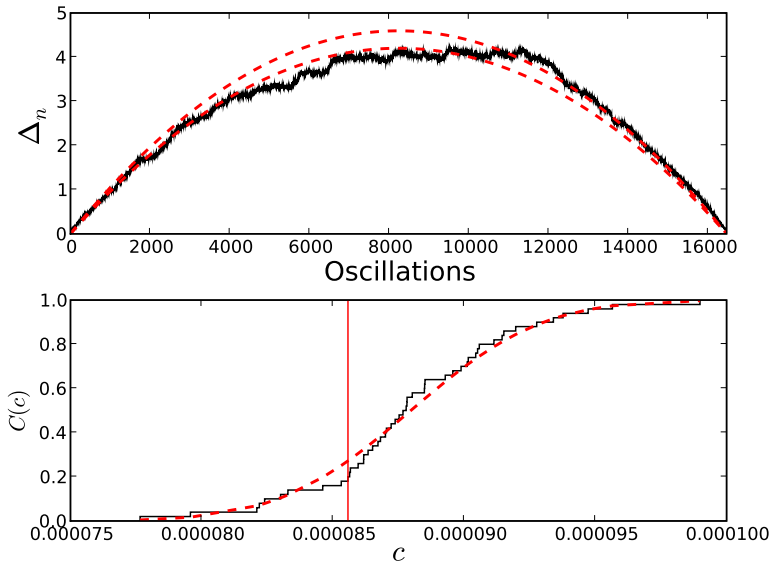

Figure B.2: The similarity of Δ_n (black line) and the corresponding theoretical functions (dashed lines) at parameter $c = \hat{D} \pm \mathrm{std}(\hat{D})$ [Eq. (B.3)] illustrate the applicability of the Brownian bridge method for an estimation of phase diffusion of the Rössler oscillator (top plot). Performing an estimation of c in 50 independent trials yields a Gaussian distribution to a good precision. This can be seen by comparing the cumulative distribution functions of the estimates $C(c)$ (black line in bottom plot) and of a Gaussian (red dashed line). The Kolmogorov-Smirnov statistics was $0.65/\sqrt{50}$ (red vertical line).

Appendix C

Approximate Isophases of the Lorenz System

The chaotic phase diffusion of the Lorenz system [Eq. (1.18)] is orders of magnitude stronger than that of the Rössler oscillator [Eq. (1.17)]. This is in line with the observation that orbit phase sets [Eq. (3.34)] are not as compatible as it was seen for the Rössler oscillator in Fig. 3.10. An optimal adjustment of phase shifts leads to a broad distribution of "states of the same phase" from which some shape can be guessed (cf. Fig. C.1). With cylindrical coordinates

$$\begin{aligned} \varphi &= \tan^{-1} \frac{z-27}{\sqrt{x^2+y^2}-12} \ ; \\ r^2 &= \left(\sqrt{x^2+y^2}-12\right)^2 + (z-27)^2 \ ; \\ h &= y \ , \end{aligned} \tag{C.1}$$

that define a monotonically growing arbitrary phase variable $\varphi(t)$, approximate isophases can still be estimated using the scheme (3.13). The result is displayed in Fig. C.1, where an approximate compliance of orbit isophase and estimated approximate isophase can be recognized. However, the correspondence is much better for the Rössler oscillator (cf. Fig. 3.15).

C.1 How to read a Stereogram

A stereogram is a plot that simulates a three-dimensional impression of an object by means of two two-dimensional projections of it. The stereograms in this work are produced in a "cross-view" fashion (as opposed to parallel-view).

In order to get a three-dimensional impression of the object each eye of the observer has to get a slightly different information by means of the two pictures. Specifically, the object on the left (right) picture is turned slightly counterclockwise (clockwise) if viewed from above. If the right (left) eye receives information only of the left (right) picture, a three-dimensional impression emerges. For this, we suggest to focus first on getting big features in each

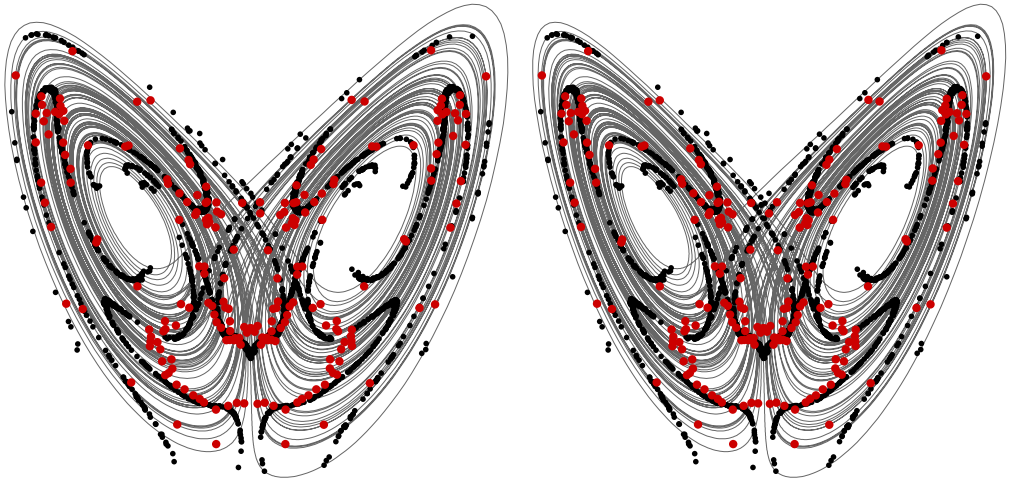

Figure C.1: Stereogram of estimated approximate isophases [Eq. (3.9)] (black points) of the Lorenz attractor [Eq. (1.18)] (grey line), together with corresponding orbit isophases [Eq. (3.34)] computed for all 6-orbits (red points). Due to larger chaotic phase diffusion, the resemblance is less pronounced both, among orbit phase sets, and among these and the approximate isophases. The conditions of estimation were: $N\Delta t = 10^4 \cdot 0.2$ s, $M = 30$, $k = 0.3$, $N_\varphi = 3$, $N_r = 3$ and $N_h = 1$.

of the pictures to coincide. After three instead of two pictures are observed one has to focus on the middle.

Problematically, the plane of focus of the eyes have to be at a different distance than what is suggested by their position. Therefore, the observer has to force her eyes to refocus. If the "middle" pictures is in the focus of both eyes the three-dimensional structure will emerge.

Looking too long at a stereogram of this work can cause dizziness.

Bibliography

[1] Andronov, A. A., Vitt, A. A., and Khaikin, S. E. *Theory of oscillators*. Pergamon, London, 1966.

[2] Anteneodo, C. and Riera, R. Arbitrary-order corrections for finite-time drift and diffusion coefficients. *Phys. Rev. E*, 80:031103, 2009. doi:10.1103/PhysRevE.80.031103.

[3] Arecchi, F. T., Meucci, R., Puccioni, G., and Tredicce, J. Experimental evidence of subharmonic bifurcations, multistability, and turbulence in a q-switched gas laser. *Phys. Rev. Lett.*, 49:1217–1220, 1982. doi:10.1103/PhysRevLett.49.1217.

[4] Artuso, R., Aurell, E., and Cvitanovic, P. Recycling of strange sets: I. Cycle expansions. *Nonlinearity*, 3:325, 1990. doi:10.1088/0951-7715/3/2/005.

[5] Artuso, R., Aurell, E., and Cvitanovic, P. Recycling of strange sets: II. Applications. *Nonlinearity*, 3:361, 1990. doi:10.1088/0951-7715/3/2/006.

[6] Balanov, A. G., Janson, N. B., and Schöll, E. Control of noise-induced oscillations by delayed feedback. *Physica D*, 199:1–12, 2004. doi:10.1016/j.physd.2004.05.008.

[7] Bartsch, R., Kantelhardt, J. W., Penzel, T., and Havlin, S. Experimental evidence for phase synchronization transitions in the human cardiorespiratory system. *Phys. Rev. Lett.*, 98:054102, 2007. doi:10.1103/PhysRevLett.98.054102.

[8] Brea, J., Russell, D. F., and Neiman, A. B. Measuring direction in the coupling of biological oscillators: A case study of electroreceptors of paddlefish. *Chaos*, 16:026111, 2006. doi:10.1063/1.2201466.

[9] Campbell, A., Gonzalez, A., Gonzalez, D. L., Piro, O., and Larrondo, H. A. Isochrones and the dynamics of kicked rotators. *Physica A*, 155:565–584, 1989. doi:10.1016/0378-4371(89)90006-X.

[10] Canavier, C. C. Phase response curve. *Scholarpedia*, 1:1332, 2006. doi:10.4249/scholarpedia.1332.

[11] DeShazer, D. J., Breban, R., Ott, E., and Roy, R. Detecting phase synchronization in a chaotic laser array. *Phys. Rev. Lett.*, 87:044101, 2001. doi:10.1103/PhysRevLett.87.044101.

[12] Dierckx, P. An algorithm for smoothing, differentiation and integration of experimental data using spline functions. *J. Comput. Appl. Math.*, 1:165 – 184, 1975.

[13] Efron, B. and Tibshirani, R. J. *An Introduction to the Bootstrap*. Chapman and Hall, New York, 1993.

[14] Ermentrout, B. and Saunders, D. Phase resetting and coupling of noisy neural oscillators. *J. Comput. Neurosci.*, 20:179–190, 2006. doi:10.1007/s10827-005-5427-0.

[15] Ermentrout, G. B. Ermentrout-Kopell canonical model. *Scholarpedia*, 3:1398, 2008. doi:10.4249/scholarpedia.1398.

[16] Faure, P. and Korn, H. Is there chaos in the brain? I. Concepts of nonlinear dynamics and methods of investigation. *Comptes Rendus de l'Académie des Sciences - Series III - Sciences de la Vie*, 324:773 – 793, 2001. doi:10.1016/S0764-4469(01)01377-4.

[17] Friedrich, R. and Peinke, J. Description of a turbulent cascade by a Fokker-Planck equation. *Phys. Rev. Lett.*, 78:863–866, 1997. doi:10.1103/PhysRevLett.78.863.

[18] Gardiner, C. W. *Handbook of Stochastic Methods*. Springer, Berlin, 3rd edn., 2004. doi:10.1002/bbpc.19850890629.

[19] Gilmore, R. Topological analysis of chaotic dynamical systems. *Rev. Mod. Phys.*, 70:1455–1529, 1998. doi:10.1103/RevModPhys.70.1455.

[20] Glass, L. and Mackey, M. C. *From Clocks to Chaos*. Princeton University Press, Princeton, 1988.

[21] Goldberger, A. L., Amaral, L. A. N., Glass, L., Hausdorff, J. M., Ivanov, P. C., Mark, R. G., Mietus, J. E., Moody, G. B., Peng, C.-K., and Stanley, H. E. PhysioBank, PhysioToolkit, and PhysioNet: Components of a new research resource for complex physiologic signals. *Circulation*, 101:e215–e220, 2000.

[22] Goldobin, D. S. and Pikovsky, A. Synchronization and desynchronization of self-sustained oscillators by common noise. *Phys. Rev. E*, 71:045201, 2005. doi:10.1103/PhysRevE.71.045201.

[23] Goldobin, D. S. and Pikovsky, A. Synchronization of self-sustained oscillators by common white noise. *Physica A*, 351:126–132, 2005. doi:10.1016/j.physa.2004.12.014.

[24] Goldobin, D. S. and Pikovsky, A. Antireliability of noise-driven neurons. *Phys. Rev. E*, 73:061906, 2006. doi:10.1103/PhysRevE.73.061906.

[25] Gollub, J. P. and Swinney, H. L. Onset of turbulence in a rotating fluid. *Phys. Rev. Lett.*, 35:927–930, 1975. doi:10.1103/PhysRevLett.35.927.

[26] Gonzalez, D. L. and Piro, O. Chaos in a nonlinear driven oscillator with exact solution. *Phys. Rev. Lett.*, 50:870–872, 1983. doi:10.1103/PhysRevLett.50.870.

[27] Grossman, P., Wilhelm, F. H., and Spoerle, M. Respiratory sinus arrhythmia, cardiac vagal control, and daily activity. *Am. J. Physiol. Heart Circ. Physiol.*, 287:H728–H734, 2004. doi:10.1152/ajpheart.00825.2003.

[28] Guralnik, Z. Exact statistics of chaotic dynamical systems. *Chaos*, 18:033114, 2008. doi:10.1063/1.2960541.

[29] Hänggi, P. and Riseborough, P. Dynamics of nonlinear dissipative oscillators. *Am. J. Phys.*, 51:347–352, 1983. doi:10.1103/PhysRevA.27.3379.

[30] Hauschildt, B., Janson, N. B., Balanov, A., and Schöll, E. Noise-induced cooperative dynamics and its control in coupled neuron models. *Phys. Rev. E*, 74:051906, 2006. doi:10.1103/PhysRevE.74.051906.

[31] Horstmann, M. T., Müller, A., Rothkegel, A., Schwabedal, J., Elger, C. E., and Lehnertz, K. Impact of computational models for an improved understanding of ictogenesis: From single neurons to networks of neurons. In *Seizure Prediction in Epilepsy: From Basic Mechanisms to Clinical Applications*. Wiley-VCH, Weinheim, 2008.

[32] Izhikevich, E. M. *Dynamical Systems in Neuroscience*. MIT Press, Cambridge, 2007.

[33] Josić, K. and Mar, D. J. Phase synchronization of chaotic systems with small phase diffusion. *Phys. Rev. E*, 64:056234, 2001. doi:10.1103/PhysRevE.64.056234.

[34] Just, W., Kantz, H., Ragwitz, M., and Schmüser, F. Nonequilibrium physics meets time series analysis: Measuring probability currents from data. *Europhys. Lett.*, 62:28–34, 2003. doi:10.1209/epl/i2003-00359-2.

[35] Kantz, H. and Schreiber, T. *Nonlinear time series analysis*. Cambridge Univ. Press, Cambridge, UK, 2nd edn., 2003.

[36] Karlin, S. and Taylor, H. M. *A Second Course in Stochastic Processes*. Academic Press, San Diego, 1981.

[37] Kawamura, Y., Nakao, H., Arai, K., Kori, H., and Kuramoto, Y. Collective phase sensitivity. *Phys. Rev. Lett.*, 101:024101, 2008. doi:10.1103/PhysRevLett.101.024101.

[38] Ko, T.-W. and Ermentrout, G. B. Phase-response curves of coupled oscillators. *Phys. Rev. E*, 79:016211, 2009. doi:10.1103/PhysRevE.79.016211.

[39] Korn, H. and Faure, P. Is there chaos in the brain? II. Experimental evidence and related models. *Comptes Rendus Biologies*, 326:787 – 840, 2003. doi:10.1016/j.crvi.2003.09.011.

[40] Kralemann, B. *Rekonstruktion invarianter Phasenmodelle aus Daten*. Ph.D. thesis, Potsdam University, 2010.

[41] Kralemann, B., Cimponeriu, L., Rosenblum, M., Pikovsky, A., and Mrowka, R. Phase dynamics of coupled oscillators reconstructed from data. *Phys. Rev. E*, 77:066205, 2008. doi:10.1103/PhysRevE.77.066205.

[42] Kuramoto, Y. *Chemical Oscillations, Waves and Turbulence*. Springer-Verlag, Berlin, Heidelberg, New York, Tokyo, 1984.

[43] Landa, P. and Rosenblum, M. Modified mackey-glass model of respiration control. *Phys. Rev. E*, 52:R36–R39, 1995. doi:10.1103/PhysRevE.52.R36.

[44] Li, T. Y. and Yorke, J. A. Period three implies chaos. *Am. Math. Monthly*, 82:985–992, 1975.

[45] Lin, K. K. and Young, L.-S. Shear-induced chaos. *Nonlinearity*, 21:899–922, 2008. doi:10.1088/0951-7715/21/5/002.

[46] Lindner, B., Garcia-Ojalvo, J., Neiman, A., and Schimansky-Geier, L. Effects of noise in excitable systems. *Phys. Rep.*, 392:321–424, 2004. doi:10.1016/j.physrep.2003.10.015.

[47] Lindner, B., Kostur, M., and Schimansky-Geier, L. Optimal diffusive transport in a tilted periodic potential. *Fluc. Noise Lett.*, 1:R25–R39, 2001. doi:10.1142/S0219477501000056.

[48] Lindner, B. and Schimansky-Geier, L. Noise-induced transport with low randomness. *Phys. Rev. Lett.*, 89:230602, 2002. doi:10.1103/PhysRevLett.89.230602.

[49] Lorenz, E. N. Deterministic nonperiodic flow. *J. Atmos. Sci.*, 20:130–141, 1963. doi:10.1175/1520-0469(1963)020.

[50] Lorrondo, H. A., Avalos, D. R., and Laura, P. A. A. Dynamics of a kicked oscillator with a delay in its parametric feedback loop: An analytical study. *Nlin. Dyn*, 11:407–419, 1996. doi:10.1007/BF00045334.

[51] Mannella, R. and Palleschi, V. Fast and precise algorithm for computer simulation of stochastic differential equations. *Phys. Rev. A*, 40:3381–3386, 1989. doi:10.1103/PhysRevA.40.3381.

[52] Memmesheimer, R.-M. and Timme, M. Designing the dynamics of spiking neural networks. *Phys. Rev. Lett.*, 97:188101, 2006. doi:10.1103/PhysRevLett.97.188101.

[53] Molenaar, D., Clercx, H. J. H., and van Heijst, G. J. F. Transition to chaos in a confined two-dimensional fluid flow. *Phys. Rev. Lett.*, 95:104503, 2005. doi:10.1103/PhysRevLett.95.104503.

[54] Müller, A. *Stochastische Synchronisation und Desynchronisation gekoppelter und ungekoppelter selbsterhaltender Oszillatoren*. Ph.D. thesis, University of Bonn, 2008.

[55] Neiman, A. B., Russell, D. F., Yakusheva, T. A., DiLullo, A., and Tass, P. A. Response clustering in transient stochastic synchronization and desynchronization of coupled neuronal bursters. *Phys. Rev. E*, 76:021908, 2007. doi:10.1103/PhysRevE.76.021908.

[56] Nelson, E. Derivation of the Schrödinger equation from Newtonian mechanics. *Phys. Rev.*, 150:1079–1085, 1966. doi:10.1103/PhysRev.150.1079.

[57] Osipov, G. V., Pikovsky, A. S., and Kurths, J. Phase synchronization of chaotic rotators. *Phys. Rev. Lett.*, 88:054102, 2002. doi:10.1103/PhysRevLett.88.054102.

[58] Osterhage, H., Mormann, F., Wagner, T., and Lehnertz, K. Detecting directional coupling in the human epileptic brain: Limitations and potential pitfalls. *Phys. Rev. E*, 77:011914, 2008. doi:10.1103/PhysRevE.77.011914.

[59] Ota, K., Nomura, M., and Aoyagi, T. Weighted spike-triggered average of a fluctuating stimulus yielding the phase response curve. *Phys. Rev. Lett.*, 103:024101, 2009. doi:10.1103/PhysRevLett.103.024101.

[60] Patidar, S., Pototsky, A., and Janson, N. B. Controlling noise-induced behavior of excitable networks. *New Journal of Physics*, 11:073001, 2009. doi:10.1088/1367-2630/11/7/073001.

[61] Peng, C.-K., Mietus, J. E., Liu, Y., Lee, C., Hausdorff, J., Stanley, M. H. E., Goldberger, A. L., and Lipsitz, L. A. Quantifying fractal dynamics of human respiration: Age and gender effects. *Ann. Biomed. Eng.*, 30:683–692, 2002.

[62] Pikovsky, A. Synchronization and stochastization of the ensamble of autogenerators by external noise. *Radiophys. Quantum Electron.*, 27:576–581, 1984.

[63] Pikovsky, A., Rosenblum, M., and Kurths, J. *Synchronization. A Universal Concept in Nonlinear Sciences.* Cambridge University Press, Cambridge, 2001.

[64] Pikovsky, A. S. and Kurths, J. Coherence resonance in a noise-driven excitable system. *Phys. Rev. Lett.*, 78:775–778, 1997. doi:10.1103/PhysRevLett.78.775.

[65] Pope, S. B. and Ching, E. S. C. Stationary probability density functions: An exact result. *Phys. Fluids A*, 5:1529–1531, 1993. doi:10.1063/1.858830.

[66] Prager, T., Lerch, H.-P., Schimansky-Geier, L., and Schöll, E. Increase of coherence in excitable systems by delayed feedback. *J. Phys. A*, 40:11045, 2007. doi:10.1088/1751-8113/40/36/005.

[67] Press, W. H., Teukolsky, S. A., Vetterling, W. T., and Flannery, B. P. *Numerical Recipes in C*. Cambridge University Press, 2nd edn., 2002.

[68] Reimann, P., Van den Broeck, C., Linke, H., Hänggi, P., Rubi, J. M., and Pérez-Madrid, A. Giant acceleration of free diffusion by use of tilted periodic potentials. *Phys. Rev. Lett.*, 87:010602, 2001. doi: 10.1103/PhysRevLett.87.010602.

[69] Reinker, S., Li, Y. X., and Kuske, R. Noise-induced coherence and network oscillations in a reduced bursting model. *Bulletin of Mathematical Biology*, 68:1401–1427, 2006. doi:10.1007/s11538-006-9089-5.

[70] Risken, H. Z. *The Fokker–Planck Equation*. Springer, Berlin, 1989.

[71] Ritt, J. Evaluation of entrainment of a nonlinear neural oscillator to white noise. *Phys. Rev. E*, 68:041915, 2003. doi:10.1103/PhysRevE.68.041915.

[72] Rosenblum, M. G., Pikovsky, A. S., and Kurths, J. Phase synchronization of chaotic oscillators. *Phys. Rev. Lett.*, 76:1804–1807, 1996. doi:10.1103/PhysRevLett.76.1804.

[73] Rössler, O. E. An equation for continuous chaos. *Phys. Lett. A*, 57:397–398, 1976. doi:10.1016/0375-9601(76)90101-8.

[74] Schmidt, R., Lang, F., and Thews, G. *Physiologie des Menschen*. Springer, Berlin, 2005.

[75] Schwabedal, J. T. C. and Lehnertz, K. Ein Verfahren zur modellassistierten Analyse des EEGs von Epilepsiepatienten. In *Biosignalverarbeitung: Innovationen bei der Erfassung und Analyse bioelektrischer und biomagnetischer Signale; Beiträge zum Workshop Biosignalverarbeitung 2008, Potsdam, 16.-18.Juli 2008*. 2008.

[76] Sharkovsky, A. N. Sharkovsky ordering. *Scholarpedia*, 3:1680, 2008. doi: 10.4249/scholarpedia.1680.

[77] Small, M. and Judd, K. Comparisons of new nonlinear modeling techniques with applications to infant respiration. *Physica D*, 117:283–298, 1998. doi:10.1016/S0167-2789(97)00311-4.

[78] Strogatz, S. H. *Nonlinear Dynamics and Chaos*. Addison-Wesley, Reading, 1994.

[79] Strogatz, S. H. From Kuramoto to Crawford: Exploring the onset of synchronization in populations of coupled oscillators. *Physica D*, 143:1–20, 2000. doi:10.1016/S0167-2789(00)00094-4.

[80] Stuart, J. T. On the non-linear mechanics of hydrodynamic stability. *J. Fluid Mech.*, 4:1–21, 1958. doi:10.1017/S0022112058000276.

[81] Sturis, J., Knudsen, C., O'Meara, N., Thomsen, J., Mosekilde, E., Van Cauter, E., and Polonsky, K. Phase-locking regions in a forced model of slow insulin and glucose oscillations. *Chaos*, 5:193–199, 1995. doi: 10.1063/1.166068.

[82] Teramae, J., Nakao, H., and Ermentrout, G. B. Stochastic phase reduction for a general class of noisy limit cycle oscillators. *Phys. Rev. Lett.*, 102:194102, 2009. doi:10.1103/PhysRevLett.102.194102.

[83] Teramae, J.-n. and Tanaka, D. Robustness of the noise-induced phase synchronization in a general class of limit cycle oscillators. *Phys. Rev. Lett.*, 93:204103, 2004. doi:10.1103/PhysRevLett.93.204103.

[84] Wagner, T., Axmacher, N., Lehnertz, K., Elger, C. E., and Fell, J. Sleep-dependent directional coupling between human neocortex and hippocampus. *Cortex*, 46:256 – 263, 2010. doi:10.1016/j.cortex.2009.05.012.

[85] Wagner, T., Fell, J., and Lehnertz, K. The detection of transient directional couplings based on phase synchronization. *New Journal of Physics*, 12:053031, 2010. doi:10.1088/1367-2630/12/5/053031.

[86] Wahba, G. *Spline Models of Observational Data*. SIAM, Philadelphia, 1990.

[87] Watts, D. J. and Strogatz, S. H. Collective dynamics of 'small-world' networks. *Nature*, 393:440–442, 1998. doi:10.1038/30918.

[88] Wechselberger, M. Canards. *Scholarpedia*, 2:1356, 2007. doi:10.4249/scholarpedia.1356.

[89] Winfree, A. T. *The Geometry of Biological Time*. Springer-Verlag, Berlin, 1980.

[90] Yoshimura, K. and Arai, K. Phase reduction of stochastic limit cycle oscillators. *Phys. Rev. Lett.*, 101:154101, 2008. doi:10.1103/PhysRevLett.101.154101.

Danksagung

An erster Stelle steht meine Dankbarkeit gegenüber meinem Doktorvater Prof. Dr. Arkadi Pikovski, der in seiner vertrauensvollen Art ein fruchtbares wissenschaftliches Arbeitsklima schaft, und der mich an das spannende Thema der Phasendynamik heran geführt hat. In diesem Zusammenhang danke ich auch Prof. Dr. Michael Rosenblum, Dr. Udo Schwarz, Dr. Markus Abel, Maik, Grisha, Zoran, Mario, Azamat, Andre, Natasha, Christin, Karsten, Sarah, Sun und vielen weiteren die täglich auf den Fluren des "goldenen Käfigs" zu sehen sind.

Die Zeit in Potsdam wäre jedoch nur halb so schön – wahrscheinlich aber auch nur halb so lang – gewesen, wenn ich nicht auch außerhalb physikalischer Kreise mit netten und interessanten Menschen in Kontakt gekommen wäre. Mit vielen von ihnen fühle ich mich seit jeher eng Verbund: Unter ihnen sind meine lieben Mitbewohnerinnen Christine und Luci, die liebe Julia, Rafi an der Trompete, Daniel der Schwarzseher, meine ewigen Mensabegleitungen Jan, Gunnar, Harald und Heiko, Wilhelm der Intellektuelle, die Mitglieder des "Jazzchor des Campus Golm" samt ihrer neuen Leiterin Maria, und nicht zuletzt die Mitglieder der Potsdamer "English Drama Group", die mich aufs Äußerste gefordert haben. Auch ihnen allen bin ich zu tiefem Dank verpflichtet.

Sehr danke ich auch meiner Mutter Anne und meinem Bruder Felix, sowie meinen langjährigen Freunden Georg, Evelien, Lukas, Ingolf und Sebastian für ihre Liebe und für ihre Hilfe den schwersten Schlag meines Lebens, nämlich den plötzlichen Tod meines Vaters Peter, zu verkraften.

In liebevoller Erinnerung meines Vaters wurde ich bei der Anfertigung der Doktorarbeit immer durch seine Disziplin und durch seine Fähigkeit zur Begeisterung inspiriert.

Ich versichere, dass ich die vorliegende Arbeit selbständig verfasst und keine anderen als die angegebenen Quellen und Hilfsmittel benutzt habe, sowie das die Arbeit bisher an keiner anderen Hochschule eingereicht worden ist.

Potsdam, den 14. September 2010

Justus Schwabedal